Doctoral Dissertations   Graduate School

8-2009

The Influence of Brick Veneer on Racking Behavior of Light Frame Wood Shear Walls

Nikola Zisi
University of Tennessee - Knoxville

To the Graduate Council:

I am submitting herewith a dissertation written by Nikola Zisi entitled "The Influence of Brick Veneer on Racking Behavior of Light Frame Wood Shear Walls." I have examined the final electronic copy of this dissertation for form and content and recommend that it be accepted in partial fulfillment of the requirements for the degree of Doctor of Philosophy, with a major in Civil Engineering.

Richard M. Bennett, Major Professor

We have read this dissertation and recommend its acceptance:

Edwin G. Burdette, Eric C. Drumm, Christopher D. Pionke

Accepted for the Council:
Dixie L. Thompson

Vice Provost and Dean of the Graduate School

(Original signatures are on file with official student records.)

To the Graduate Council:

I am submitting herewith a dissertation written by Nikola Zisi entitled "The Influence of Brick Veneer on Racking Behavior of Light Frame Wood Shear Walls." I have examined the final electronic copy of this dissertation for form and content and recommend that it be accepted in partial fulfillment of the requirements for the degree of Doctor of Philosophy, with a major in Civil Engineering.

<u>Richard M. Bennett, Major Professor</u>

We have read this dissertation
and recommend its acceptance:

<u>Edwin G. Burdette</u>

<u>Eric C. Drumm</u>

<u>Christopher D. Pionke</u>

Accepted for the Council:

<u>Carolyn R. Hodges, Vice Provost and
Dean of the Graduate School</u>

The Influence of Brick Veneer on Racking Behavior of
Light Frame Wood Shear Walls

A Dissertation
Presented for the
Doctor of Philosophy
Degree
The University of Tennessee, Knoxville

Nikola Zisi
August 2009

improving the open-source software framework that utilizes a variety of nonlinear material models, elements, and solution algorithms which I found indispensible in modeling and analyzing structural response.

Last, but certainly not least, the unwavering support, continual encouragement and enduring patience of my family is deeply and sincerely appreciated.

ABSTRACT

The racking behavior of an anchored brick veneer – wood frame wall system was investigated analytically. The core wall model simulated a wood frame sheathed with oriented strand board. Brick veneer was then tied to the exterior wall face, and gypsum wallboard sheathing was added on the interior wall face. Two-dimensional linear elastic beam and continuum type elements were used to model these principal wall components. Gap elements were used to prevent sheathing overlap and to model panel bearing at the base. The veneer was supported on compression-only spring elements in the vertical direction and perfectly plastic spring elements in the horizontal direction. The fasteners connecting the sheathing to the frame backing, and the ties anchoring the veneer were modeled with pairs of orthogonal independent nonlinear inelastic springs. Common force-displacement relations were used for the springs that approximated the fasteners, while an experimental study was carried out to determine constitutive relations for corrugated metal ties that anchor the brick veneer to its wood frame backing.

Connection subassemblies were tested under monotonic and cyclic shear loading, and it was determined that fastener slippage during cyclic loading enabled by the localized damage of the surrounding wood fibers diminished the energy absorption capacity of the connection and caused pronounced pinching in the hystereses. Considering corrugated ties with minimum thickness permitted by the MSJC Code, tie design and bent eccentricity were found to be the most important factors, while tie location in the bed joint, fastener type and fastener quantity were influential to a lesser degree.

Of particular interest in the analytical investigation were the effects resulting from the inclusion of brick veneer on the outer wall face and/or gypsum wallboard sheathing on the interior wall face, as well as the viability of the created integral wall system. It was determined that both brick veneer and wallboard sheathing stiffen significantly the core light frame wood shear wall and alter its response. Their simultaneous presence increased racking wall strength, but diminished its ductility. The addition of anchored brick veneer limited wood shear wall displacements and reduced wall's base shear under dynamic excitation.

TABLE OF CONTENTS

LIST OF TABLES

LIST OF FIGURES

CHAPTER I - INTRODUCTION

Composition of Brick Veneer-Light Frame Wood Shear Walls

Light Frame Wood Shear Walls

Light frame wood shear walls are the primary lateral load bearing system used in low rise residential construction in North America (Fig. 1.1). These shear walls consist of a dimensional lumber frame sheathed with plywood or oriented strand board (OSB) to create a stiff wall assembly (Fig. 1.2). Lateral forces induced into the wall from winds or earthquakes are resisted primarily by racking of the sheathing and are transferred to framing members via nailed connections. In the past two decades extensive experimental and analytical work has been carried out to determine the racking behavior of such walls. A review of this research is detailed in a bibliography written by van de Lindt (2004). Through numerous experiments researchers have verified that light frame wood shear walls are capable of dissipating large amounts of energy through the summation of individual fastener deformations. Interestingly, the behavior of the nailed sheathing-to-wall connection is the one that governs the response of the whole shear wall assembly (Fig. 1.3). The load deformation relation of such shear walls during cyclic loading is characterized by pinched hystereses that show both stiffness degradation and strength deterioration (Dolan and Madsen 1992 b, Shenton et al. 1998, Folz and Filiatrault 2001).

Studies on the effect of sheathing thickness, sheathing size, nail type, nail spacing, nail head penetration and the use of blocking on the wall behavior showed that nail spacing had a more prominent effect on the wall stiffness than did nail type. Excessive nail head penetration could significantly reduce wall strength and displacement capacity. A considerable increase in panel thickness from 7/16 to 5/8 inch resulted in only moderate strength increase, while walls built with oversized sheathing panels showed increase in stiffness and strength but a reduction in energy dissipation capacity. It was also found that the use of blocking had a smaller but still considerable effect on the wall stiffness (Atherton 1983, Falk and Itani 1989, Lam et al. 1997, Jones and Fonseca 2002). Tests on both small and full scale wood shear walls sheathed with

1

DISTRIBUTION OF LATERAL LOADS ON BUILDING

Roof (horizontal diaphragm) carries load to end walls

Wind load, F (lb per sq ft)

Side wall carries load to roof diaphragm at top, and to foundation at bottom

End wall (vertical diaphragm or shear wall) carries load to foundation

v (lb per lin ft of diaphragm width) $= \dfrac{wL}{2b}$

w (lb per lin ft of wall) $= F\dfrac{h}{2}$

T (lb) $= C = vh$
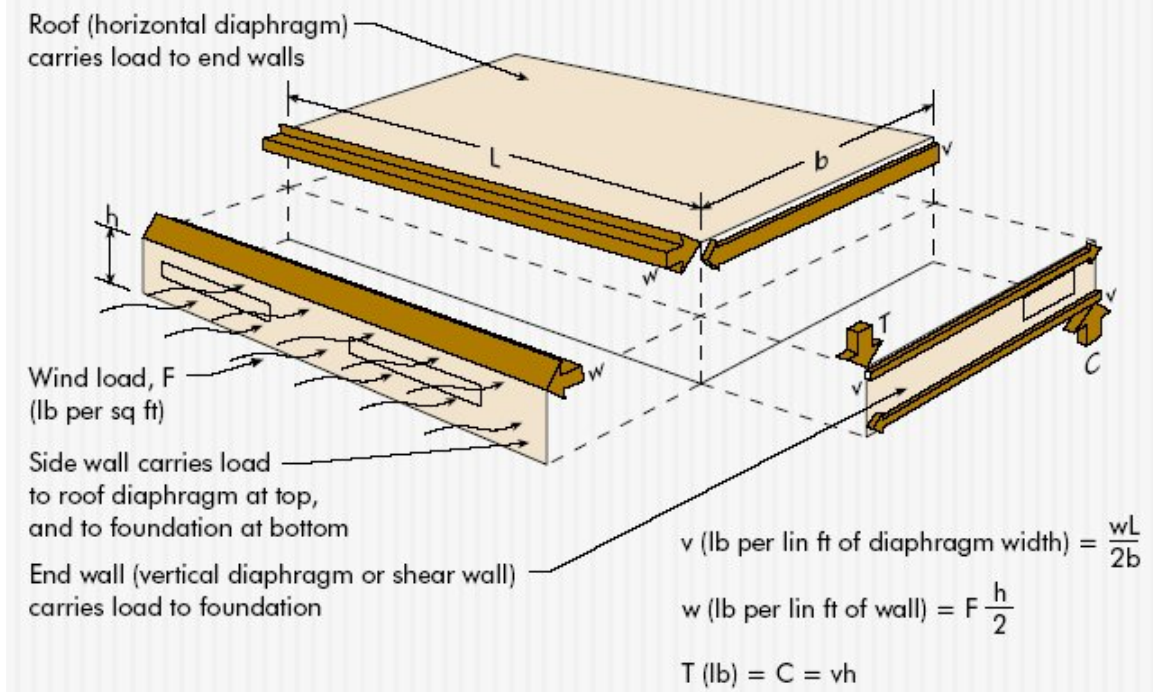
Fig. 1.1. Distribution of lateral loads on building
(source: APA 2001)
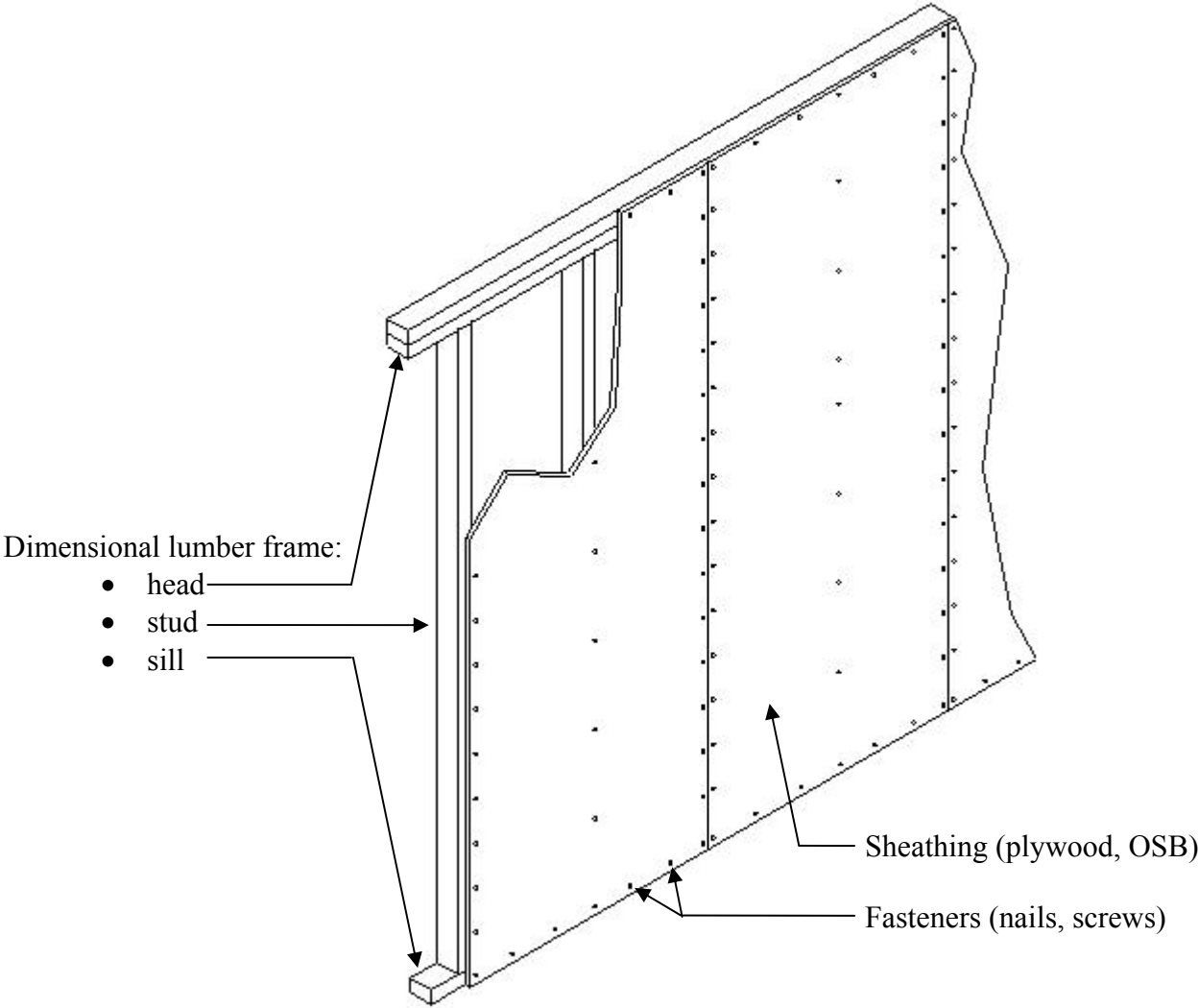
Fig. 1.2. Structural components of a light frame wood shear wall
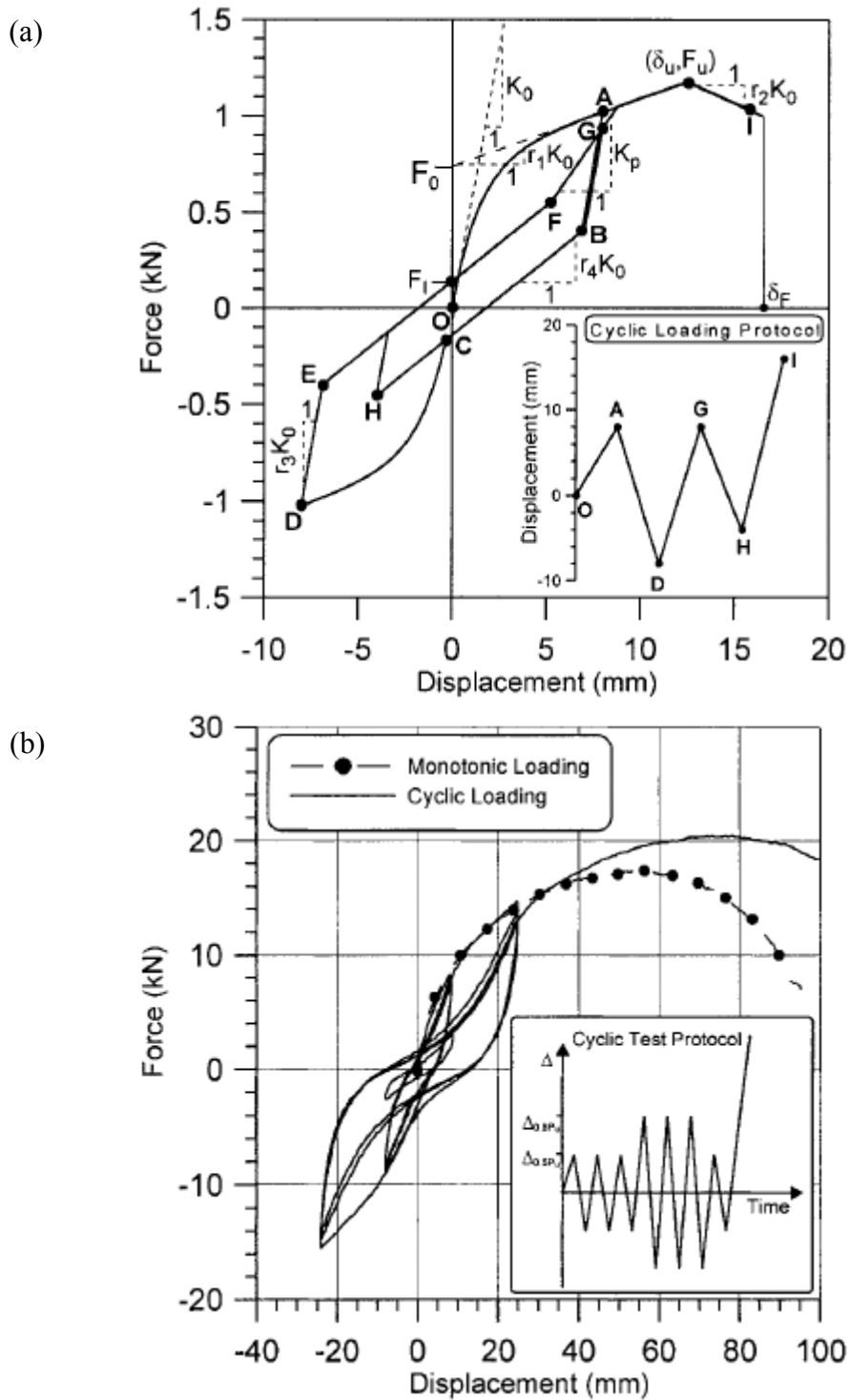
Fig. 1.3. Behavior under cyclic loading: (a) 50 mm long spiral nail, and (b) Light frame wood shear wall assembly 2.44 m square

(source: Folz and Filiatrault 2001)

4

plywood on the outside and gypsum wallboard (GWB) on the inside have shown that racking strength was linearly proportional to the wall length (Patton-Mallory et al. 1985). It was confirmed that wall openings for doors and windows had considerable effect on the racking strength, and a recommendation was given that the net wall length without the openings should be used in the formulas for calculating racking resistance. A conclusion was also made that gypsum wallboard significantly contributes to the shear wall performance. Its resistance was additive to the resistance provided by the plywood sheathing. This finding was recently corroborated on a shaking table test of a two story residential house (Filiatrault et al. 2002). It appears that a structure incorporated with wall finish materials exhibits a substantial increase in lateral stiffness and a considerable reduction in its displacement response (Fig. 1.4).

Masonry Walls

Masonry is one of the oldest building materials known to mankind. It represents a composite made of brick, concrete, or stone units jointed with mortar (Fig. 1.5). The large number of factors that influence in-plane brick masonry behavior and strength such as bond pattern, brick anisotropy, brick size, mortar joint width, brick and mortar material properties, and quality of workmanship make the simulation of masonry structures very difficult (Lourenco and Rots 1997). Masonry walls subjected to in-plane loading respond in a state of plane stress, while the masonry as a material exhibits distinct directional properties because the mortar joints act as planes of weakness. The failure mechanisms that can develop in masonry are pure joint failures, pure brick failures, or combined joint and brick failures (Fig. 1.6). Which of these mechanisms will develop depends on the stress state in regard to the orientation of the material axis defined with the bed and head joints. Experimental and analytical research carried out on masonry walls subjected to horizontal shearing forces superimposed on the vertical forces, have shown the influence of wall geometry on the failure mechanism, the strengthening effect of the compressive vertical forces, the stiffness degradation with increasing lateral displacements and the pinched hysteretic response under cyclic loading (Fig. 1.7) (Gambarotta and Lagomarsino 1997, Lourenco et al. 1998).
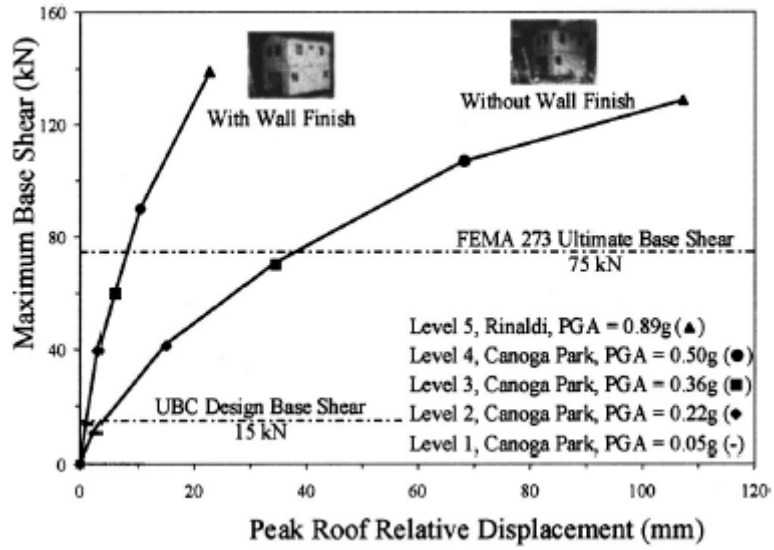
Fig. 1.4. Experimental capacity spectra of test structure with and without wall finish materials (source: Filiatrault et al. 2002)
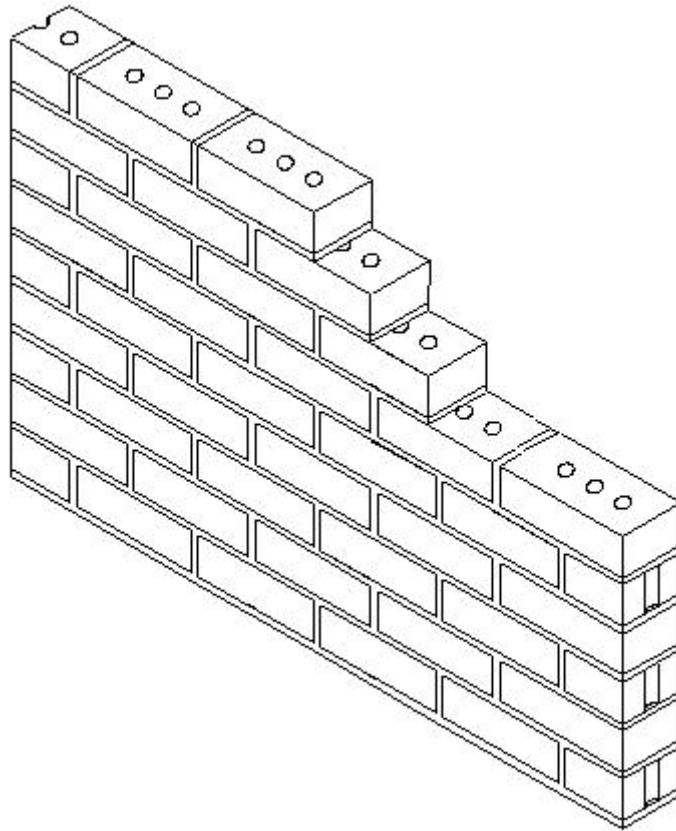
Fig. 1.5. Single wythe masonry wall
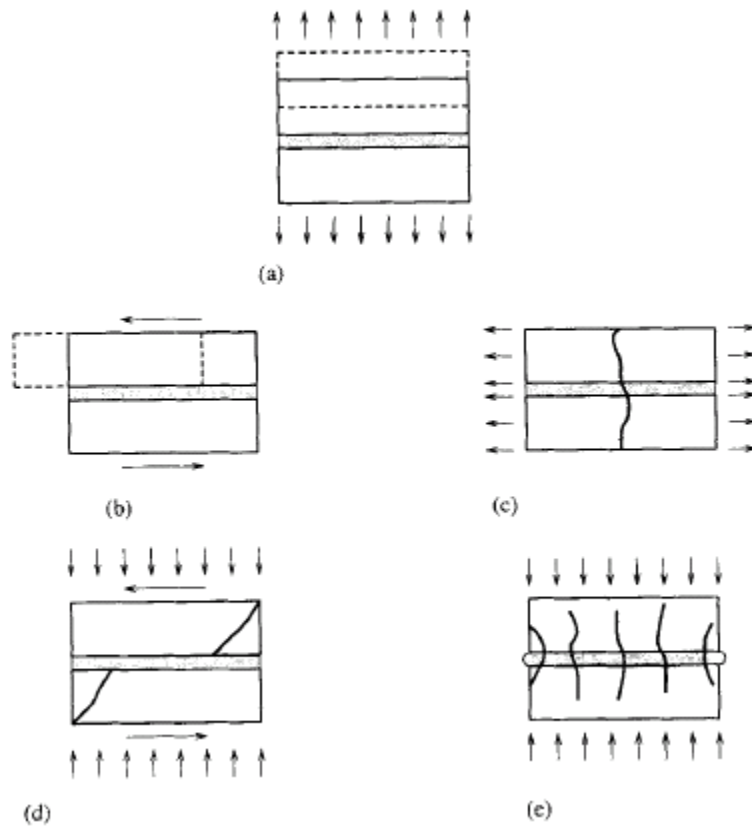
pure joint failures
  (a) joint tension cracking
  (b) joint slip
pure brick failures
  (c) brick direct tension crack
combined joint and brick failures
  (d) brick diagonal tension crack
  (e) masonry crushing

Fig. 1.6. Basic failure mechanisms in masonry subjected to in-plane loads
(source: Lourenco and Rots 1997)
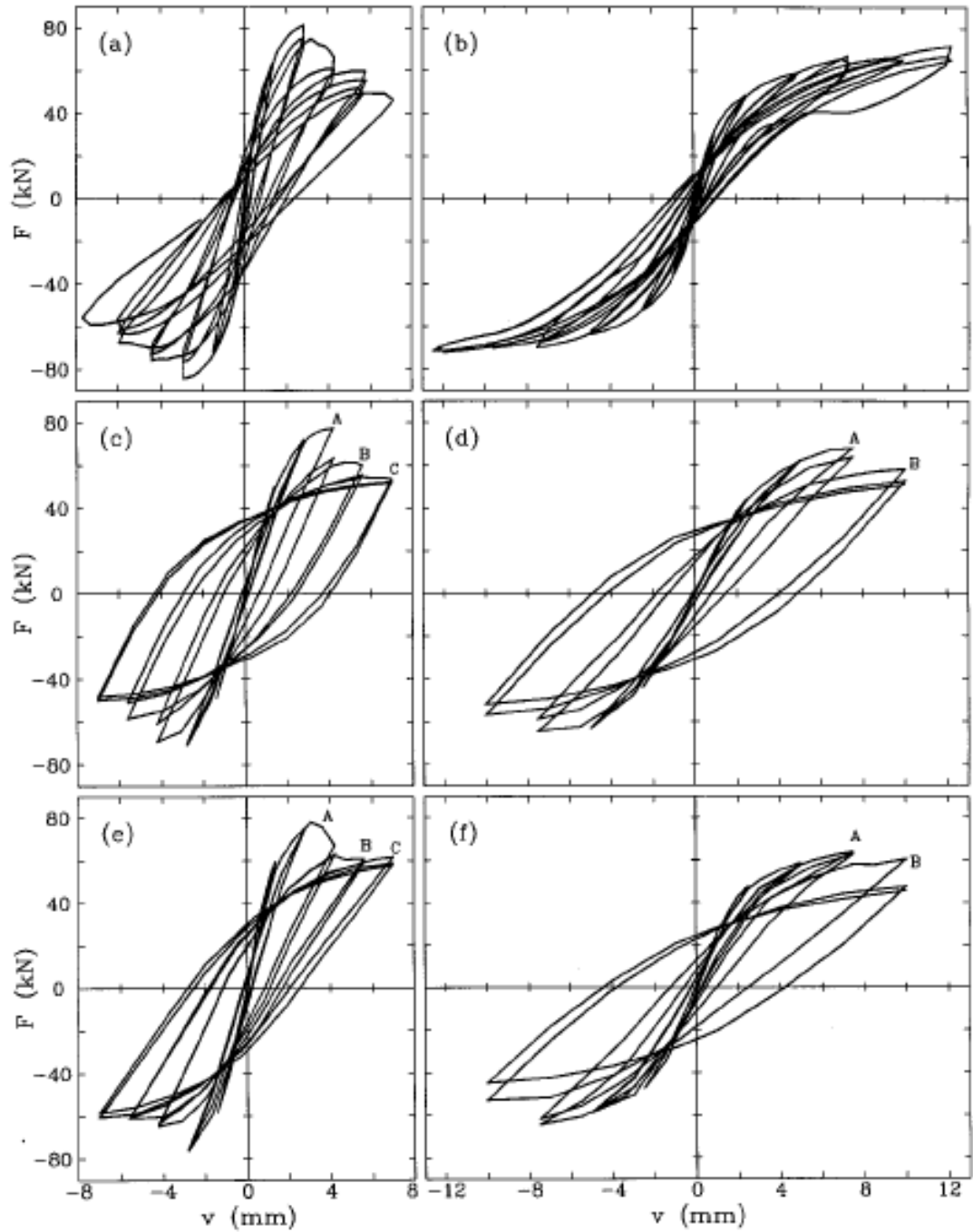
Fig. 1.7. Rectangular masonry panel behavior under in-plane cyclic loading. Experimental response: (a) low wall (1.00 x 1.35 m); (b) high wall (1.00 x 2.00 m). Analytical response by a composite model: (c) low wall; (d) high wall. Analytical response by a continuum model: (e) low wall; (f) high wall

(source: Gambarotta and Lagomarsino 1997 b)

9

Combining the Pieces Together: Brick Veneer-Light Frame Wood Shear Walls

When brick masonry is used as a facade in residential construction, its contribution to the light frame wood shear wall racking resistance is neglected in the calculations. It is considered that such walls are loaded only with their self-weight, hence they are named brick veneer (Fig. 1.8). In case of an earthquake the considerable self-weight of the brick veneer is mobilized in the horizontal direction, and the induced increased inertial forces have to be taken by the lateral load carrying system to whose stiffness and strength the veneer is not considered to contribute. However, the higher initial stiffness of the brick veneer compared to the stiffness of the wood shear wall can attract a portion of the racking load if the ties used to connect the two have the ability to transfer that load (Fig. 1.9). Hence, a similar argument stated above for the contribution of wall finish materials on the wall performance under lateral loads can also be made for the brick veneer. Namely, the exclusion of the brick veneer from experimental or analytical studies could result in an underestimate of the lateral stiffness and an overestimate in the displacements, which ultimately yield excessively conservative approximations.

A study carried out by Johnson and McGinley (2003) on small wall specimens loaded in uniform double shear throughout the wall height verified that standard 22 gauge corrugated metal ties, the type most commonly used in North America to tie the brick veneer to its wood wall backing, have considerable capacity to transfer racking loads from the wood wall to the brick veneer. The shear transfer was greatly enhanced when additional truss type horizontal joint reinforcement was laid into the veneer and fastened to the backing wall (Fig. 1.10). These unidirectional tests confirmed that corrugated metal ties could transfer shear force from the wood wall to the brick veneer and raised the need for further investigation aiming to characterize individual tie load-displacement curves crucial for in-plane analytical modeling of brick-wood wall assemblies.

Allen and Lapish (1986) performed an extensive experimental study on the behavior of brick veneer-light frame wood shear wall assemblies. They reported that stiff strip metal ties nailed to the backing could transfer a substantial racking load component from the timber frame into the brick veneer. The transferred force was sufficient to break the brick mortar bond at the base beam. At higher deflections, the strength of the tested ties was sufficient to rock the brick veneer
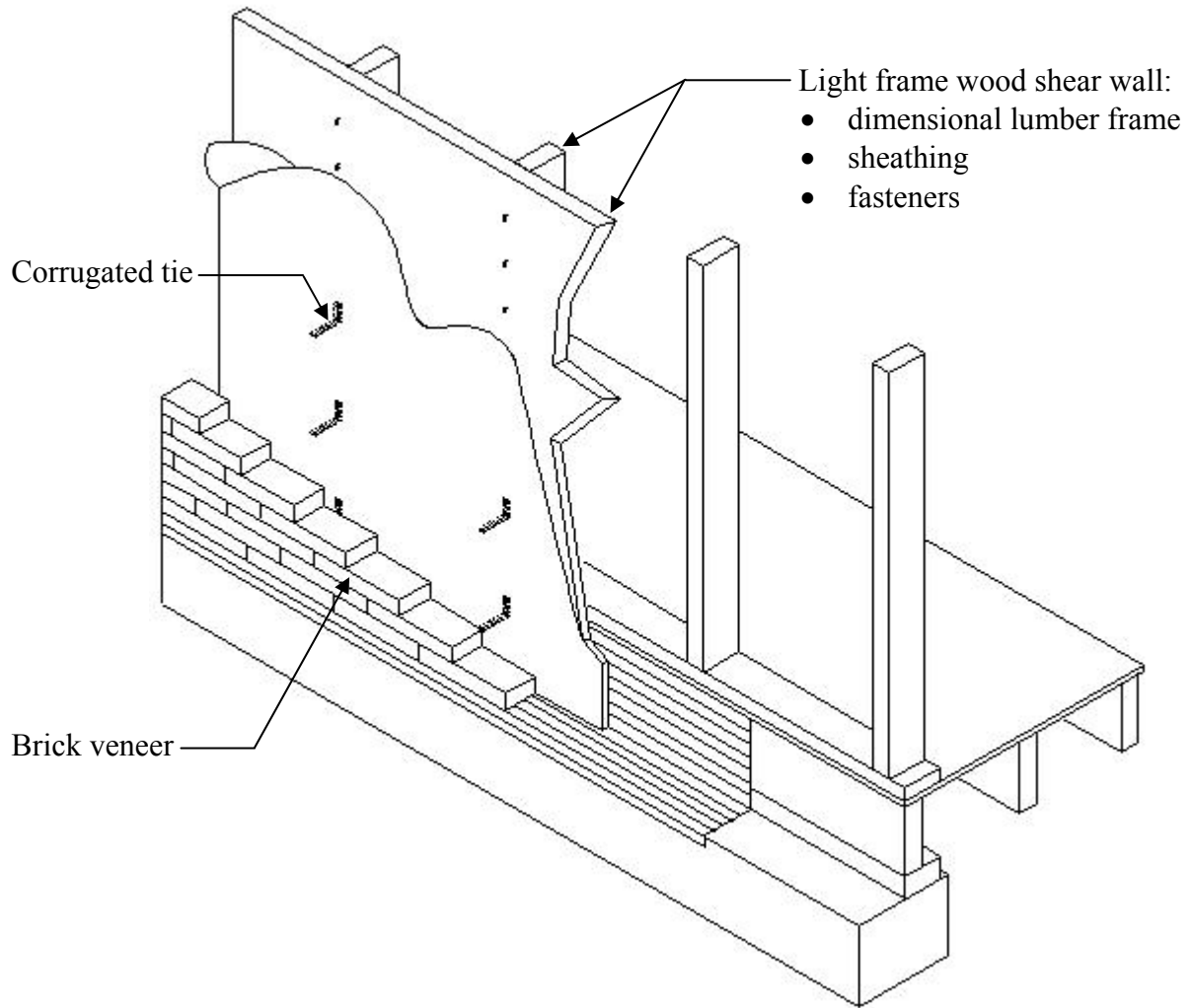
Fig. 1.8. Components of an anchored brick veneer-light frame wood shear wall
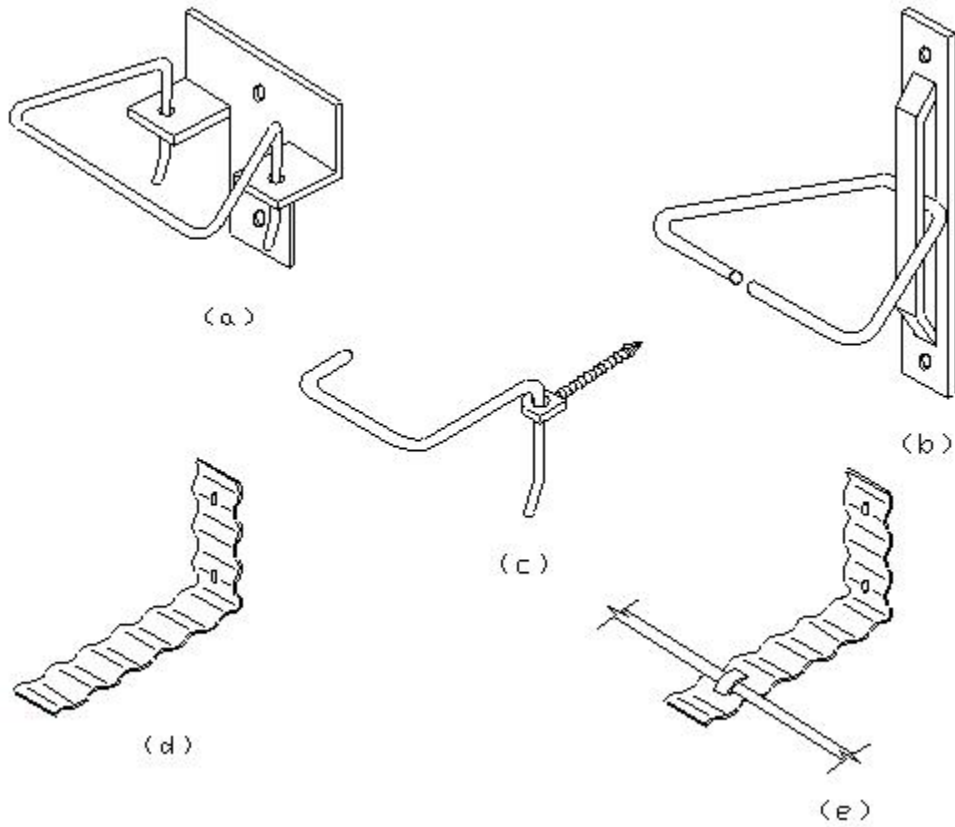
Fig. 1.9. Unit ties: a) trapezoidal wire tie, b) triangular wire tie, c) wire tie, d) corrugated strip metal tie, and e) corrugated strip metal tie with joint reinforcement

(source: BIA Technical Notes 28 2002)

Top View

2" (51 mm)

-Corrugated Ties At 16" OC
(406 mm)

(200 mm) 7⅞"

(800 mm) 2'-7½"

-Truss For Wall Type II and III

(200 mm) 7⅞"

-Corrugated Ties At 16" OC
(406 mm)

(205 mm) 8 1/16"

3'-3⅝"
(1006 mm)

Side View

(b)

Load vs Deflection

Shear Load (lb)

6000 ─ (26.7 kN)
5000
4000
3000
2000
1000
0

0   0.5   1   1.5   2   2.5 (63.5 mm)

Average Deflection (in)

Wall II-3
Wall III-2
Wall I-1
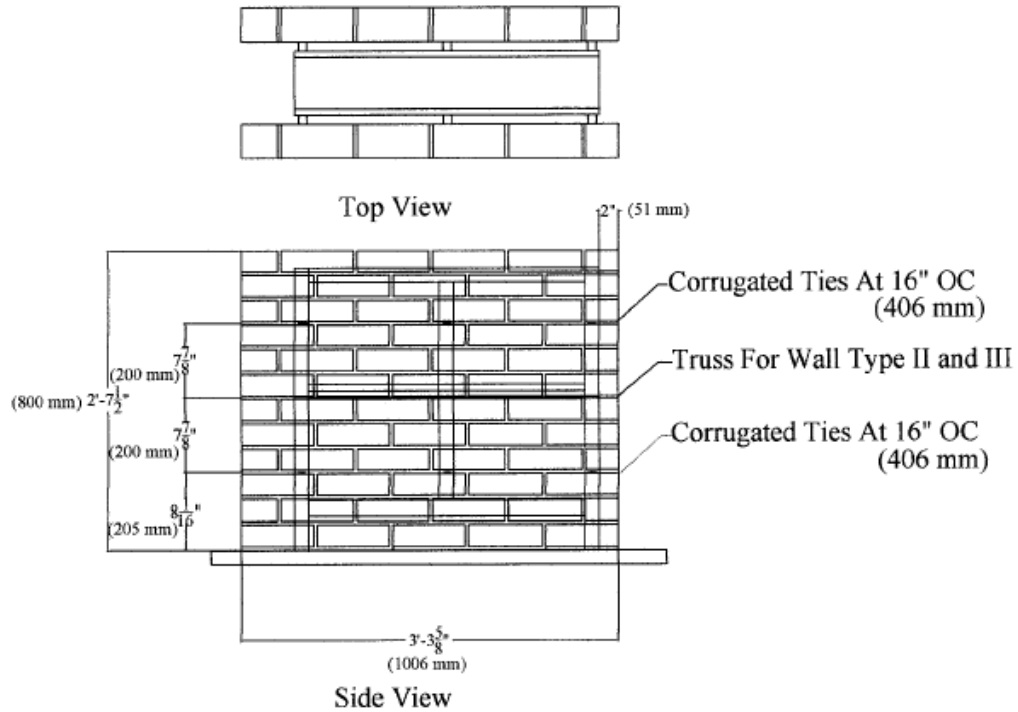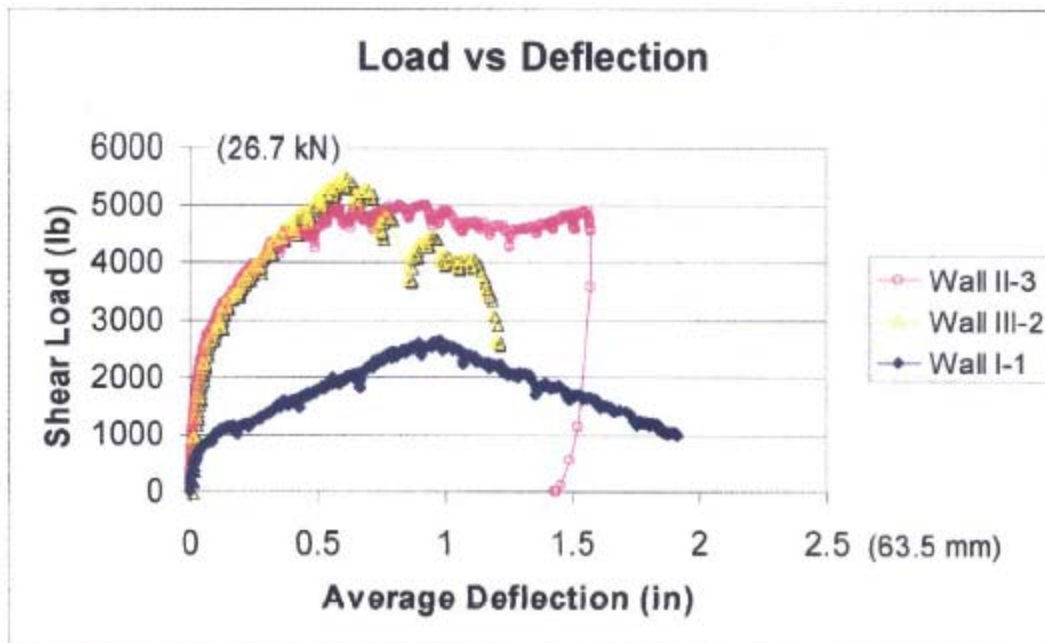
Fig. 1.10. (a) Brick veneer-light frame wood wall specimen for testing in double shear, and (b) Typical load deflection performance of wall specimens with brick veneer attached with corrugated ties (Wall I), and with ties and joint reinforcement (Walls II and III)

(source: Johnson and McGinley 2003)

13

in unison with the racking of the timber frame. It was indicated that the presence of brick veneer markedly increased the racking strength of the brick-wood wall assembly over the strength of a comparable light frame wood shear wall. However, the existence of brick veneer had an adverse effect on the wall ductility (Fig. 1.11). The study revealed the pinched hysteretic response under cycling loading in both cases of walls without and with brick veneer attached (Fig. 1.12).

Shelton and King (1994) examined the veneer-frame interaction on individual veneer elements and complete veneer systems loaded with both in-plane and out-of-plane forces. The light frame timber wall was sheathed with plasterboard on the inner face and no other in-plane bracing was used. Mild steel strip ties were used to tie the brick veneer to the frame backing. They reported similar wall behavior under lateral loads as in the earlier work presented by Allen and Lapish (1986). At an intermediate stage of the in-plane tests the frame and the veneer were each resisting about half the applied load (Fig. 1.13). A recommendation was given for using screws to fix the ties to the backing frame rather than nails. This method had the dual advantage of fewer disturbances during installation and higher pullout resistance during axial loading. Installing the ties on bedding mortar proved to be superior over installing them dry on the bricks. Elemental tie tests showed a potential for doubling and even tripling the axial resistance when both superior installation methods were implemented.

Experimental Research

While the experimental work of Allen and Lapish (1986) and Shelton and King (1994) provides an insight into the interaction between the brick veneer and the light frame wood shear walls, it is representative of the common construction practice found in New Zealand which differs from the one in North America. First there is the distinction in the type of ties used. While rather stiff mild steel strip ties are being used in New Zealand, more flexible corrugated metal ties are commonly used in North America. This difference is considerable because tie stiffness and tie behavior under lateral loads are essential for the lateral force transfer and hence the behavior of the whole brick veneer-light frame wall assembly. Choi and LaFave (2004) researched the behavior of corrugated metal ties in brick-tie-wood subassemblies under axial (out-of-plane) and lateral (in-plane) loading. Both monotonic and cyclic loading cases were considered. In the case of axial

(a)

STEEL ANGLE BOLTED TO TOP PLATE.

100 x 50 PLATE

"U" STRAP

600mm CRES.

100 x 50 STUDS

NOGGINGS 300 mm CRS.

PLYWOOD

BRICK VENEER

WALL TIES.

PLASTER BOARD

100 x 50 PLATE

"U" STRAP

CONCRETE BASE

M16 BOLTS

(b)

30 kN   **Figure Thirteen**

PANEL No 4

PANEL No 2

20

10

(HEAVY DUTY END STUD TO BASE FIXING.)

10   20 (MM)   30   40
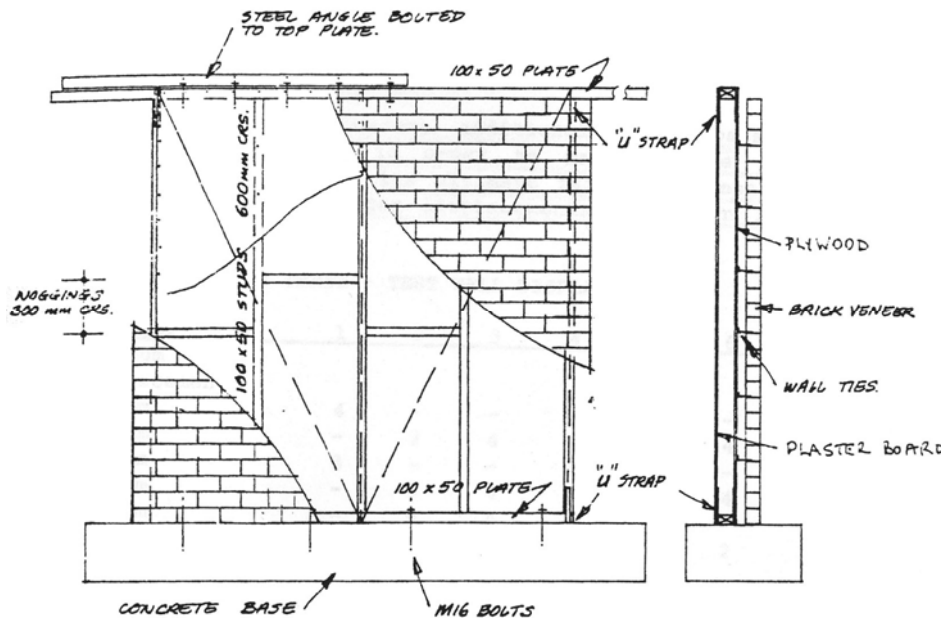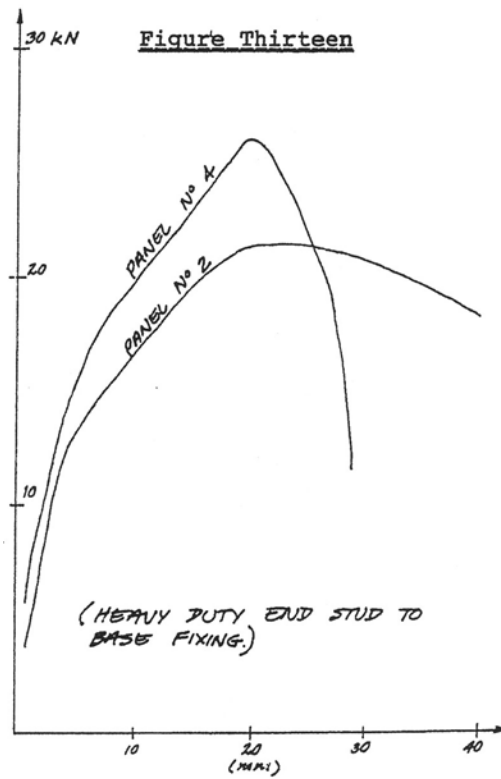
Fig. 1.11. (a) Brick veneer-light frame wood shear wall specimen, 2.44 m square, and (b) Racking force vs. top wall displacement

(source: Allen and Lapish 1986)

15
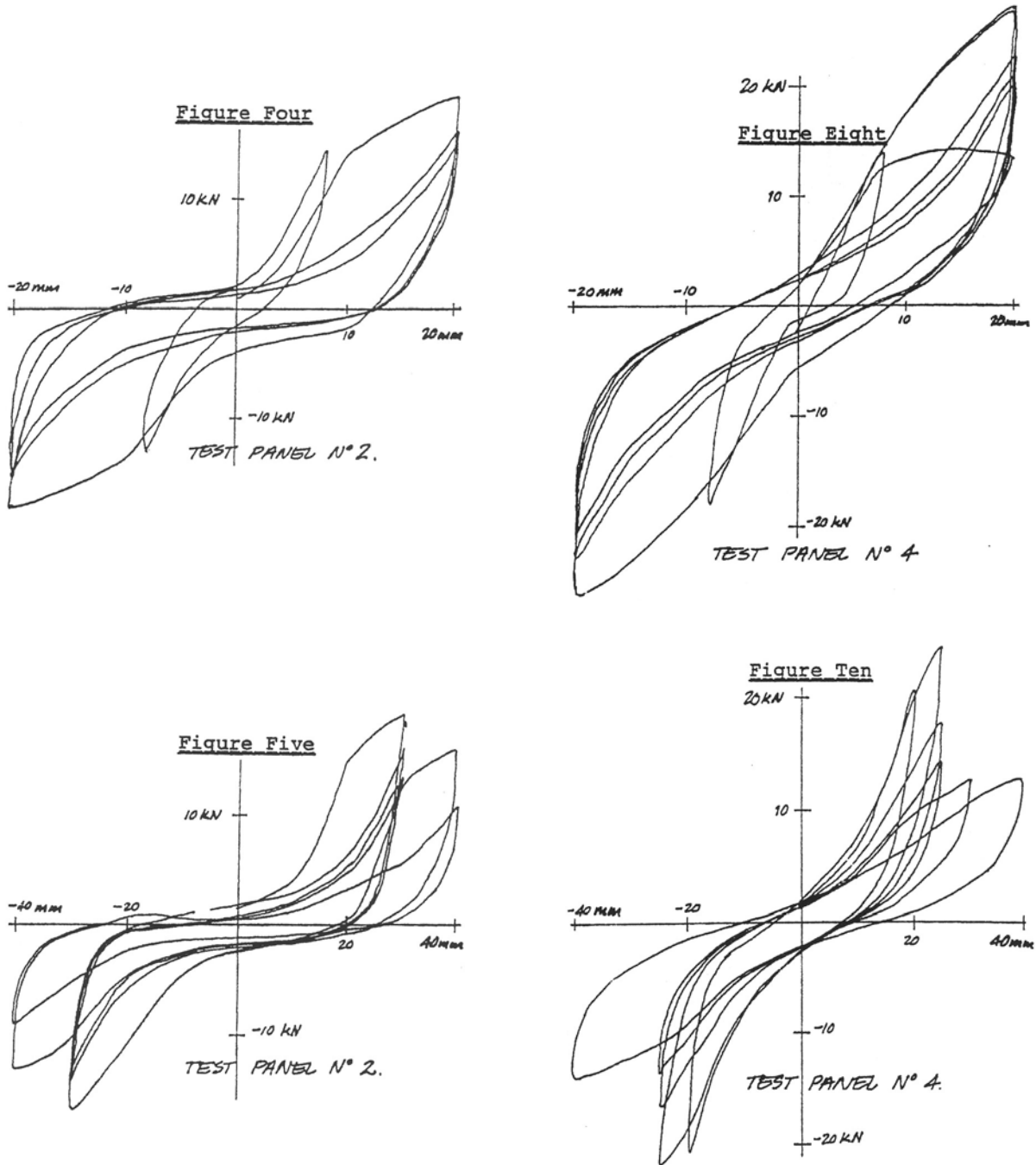
Fig. 1.12. Racking force vs. top wall displacement for 2.44 m square light-frame wood shear walls without (left, panel #2), and with brick veneer (right, panel #4), at smaller (top) and larger (bottom) displacement magnitudes

(source: Allen and Lapish 1986)

16

(a)

(b)

(c)
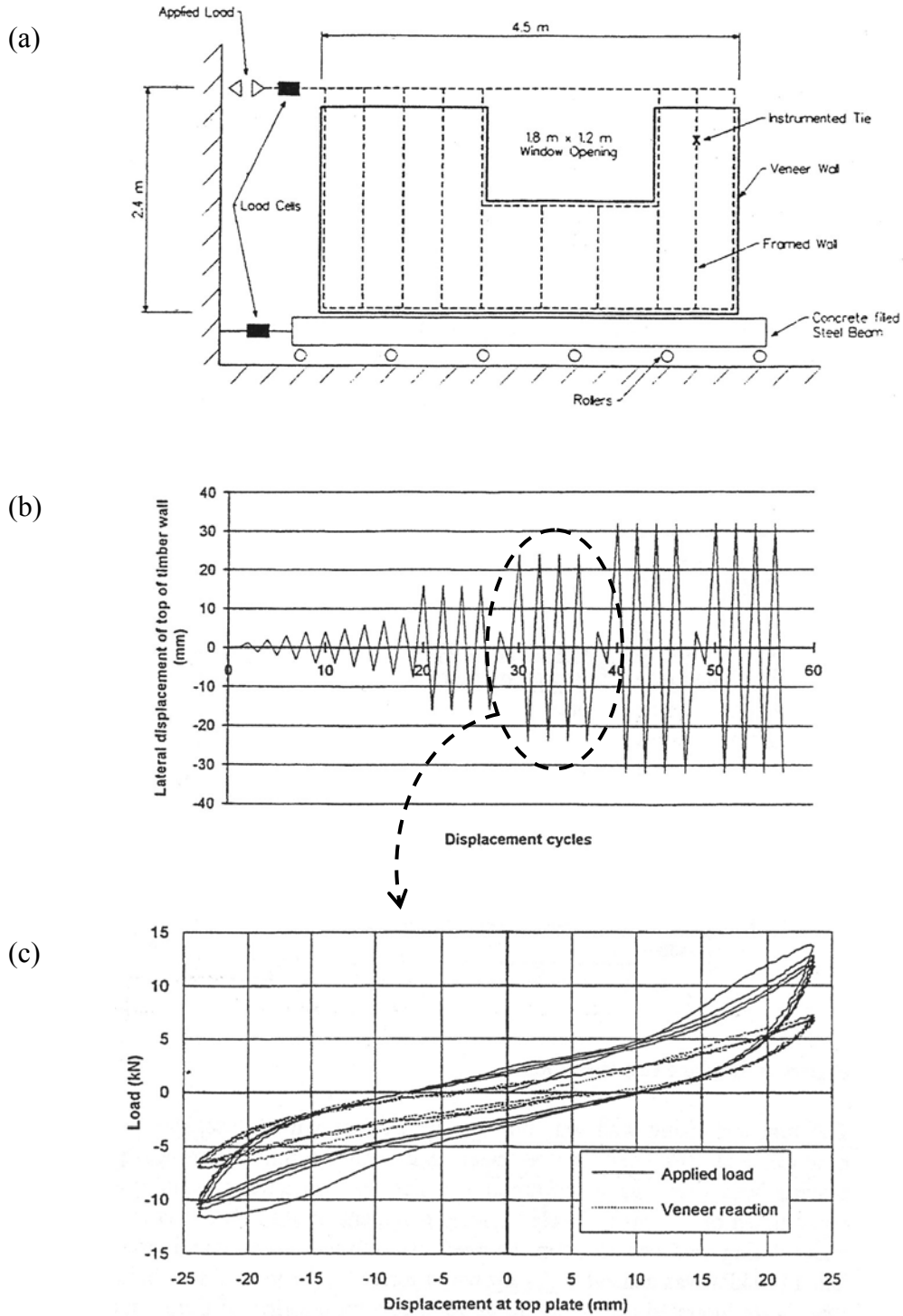
Fig. 1.13. (a) Brick veneer-light frame wood shear wall specimen, (b) Displacement history, and (c) Racking force vs. top wall displacement hystereses at intermediate loading stages

(source: Shelton and King 1994)

17

loading the primary failure modes were identified as being ones of nail pullout from the wood in nail-connected tension tests, tie pullout from the mortar joint in screw connected tension tests, and buckling of the tie in both nailed and screwed compression tests. The load displacement relation of the subassembly under cyclic axial loading was characterized by quite stable nonsymmetrical pinched hystereses that show both stiffness degradation and strength deterioration (Fig. 1.14.b). Nail pullout from the wood was identified as the primary failure mode in the case of monotonic lateral loading, while tie fracture was recognized as a predominant failure mode in the case of cyclic lateral loading. Idealized load displacement relations for monotonic lateral (shear) loading and envelope curves for cyclic lateral loading were published demonstrating the tie thickness, fastener type and bent eccentricity effects (Fig. 1.14.c). As an extension to their work, similar brick-tie-wood subassemblies were tested under cyclic lateral loading in order to identify additional influencing parameters, verify observed failure modes and determine lateral cyclic load-displacement curves necessary for in-plane analytical modeling of a whole wall assembly. The results of this experimental investigation are presented in Chapter 2.

It appears that the published experiments conducted in New Zealand didn't address the effect of flashing on in-plane wall behavior. Continuous flashing is installed in the wall base primarily to drain the moisture out of the wall cavity and to prevent capillary rising of water into the wall system. The flashing acts as a bond breaker between the brick veneer and its concrete foundation, allowing some slippage to occur and hence controls their susceptibility to cracking due to moisture and thermal movements. However, breaking the bond has an adverse effect on the shear strength of the veneer wall (McGinley and Borchelt 1990). Under these conditions frictional forces arising from vertical compressive loads above the plane of the flashing provide the shear resistance at the joint. Several research studies carried out by Thrischuk and Suter (1996), Rajakaruna (1997), Zhuge and Mills (1998), and Griffith and Page (1998) investigated the shear behavior of joints with flashing materials in common use in their native countries. The work by Griffith and Page conducted on flashing materials in concrete-mortar-concrete joints stands out for addressing both unidirectional and cyclic quasi-static loading. Shear tests on numerous concrete brick triplets revealed very stable hystereses that closely follow an elastic-perfectly plastic shear load-displacement skeleton curve. Apparently there was no degradation of the joint even after fifty cycles of shear displacement. An increase in the precompression level
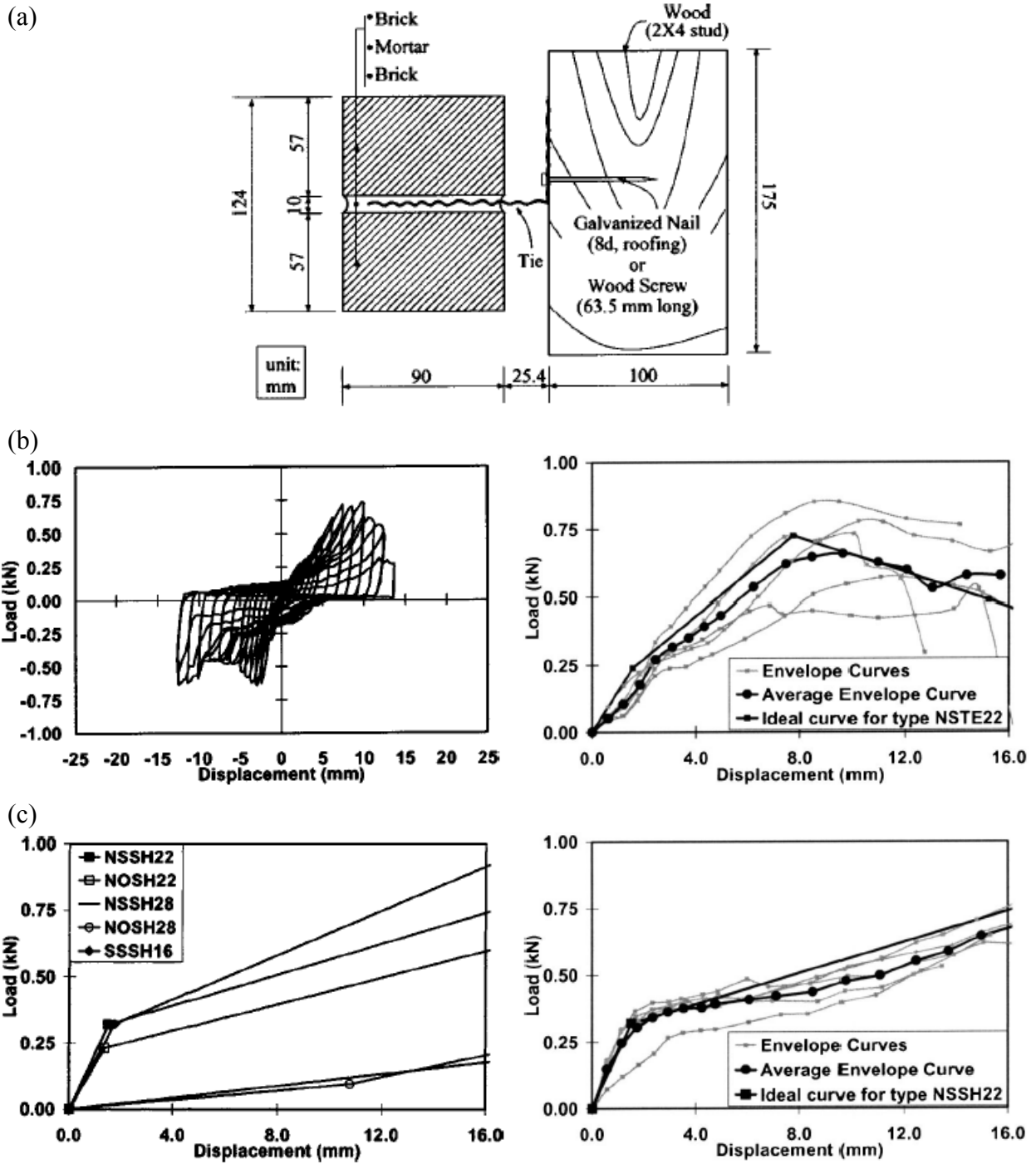
Fig. 1.14. (a) Brick-tie-wood specimen, (b) Load vs. displacement history, and Envelope curves for specimens with 22 ga corrugated ties under cyclic axial loading, (c) Idealized load displacement relations under monotonic lateral loading, and Envelope curves for specimens with 22 ga corrugated ties under cyclic lateral loading

(source: Choi and LaFave 2004)

19

shifted the skeleton curve towards higher shear resistance values, and the subsequent hystereses encompassed a larger area (Fig. 1.15). Similar experiments on brick-mortar-concrete joints with flashing materials commonly used in North America are needed to investigate whether the difference in the materials significantly affects the shear load-displacement behavior. Such curves can then be used to realistically build the analytical model of the whole wall assembly and study the effect the flashing has on wall strength and deformation.

Finally, experiments on full-scale brick veneer-light frame wood shear wall assemblies loaded with in-plane forces can help understand and improve the behavior of such shear walls under dynamic loading. The results emerging from such experiments are invaluable for calibrating analytical models, which is a necessary prerequisite for meaningful parametric and reliability studies needed for improvement of the design approaches and codes.

Analytical Research

Light Frame Wood Shear Walls

Modeling of light frame wood shear walls has evolved over the last three decades from simple racking equations for displacement and ultimate capacity to complex nonlinear dynamic models. There are two distinct modeling approaches in current practice. The first approach is based on simpler, reduced degrees of freedom models. According to these models the nonlinear load-deformation behavior of the sheathing-to-framing connectors fully governs the nonlinear global wall response. The sheathing is assumed to develop only elastic in-plane shear forces, while the framing members are usually assumed to be rigid in bending. The earlier models that follow this modeling approach were originally developed for static analysis, but they could be updated for cyclic and dynamic analysis as well (Easley et al. 1982, McCutcheon 1985, Gupta and Kuo 1987). The latest models are formulated for all analysis options (Filiatrault 1990, Dinehart and Shenton 2000, Folz and Filiatrault 2001). The models that fall into this category enable low cost analysis without compromising much on the accuracy. In general, they provide satisfactory agreement with the load-displacement response obtained from experimental investigations. However, due to their simplicity, they are not able to capture the detailed interaction and load sharing between the components of the shear wall under the imposed lateral loading.

(a)

(b)
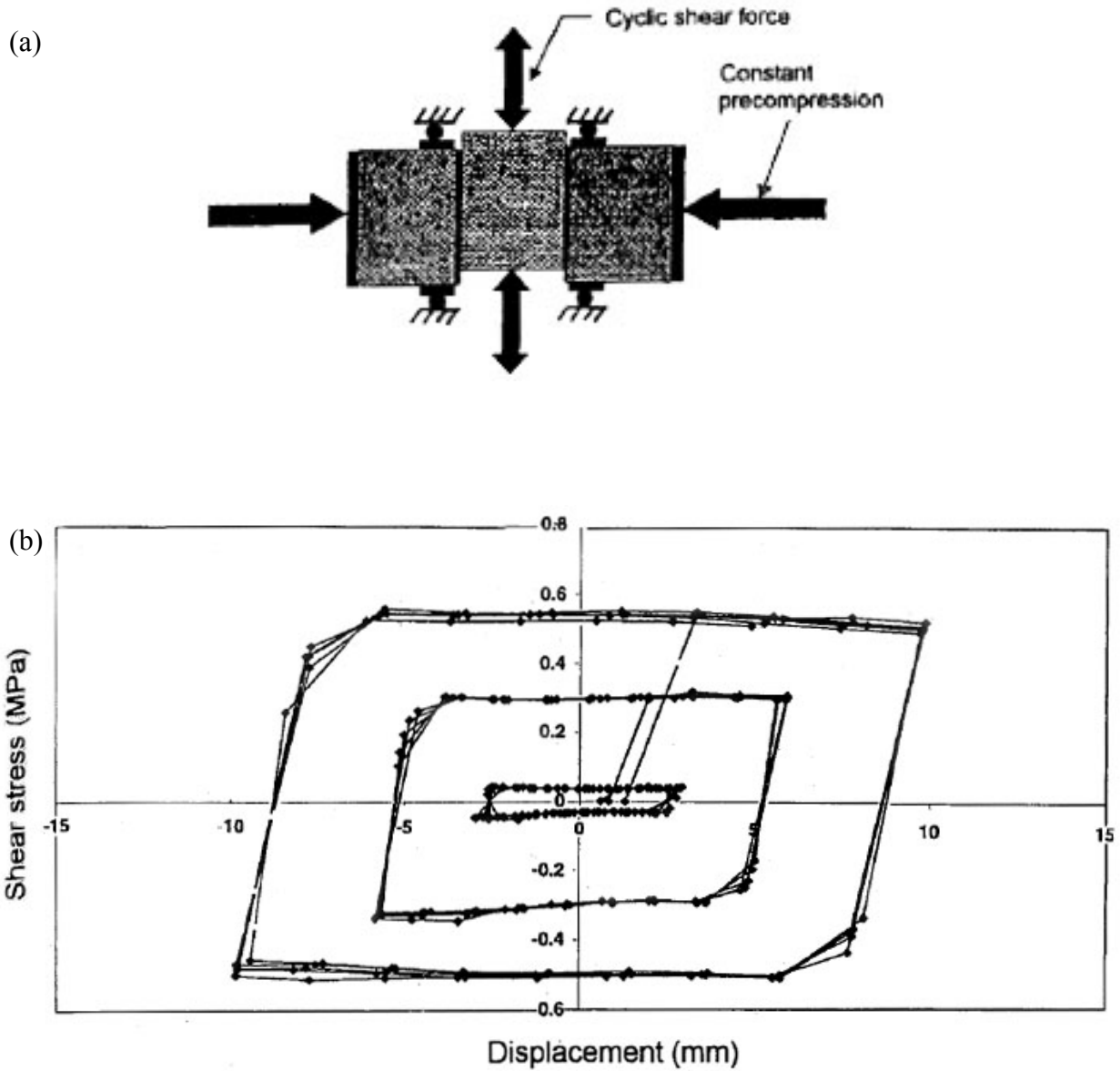
Fig. 1.15.(a) Schematic diagram of test set up for cyclic shear tests, (b) Typical cyclic shear test on a joint containing a damp-proof course membrane[1]

(source: Griffith and Page 1998)

On the other end of the light frame wood shear wall modeling spectrum lie the sophisticated finite element models (Itani and Cheung 1984, Gutkowski and Castillo 1988, Falk and Itani 1989, Dolan and Foschi 1991, White and Dolan 1995, Tarabia and Itani, 1997). In these models the framing members are approximated with linear elastic beam elements usually pinned at their ends. The sheathing is typically represented by linear elastic, orthotropic plane stress elements, while some researchers have also tried the corresponding plate bending elements. The sheathing-to-framing connectors are modeled with a pair of independent orthogonal springs that follow nonlinear load-deformation relations. These relations evolved from relatively simple exponential, power or logarithmic curves suitable for quasi-static analysis to complete hysteretic relations that enable cyclic and dynamic analysis. Gap elements have been introduced along the interface between adjacent sheathing panels to account for eventual bearing. Also, flexible supports with some degree of fixity have been tried instead of the pinned stud connections. These sophisticated models are able to capture more fully the intercomponent response within the wall. However, due to their increased complexity, these models require much greater computational effort. Interestingly, the overall global load-displacement estimates from these models show essentially the same level of correlation with experimental data as the simpler models discussed previously. Hence, when both approaches provide the same level of accuracy, the choice between the two depends mainly on the scale of the particular problem and the type of software available.

Masonry Walls

Modeling of in-plane loaded masonry walls has come a long way from the early approximations with plane stress finite elements having linear elastic homogenous isotropic properties. A complete sophisticated model for masonry requires the elastic properties, a yield criterion, inelastic stress-strain relations and a failure criterion. Several contemporary models that satisfy these requirements can be grouped in two categories according to the way they approach the material modeling. In the first category are all the models that treat the masonry as a continuum. Some of the models that fall into this category are: Page et al. (1985), Andreaus (1996), Papa and Nappi (1997), Gambarotta and Lagomarsino (1997 b), Zhuge et al. (1998), Lourenco et al. (1998), Asteris and Tzamtzis (2003). These macro models approximate masonry as a one-phase material with averaged homogeneous isotropic or anisotropic properties and constitutive

relations that are different from the ones of the component materials. The accompanying failure criteria under biaxial stress are defined with a three dimensional failure surface determined either with the two principal stresses and their orientation to the bed joints (σ_1, σ_2, θ), or with the two normal stresses: normal and parallel to bed joints, and shear stress on bed joint (σ_n, σ_p, τ). A single finite element in these continuum models usually encompasses several brick courses and several bed and head joints reducing in that way the overall number of degrees of freedom. These model formulations can either be incorporated into a general purpose finite element program, or the built-in model for brittle material such as concrete can be tailored with appropriate masonry parameters. The models that fall into this category enable relatively low cost analysis and are suitable for studying global wall behavior.

The second category consists of all the models that incorporate discontinuous masonry formulations. Typical models that follow this approach are: Page (1978), Ali et al. (1986), Lotfi and Shing (1994), Ghosh et al. (1994), Gambarotta and Lagomarsino (1997 a), Lourenco and Rots (1997), Tzamtzis and Asteris (2003). These micro models approximate masonry as a two-phase material. Each material is modeled separately with its own constitutive relations and failure criteria. Two distinct approaches adhere to the discontinuous masonry formulation. According to the first approach the (brick) units are modeled as a continuum, while nondimensional interface elements are used to model the mortar joints. In the second approach the (brick) units and the mortar are modeled as continuums, while the brick-mortar interface is modeled with nondimenional interface elements. While the use of discontinuous masonry models leads to more accurate results, the level of refinement requires large computational effort. Hence at present these models are more appropriate for studying local masonry behavior.

CHAPTER II - EXPERIMENTAL

Shear Behavior of Corrugated Tie Connections in Anchored Brick Veneer - Wood Frame Wall Systems

Abstract

An experimental study was carried out to investigate the shear behavior of corrugated metal ties anchoring brick veneer walls to light wood frame backing. Connection subassemblies were tested under monotonic and cyclic shear loading, and statistical analyses were conducted to identify and quantify the parameters influencing this behavior. Force-displacement curves obtained under monotonic loading can be considered an upper bound for the hysteresis loop envelopes. Fastener slippage during cyclic loading enabled by the localized damage of the surrounding wood fibers diminished the energy absorption capacity of the connection and caused pronounced pinching in the hystereses. Considering corrugated ties with minimum thickness permitted by the MSJC Code, tie design and bent eccentricity were found to be the most important factors, while tie location in the bed joint, fastener type and fastener quantity were influential to a lesser degree.

Introduction

Brick masonry is frequently used as a façade in residential construction in North America primarily due to its aesthetic appearance. Typically such brick veneers are anchored over an air cavity to light frame wood shear walls, with the wood shear wall being considered as the primary lateral load-resisting system and the brick considered to be nonstructural. The shear walls consist of a dimensional lumber frame sheathed with plywood or oriented strand board to create a stiff wall assembly. The synergy created with the integral wall system manifests in improved moisture resistance, fire resistance, resistance to heat transfer, and favorable acoustics (BIA 2002). The MSJC Code (MSJC 2008) does not recognize any synergy regarding the in-plane

24

load resistance, assuming the wood frame wall to bear all racking loads although BIA Tech Notes (2002) acknowledge that brick veneers do carry a proportionate share of the lateral load. Since both wall faces have proven shear capability on their own it depends on the properties of the anchoring system whether any synergy is being achieved in this regard. If the anchoring system possesses sufficient stiffness and strength in the in-plane wall direction then considerable load transfer between the two wall faces can be achieved. In such a case it is anticipated that the larger shear stiffness of the brick veneer will attract lower intensity racking loads, while additional higher intensity loads will be carried jointly by the integral system or by the more ductile wood frame wall if the brittle brick veneer suffers serious damage.

Several researchers have conducted experimental investigations in order to examine the load distribution. In a comprehensive study of brick veneer-light frame wood shear wall assemblies, Allen and Lapish (1986) reported that stiff strip metal ties nailed to the backing could transfer a substantial racking load component from the wood frame into the brick veneer. The transferred force was sufficient to break the brick mortar bond at the base beam. At higher deflections, the strength of the tested ties was sufficient to rock the brick veneer in unison with the racking of the timber frame. The presence of brick veneer markedly increased the racking strength of the brick-wood wall assembly over the strength of a comparable light frame wood shear wall. However, the existence of brick veneer had an adverse effect on the wall ductility.

A significant finding in a similar investigation carried out on complete veneer wall systems utilizing mild steel strip ties was that at an intermediate loading stage the frame and the veneer were each resisting about half the applied in-plane load (Shelton and King 1994). The study favored screws over nails as tie fasteners to the wood backup due to the dual advantage of fewer disturbances during installation and higher pullout resistance. Installing the ties on bedding mortar proved to be superior over installing them dry on the bricks.

A study performed on small wall specimens loaded in uniform double shear throughout the wall height verified that properly spaced standard 22 gauge corrugated metal ties, the type most commonly used in North America to tie the brick veneer to its wood wall backing, have considerable capacity to transfer racking loads from the wood wall to the brick veneer. The shear

transfer was greatly enhanced when additional truss type horizontal joint reinforcement was laid into the veneer and fastened to the backing wall (Johnson and McGinley 2003).

A comprehensive behavioral study conducted by Choi and LaFave (2004) on brick veneer–wood frame subassemblies anchored with corrugated metal ties addressed among other things in-plane wall loading. Idealized force-displacement relations for monotonic shear loading and envelope curves for cyclic shear loading were published demonstrating the tie thickness, fastener type and bent eccentricity effects. Nail pullout from the wood was identified as the primary failure mode in the case of monotonic loading, while tie fracture was recognized as a predominant failure mode in the case of cyclic loading.

The experimental study reported herein presents an extension of Choi and LaFave (2004), with this study focusing exclusively on in-plane wall loads induced from wind or earthquake that introduce shear in the tied connection. The significance of multiple effects on the behavior of corrugated metal tie connections was statistically investigated, and characteristic load-displacement curves from monotonic loading along with typical hysteretic curves from cyclic loading necessary for in-plane analytical wall modeling are published.

Materials and Methods

Test Specimens

In order to grasp the localized behavior of the entire connection, rather than the behavior of the tie itself this study utilized brick-tie-wood subassembly specimens similar to the ones used in the work of Choi and LaFave (2004). A typical specimen mounted onto the test apparatus is shown in Fig. 2.1. The wood portion of the connection consisted of a 2×4 stud piece of Standard Grade Spruce-Pine-Fir. A 11.1 mm thick Southern pine OSB sheathing strip was nailed to the stud piece. A 22 gauge corrugated sheet metal tie was fastened to the wood portion and bent before the bricks were attached. The brick couplet consisted of two standard size ASTM C216 bricks (100×67×200 mm) with three holes. A professional mason used type N masonry cement mortar to assemble the connection. Compression tests of three 180 days old mortar cubes kept in a wet room showed an average strength of 15.1 MPa.
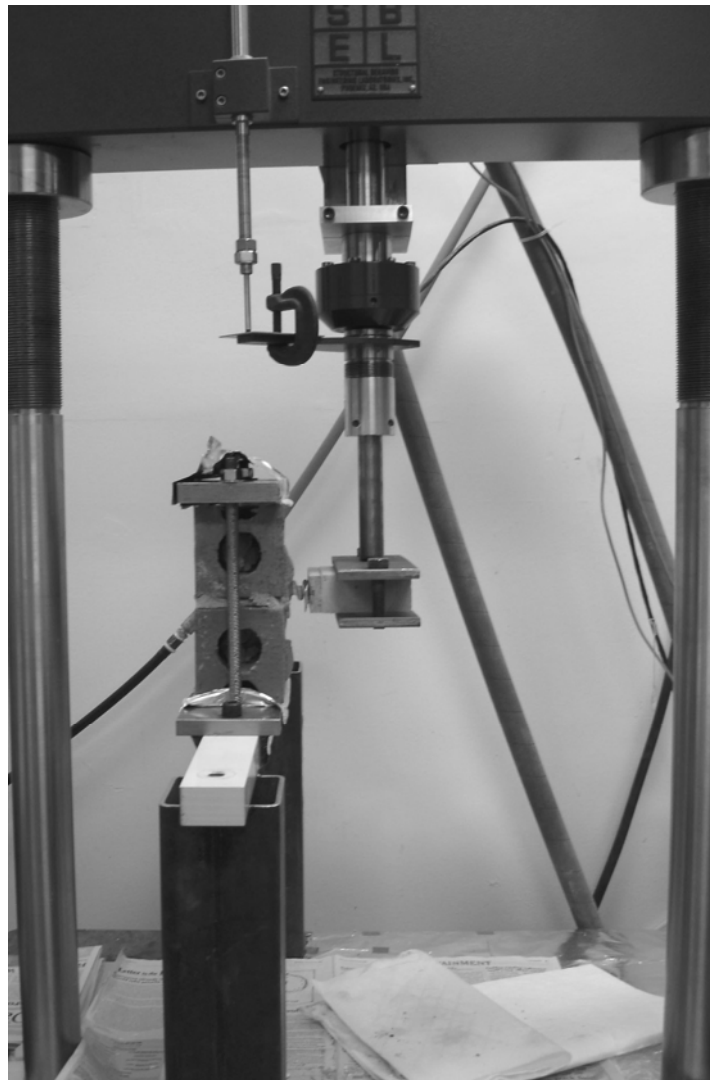
Fig. 2.1. Test setup

Test Program

The study was based on a test program (Table 2.1) designed to evaluate the effect of multiple factors on the shear behavior of corrugated ties in brick veneer wall systems. Six specimens were made for each distinctive set. Apparatus malfunction caused destruction of two specimens leaving the sets marked B and L with five specimens each, hence reducing the total specimen count to 76.

The study considered the use of two corrugated tie designs, labeled narrow and wide, as shown in Fig. 2.2. Both ties were 22 gauge (0.79 mm thick), complying with the minimum thickness permitted by the MSJC Code (MSJC 2008). The ties came predrilled with regular hole diameters of 3.8 mm for the narrow ties, and 5.6 mm for the wide ties. In order to investigate the hole size effect, some of the wide ties were drilled to a smaller 3.8 mm hole that matched the one present in the narrow ties.

The effect of two fastener types, 8d 63.5 mm long common nails, and 6×41 mm screws was investigated. In order to evaluate the fastener quantity effect, one set of specimens was assembled with two nails instead of a single one commonly used in practice.

Three bent eccentricities were considered. The minimum eccentricity, 4 mm for the narrow ties and 5 mm for the wide ties was obtained by bending the ties as close as possible to the fastener head. MSJC Code (MSJC 2008) maximum permitted bent eccentricity of 12.7 mm as well as excessive eccentricity of 25.4 mm were also investigated.

The effect of tie location in bed joint was examined by comparing the behavior of subassemblies with ties placed centered in the joint and subassemblies with ties placed flush on the underlying brick and then topped with mortar. The latter practice isn't compliant with the MSJC Code (MSJC, 2008), yet it is often present in construction.

Two tie positions with respect to the head joint were considered: offset, and no offset. The set of specimens with offset had a brick couplet made of two whole bricks. Placing the tie in the middle produced a half brick length offset from the head joint. All other specimens had a brick couplet

Table 2.1. Test program overview

Group	Count	Tie Type	Hole, Diam. (mm)	Fastener	Bent Ecc.	Tie Loc. Bed Joint	Tie Loc. Head Joint	Load Type
Ctrl	6	narrow	regular, 3.8	nail	min	centered	no offset	cyclic
A	6	narrow	regular, 3.8	nail	min	centered	no offset	monot.
B	5	narrow	regular, 3.8	screw	min	centered	no offset	cyclic
C	6	narrow	regular, 3.8	nail	max	centered	no offset	cyclic
D	6	narrow	regular, 3.8	nail	excess.	centered	no offset	cyclic
E	6	wide	regular, 5.6	nail	min	centered	no offset	cyclic
F	6	wide	regular, 5.6	nail	max	centered	no offset	cyclic
G	6	wide	regular, 5.6	nail	excess.	centered	no offset	cyclic
H	6	narrow	regular, 3.8	nail	min	flush	no offset	cyclic
I	6	wide	regular, 5.6	nail	min	flush	no offset	cyclic
J	6	narrow	regular, 3.8	nail	min	centered	offset	cyclic
K	6	narrow	regular, 3.8	2 nails	min	centered	no offset	cyclic
L	5	wide	smaller, 3.8	nail	min	centered	no offset	cyclic

built with one full brick and two half brick cuttings with a head joint connecting them, typical of running bond. Placing the tie in the middle resulted in a lack of tie offset with respect to the head joint.

Test Setup and Testing Procedure

All testing was carried out at least 150 days after construction. Part of the test setup is shown in Fig. 2.1. The testing apparatus consisted of a two-part custom specimen attachment rig, a universal testing frame, and a data acquisition system. Fast setting gypsum was used on both sides of the brick couplet contacting the attachment rig in order to level the surface and avoid brick couplet split caused by application of uneven loads to the bed joint. Controlled down and up movement of the testing machine's movable arm produced the desired shear on the tie (in-plane wall direction). Besides the inherent stiffness of the attachment rig itself, no attempt was made to constrain the axial movement of the tie (out-of-plane wall direction), which was deemed as more realistic representation of field conditions. This axial movement became apparent with larger in-plane displacements.

The tests were performed under either monotonic or cyclic load conditions. The loading rate for the monotonic tests was 1.27 mm/min, while cyclic tests were performed at a rate of 1 cycle/min. The cyclic tests, illustrated in Fig. 2.3, started with cycles having amplitudes of 0.64, 1.27 and 1.91 mm followed by three cycles with amplitude of 2.54 mm. They continued with four series composed of a leading 1.27 mm amplitude cycle followed by three repetitions of cycles at amplitudes being multiples of 2.54 mm, up to 12.7 mm. The second to last cycle had an amplitude of 25.4 mm, which was considered terminal for the connection.

Displacement control was used in all tests. The sampling rate was four readings per second. Measured force-displacement relations were used as a base to extract envelopes and compute initial stiffness and absorbed energy for all cyclic tests. An envelope curve for cyclic loading was constructed by extracting peak force values in each leading cycle at each displacement level in both loading directions. Initial stiffness was obtained as the maximum of the slope of a least square straight line fitted over any 50% of the measured force-displacement curve in the loading part of the first 1.27 mm (0.05 in) cycle. Values of r^2 for the linear regression were typically

30
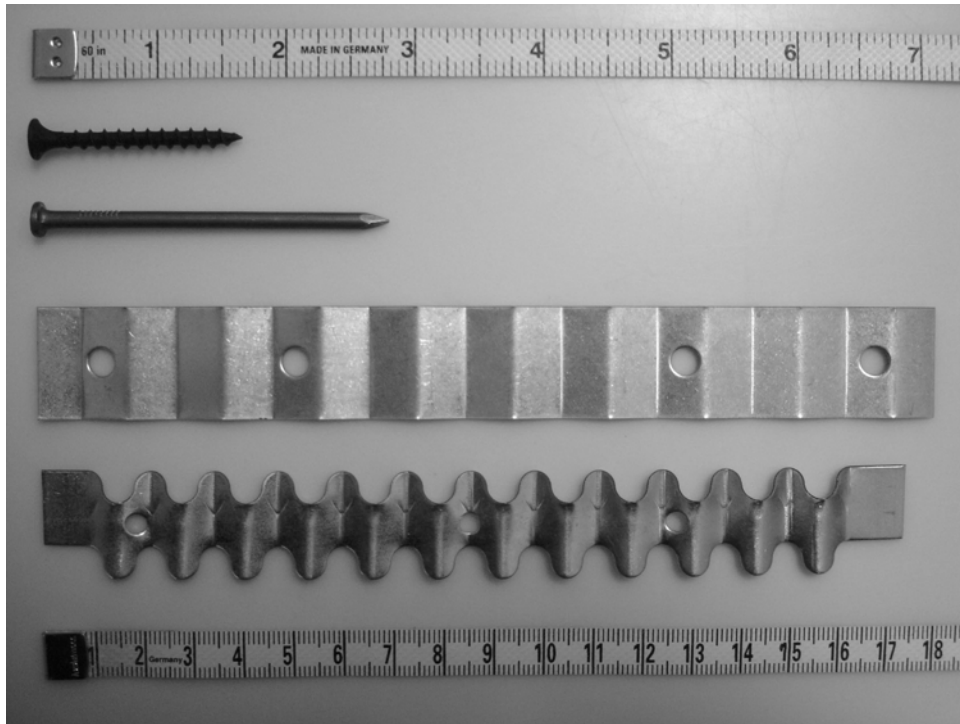
Fig. 2.2. Considered fastener types (screw, nail) and tie designs (wide, narrow)
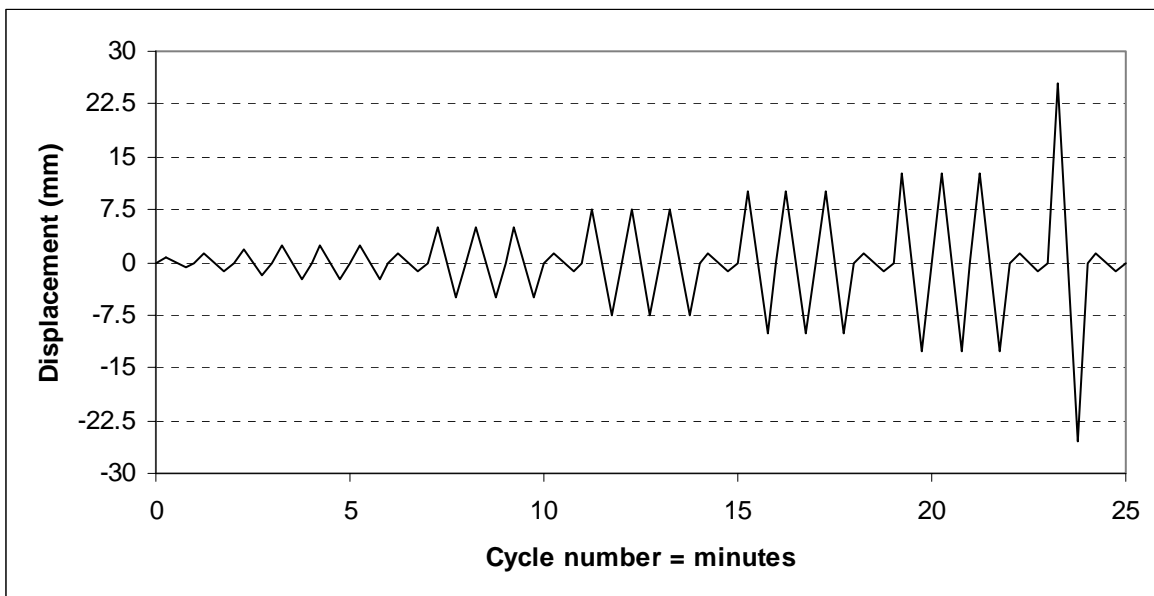
Fig. 2.3. Displacement history for cyclic tests

31

greater than 0.97. Absorbed energy in each cycle was computed by summing incremental areas under the force-displacement curve. Linear force distribution was assumed over each displacement interval.

Results and Discussion

Behavior Under Cyclic Loading

A typical load-displacement curve from cyclic loading for a specimen with a narrow tie design is shown in Fig. 2.4. Nonlinear hysteretic behavior is present even for small displacements. During the initial loading stages the hystereses are quite symmetrical; however pinching becomes pronounced with the increase in displacements. This reduction in energy absorption is caused by irreversible damage in the wood fibers surrounding the fastener. The loss of fastener contact with virgin wood visually manifests as slippage, and produces stiffness loss evident in the graph. When the contact is restored the stiffness picks up sharply. Repetitive cycling at a given displacement level causes strength reduction that attenuates as the cycling progresses. A tendency in the curve to pass near the previously achieved strength value is noticeable when moving from smaller to larger displacement levels. As the displacements increase the hystereses become asymmetrical. This behavior is primarily caused by a permanent twist in the tie. The specific narrow tie design results in a predetermined line of weakness that follows the shortest distance between the tie sides. It goes from the corrugation valley nearest to the fastener to the corrugation ridge on the opposite tie side. A displacement excursion in the nonlinear range in one loading direction activates this weak spot and adversely affects the subsequent strength achieved in the same direction during incremental cycles.

Similar behavior was recorded in specimens constructed with wide ties (Fig. 2.5). It is noticeable that these specimens achieve higher strength and absorb more energy which was expected considering their full body design. A specific to the wide ties was a larger diameter hole that permitted additional fastener slippage resulting in brief, abrupt drop in stiffness as shown with two ovals in Fig. 2.5. Switching to a smaller diameter hole eliminated this undesirable behavior.
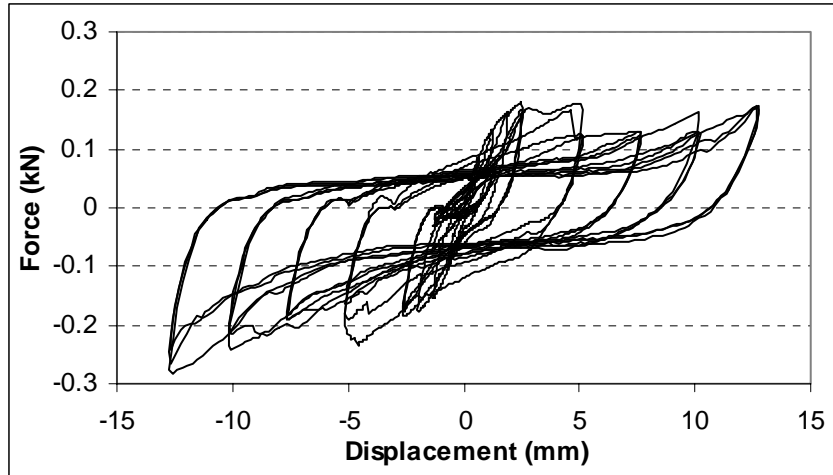
Fig. 2.4. Typical force-displacement curve for specimens with narrow ties
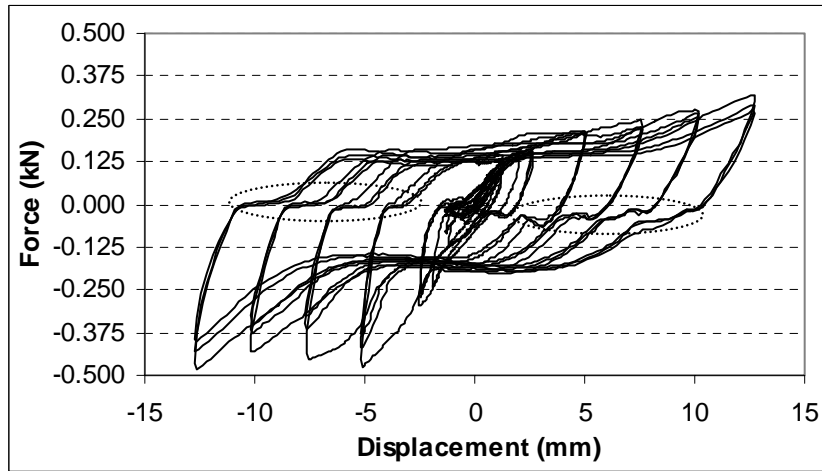
Fig. 2.5. Typical force-displacement curve for specimens with wide ties

Initial Stiffness

The initial stiffness summary statistics are given in Table 2.2. Data analysis revealed three extreme outliers on the high side, which were removed from the set. They were associated with specimens in which excessive mortar droppings engulfed the ties and spanned almost the whole cavity.

Statistical analyses for relevance of considered effects were carried out on specimen groups clustered logically in order to study several effects simultaneously. A 5% significance level ($\alpha =$ 0.05) was used for decision making in all statistical tests. The first cluster consisted of specimens with narrow ties from groups labeled Ctrl, B, J and K. The effects covered in this cluster were fastener type, tie location with respect to head joint and fastener quantity. The distribution of initial stiffness means and mean ranks as shown in Fig. 2.6 points to apparently higher initial stiffness values for specimens with two nails. The underlying data was analyzed using one-way analysis of variance (ANOVA). Summary of results is given in Table 2.3. Levene's test was used to determine homogeneity of residual variance (homoscadasticity). Normality of the data was checked by testing for skewness and kurtosis in the residuals and by performing the D'Agostino-Pearson omnibus normality test of the residuals. Since the data were found to be normal, and variances were homogeneous, the parametric F test was used to test for equality of means. For completeness, the nonparametric Kruskal-Wallis test on ranks was also used to check for equality of medians. Both tests indicated lack of significant difference between the means or medians.

Specimen groups Ctrl, C, D, E, F and G were clustered together and analyzed using two-way ANOVA in order to simultaneously investigate tie design and bent eccentricity effects. Two levels of tie design (narrow and wide) and three levels of bent eccentricity (min, code max, and excessive) were considered. Group means along with marginal unweighted means collapsing over the effects are shown in Table 2.4. A summary of statistical analysis results is presented in Table 2.5. Variance homogeneity was verified with Levene's test and normality was confirmed with a series of skewness, kurtosis and an omnibus test. These results allowed the use of a parametric all or nothing F test to check the null hypothesis that all group means are equal. The

Table 2.2. Initial stiffness summary statistics

Group	Count	Median (kN/mm)	Mean (kN/mm)	COV (%)
Ctrl	6	0.0943	0.0839	31.96
B	5	0.0983	0.0847	27.43
C	6	0.0639	0.0563	40.00
D	6	0.0249	0.0247	43.18
E	4	0.1351	0.1446	18.94
F	6	0.0775	0.0780	22.39
G	6	0.0357	0.0350	20.70
H	6	0.1302	0.1293	27.33
I	5	0.2263	0.2190	19.17
J	6	0.0776	0.0825	33.69
K	6	0.1037	0.1155	20.65
L	5	0.1438	0.1438	21.56
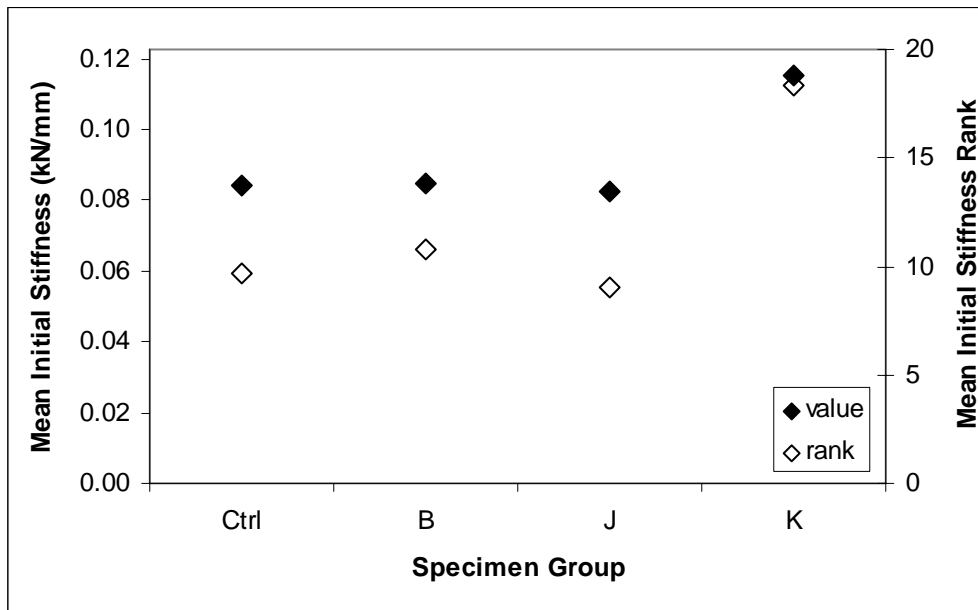
Fig. 2.6. Initial stiffness means and mean ranks for specimen groups with narrow ties

Table 2.3. Summary of statistical tests for initial stiffness in specimens with narrow ties

Parameter	Test	Statistics	p value	H_0
Variance	F	0.10	0.962	OK
Skewness	Z	1.02	0.308	OK
Curtosis	Z	0.17	0.864	OK
Normality	χ^2	1.07	0.586	OK
Mean	F	2.30	0.110	OK
Median	χ^2	7.27	0.064	OK

Table 2.4. Mean initial stiffness (kN/mm) for tie design and bent eccentricity effects

Tie Design	Bent Eccentricity			Mean
	Min	Max	Exc	
Narrow	0.0839	0.0563	0.0247	0.0550
Wide	0.1446	0.0780	0.0350	0.0858
Mean	0.1142	0.0672	0.0298	

Table 2.5. Summary of statistical tests for initial stiffness considering tie design and bent eccentricity effects

Parameter	Test	Statistics	p value	H_0
Variance	F	1.97	0.115	OK
Skewness	Z	-0.19	0.849	OK
Curtosis	Z	0.13	0.901	OK
Normality	χ^2	0.05	0.974	OK
Mean – all	F	22.98	<.0001	NG
Mean – Tie Type	F	20.66	<.0001	NG
Mean – Bent Ecc	F	49.54	<.0001	NG
Interaction	F	4.70	0.017	NG

hypothesis was rejected at the 5% significance level. Subsequent two F tests lead to a conclusion to reject the null hypotheses that marginal means for a considered effect are equal. Tukey's all possible pairwise comparison tests showed that each marginal mean is unique and cannot be grouped with the companion(s) for the considered effect. For completeness a two-way ANOVA was carried out on the ranks, a nonparametric alternative equivalent to a Kruskal-Wallis test, and the results came out identical.

The significance of both effects can be easily seen in Fig. 2.7. Two distinct lines, one for each tie design, identify the presence of this effect. The wide tie design shows superior performance with considerably higher initial stiffness values. Both lines are sloped with the highest stiffness values at the minimum eccentricity level and the lowest values at the excessive eccentricity level. Clearly the increase in bent eccentricity adversely affects initial stiffness values. The lines are not exactly parallel. While the slope of the line for the narrow ties is constant, the slope of the line for wide ties varies along the eccentricity levels pointing to the presence of an interaction effect as confirmed with the last of the parametric tests summarized in Table 2.5.

Specimen groups Ctrl, H, E, and I composed a cluster intended to simultaneously investigate tie design and tie location in bed joint effects using two-way ANOVA. Two aforementioned tie design levels (narrow and wide) were investigated along with two levels of tie location (centered and flush). Mean data is given in Table 2.6, and summary results of performed statistical analyses is presented in Table 2.7. The same analysis procedure described in the preceding cluster was followed. Residual variances were found to be identical, but there was kurtosis in the residuals, a sign of concern when parametric tests are based on small sample sizes. Therefore more emphasis was put on alternative nonparametric rank based tests. The results came out identical for both parametric and nonparametric statistical tests. The means or medians were different, and both effects were present. No interaction between the effects was found.

The significance of both effects can be seen in Fig. 2.8. Once again the wide tie design shows superior performance with considerably higher initial stiffness values than the narrow tie design. The presence of tie location effect is indicated with the existence of a slope in the lines. In both cases notably higher initial stiffness values were recorded when ties were placed flush in the bed
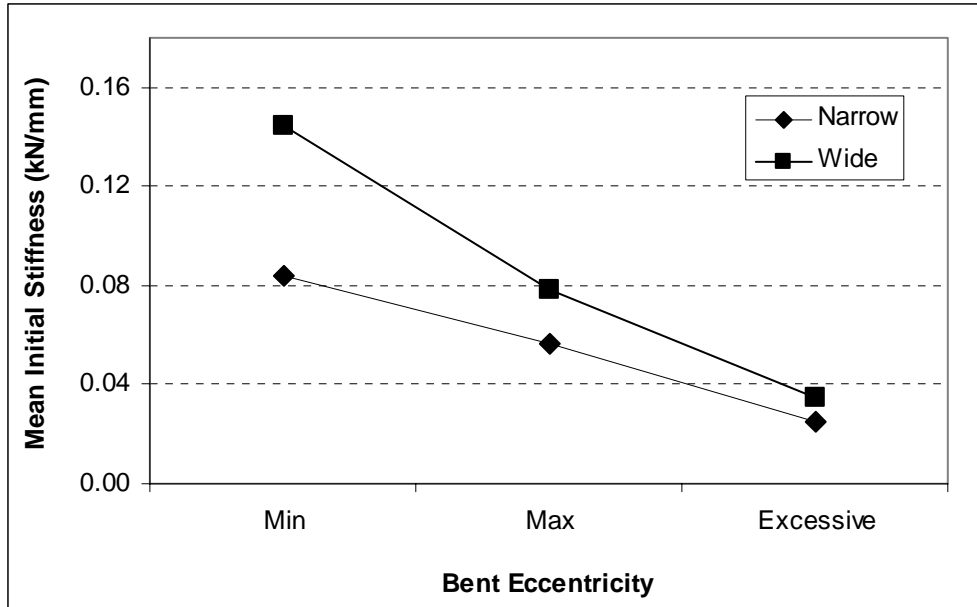
Fig. 2.7. Initial stiffness means for tie design and bent eccentricity effects
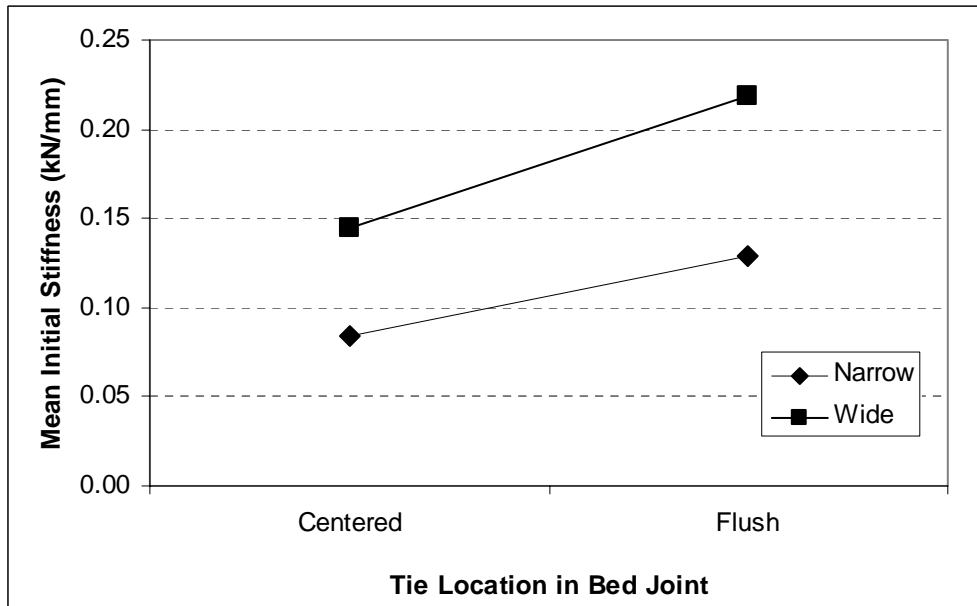
Fig. 2.8. Initial stiffness means for tie design and tie location in bed joint effects

Table 2.6. Mean initial stiffness (kN/mm) for tie design and tie location effects

Tie Design	Tie location in bed joint		
	Centered	Flush	Mean
Narrow	0.0839	0.1293	0.1066
Wide	0.1446	0.2190	0.1818
Mean	0.1142	0.1742	

Table 2.7. Summary of statistical tests for initial stiffness considering tie design and tie location effects

Parameter	Test	Statistics	p value	H_0
Variance	F	1.50	0.251	OK
Skewness	Z	-0.15	0.880	OK
Curtosis	Z	-2.25	0.024	NG
Normality	χ^2	5.09	0.079	OK
Mean – all	F	15.05	<.0001	NG
Mean – Tie Type	F	25.61	<.0001	NG
Mean – Tie Loc	F	16.29	0.001	NG
Interaction	F	0.96	0.342	OK

joint. The existence of the latter effect, and its nature, came as a surprise. A closer look at the specimens and the construction timing pointed to the reason for this inconsistency. Specimens with ties placed flush on the underlying brick and topped with mortar had considerably larger amounts of mortar droppings in the cavity than the ones placed on a mortar bed and then topped with another mortar layer. The former specimens were built last in the sequence and after a long day quality seemed to deteriorate. The droppings weren't properly trimmed and they obviously increased the initial stiffness of the specimens. If proper construction practice were followed, it is doubtful this effect would be present.

Finally, the effect of fastener hole diameter on initial stiffness was investigated in a side-by-side comparison of specimen groups E and L, both constructed with wide ties. Levene's test revealed that variances were equal (F = 0.13, p = 0.728). Small sample sizes required the use of a pooled variance t-test to check equality of means (t = 0.04, p = 0.972). The nonparametric Wilcoxon rank sums test (Mann-Whitney U test) was carried out for completeness (Z = 0.123, p = 0.903). The tests failed to refute the null hypothesis that initial stiffness means or medians were equal. Hence, it can be concluded that the fastener hole size has no significant affect on initial stiffness.

Energy Absorption Capacity

Loss in energy absorption capacity with repetitive cycling at all displacement levels was commonly found in all tested specimen varieties. In order to investigate the significance of this loss the control specimens were taken as a representative group on which one-way repetitive measures ANOVA was carried out. The six sample mean absorbed energy values for the three repetitive cycles at each displacement level are shown in Fig. 2.9, and a summary of the statistical analyses is given in Table 2.8. A 5 % significance level was used for decision making. At the majority of considered displacement levels the sphericity tests rejected the null hypothesis that the data are uncorrelated, exposing a positive bias in F tests of correlated data with heterogeneous variances. Therefore at all displacement levels the Greenhouse-Geisser correction was used to alter the significance of the F tests. The so called all or nothing tests for means rejected the null hypothesis that all means are equal, and subsequent one-sided Dunnett's tests confirmed that statistically significant differences exist between the absorbed energy in the first and each of the consecutive repetitive cycles.
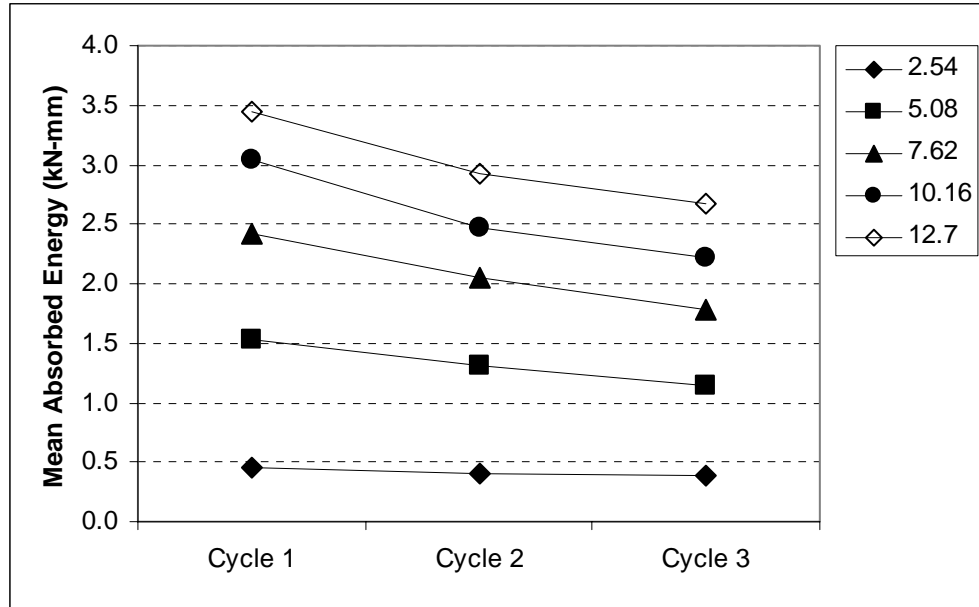
Fig. 2.9. Mean absorbed energy at five displacement levels for Ctrl specimens

Table 2.8. Summary of statistical tests for energy absorption capacity of Ctrl specimens

Displ.	Parameter	Test	Statistics	p value	H_0
2.54	correlation	χ^2	9.35	0.0093	NG
	mean	F	9.00	0.0276	NG
5.08	correlation	χ^2	5.11	0.0776	OK
	mean	F	9.44	0.0209	NG
7.62	correlation	χ^2	3.31	0.1911	OK
	mean	F	20.90	0.0025	NG
10.16	correlation	χ^2	6.60	0.0370	NG
	mean	F	67.88	0.0002	NG
12.70	correlation	χ^2	8.00	0.0183	NG
	mean	F	66.56	0.0003	NG

41

confirmed that statistically significant differences exist between the absorbed energy in the first and each of the consecutive repetitive cycles.

Absorbed Energy

Mean absorbed energy at several displacement levels are given in Table 2.9. The absorbed energy was taken as a cycle average for the displacement levels where repetitive cycling was conducted. Statistical analyses were carried out on the same group clusters as described before for initial stiffness. The distribution of mean absorbed energy for the first cluster is shown in Fig. 2.10. Narrow tie specimens fastened with two nails (K) have the highest values from the beginning, followed by the specimens fastened with screws (B). There is very little difference between the control group and the specimens with tie offset with respect to the head joint (J). The underlying data was analyzed at the considered displacement levels using one-way ANOVA. Homoscadasticity and normality were checked first, followed by the so called all or nothing parametric and nonparametric (Kruskal-Wallis) tests for equality of means or medians. The latter tests confirmed the existence of significant differences only at higher displacement levels. Subsequent two-sided Dunnet's all pairwise comparisons of means or ranks to a control group revealed the importance of the nail quantity effect at and above the 5 mm displacement level. A summary of the statistical tests is given in Table 2.10, and means that differ significantly from the control are indicated with arrows in Fig. 2.10.

Tie design and bent eccentricity effects on absorbed energy were simultaneously investigated using two-way ANOVA of data from the second cluster composed of specimen groups Ctrl, C, D, E, F and G. This clustering enabled the consideration of two tie design levels and three bent eccentricity levels that matched the ones used in the initial stiffness investigation. A separate ANOVA was performed at each of the representative displacement levels. Homoscadasticity couldn't be verified in all cases, and the normality assumption couldn't be verified in most cases either. Hence, emphasis was placed on results obtained from nonparametric tests on ranks rather than on parametric tests on actual data. These tests verified the existence of both effects at each considered displacement level. Subsequent Tukey's all possible pairwise comparison tests showed that each level of each effect was decisive across the board.

42

Table 2.9. Mean absorbed energy (kN-mm) at six displacement levels

Group	Displacement (mm)					
	1.27	2.54	5.08	7.62	10.16	12.70
Ctrl	0.112	0.414	1.322	2.082	2.578	3.019
B	0.134	0.446	1.371	2.156	2.908	3.601
C	0.071	0.189	0.582	1.053	1.613	2.197
D	0.033	0.068	0.216	0.378	0.574	0.817
E	0.200	0.640	2.071	3.401	4.728	6.205
F	0.088	0.276	0.936	1.619	2.443	3.403
G	0.035	0.122	0.468	0.934	1.500	2.124
H	0.137	0.412	1.357	1.945	2.604	3.152
I	0.195	0.550	1.804	2.890	3.630	4.733
J	0.109	0.376	1.274	1.914	2.464	2.917
K	0.131	0.502	1.724	2.779	3.395	3.841
L	0.210	0.649	2.110	3.699	5.366	7.138
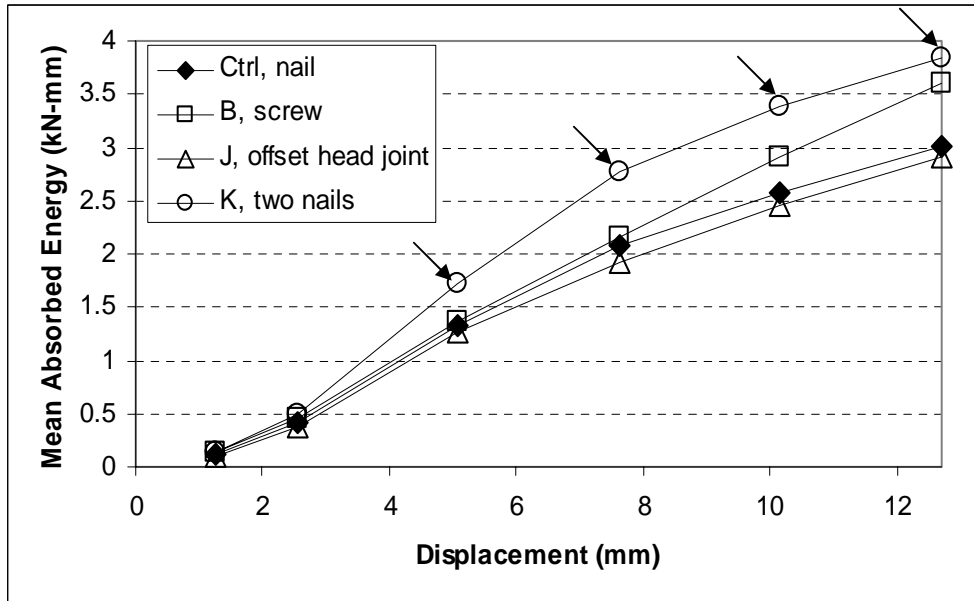
Fig. 2.10. Mean absorbed energy for specimen groups with narrow ties

Table 2.10. Summary of statistical tests for absorbed energy in narrow tie groups

Displ.	Parameter	Test	Statistics	p value	H_0
	variance	F	1.66	0.209	OK
1.27	mean	F	1.26	0.317	OK
	median	χ^2	3.82	0.281	OK
	variance	F	1.50	0.246	OK
2.54	mean	F	2.84	0.066	OK
	median	χ^2	10.01	0.019	NG
	variance	F	0.47	0.705	OK
5.08	mean	F	6.56	0.003	NG
	median	χ^2	12.25	0.007	NG
	variance	F	0.42	0.741	OK
7.62	mean	F	10.04	0.000	NG
	median	χ^2	13.04	0.005	NG
	variance	F	0.68	0.578	OK
10.16	mean	F	5.14	0.009	NG
	median	χ^2	10.15	0.017	NG
	variance	F	1.33	0.293	OK
12.7	mean	F	4.68	0.013	NG
	median	χ^2	10.06	0.018	NG

44

The significance of both effects can be seen in Fig. 2.11. The effect of tie design is evident from the existence of three pairs of distinctive lines corresponding to the minimum, code maximum and excessive bent eccentricities. In each set the dashed line associated with wide tie design lies above the corresponding solid line associated with narrow tie design. This clearly points to the superior energy absorption capacity of the wide tie design. The bent eccentricity effect is revealed from the existence of two sets of three distinctive lines corresponding to narrow and wide tie designs. In each of the two sets the line associated with the minimum bent eccentricity is the highest and the one corresponding to the excessive eccentricity is the lowest. This confirms the superior energy absorption of smaller bent eccentricities.

Two-way ANOVA of data from the third group cluster was utilized to simultaneously investigate tie design and tie location with respect to bed joint effects on absorbed energy. The analyses considered the aforementioned two tie design levels, and two tie location levels that corresponded to the ones used in the initial stiffness investigation. A separate ANOVA was performed at each of the representative displacement levels. Emphasis was placed on results obtained from nonparametric tests on ranks rather than on parametric tests on actual data because the outcomes from the performed tests for equality of residual variance and normality of the residuals were not uniformly affirmative across the considered displacement levels. The analyses confirmed the significance of the tie design effect only. Neither tie location, nor interaction effects were statistically important. The graph of mean absorbed energy, Fig. 2.12, illustrates these statistical outcomes. The existence of two distinctive pairs of lines corresponding to the narrow and wide tie designs points to the presence of the tie design effect. The lack of statistical significance for the tie location effect comes primarily from the specimens with narrow tie design. For these specimens the two lines corresponding to the central and flush tie locations in the bed joint almost overlap each other. Clearly for the narrow tie design the amount of absorbed energy at each of the considered displacement levels wasn't affected by the way the ties were laid in the bed joint. Contrary to this behavior the amount of absorbed energy in specimens with wide tie design depends on tie location in the bed joint at displacement levels of 5 mm and above. The specimens with ties laid centrally in the joint have superior energy absorbance over the ones laid flush on the brick and topped with mortar. In the latter case the considerable width of the tie prevents the topping mortar to penetrate into the underlying brick cavity resulting
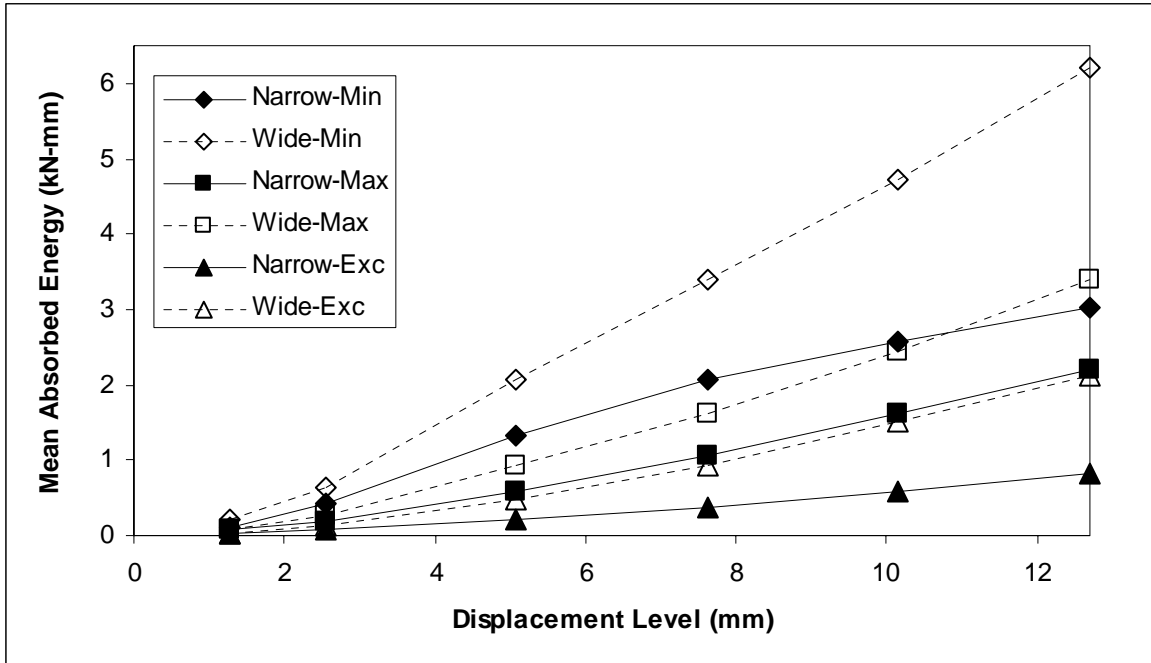
Fig. 2.11. Mean absorbed energy for tie design and bent eccentricity effects
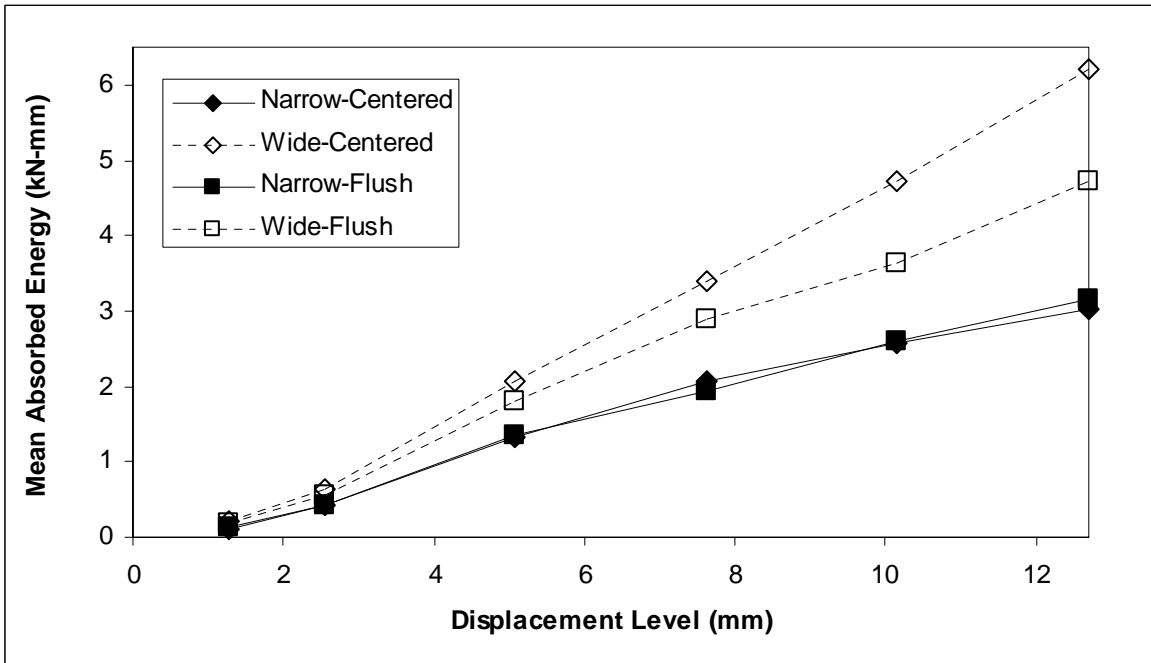
Fig. 2.12. Mean absorbed energy for tie design and tie location in bed joint effects

in connection weakness. This flaw becomes prominent at larger displacements when the tie is loosened in the mortar joint and slips from side to side during cycling. The tie slip causes the force capacity to level off, resulting in narrower hystereses which consequently reduces the amount of absorbed energy.

Mean absorbed energy values for wide tie specimens with two fastener hole sizes are plotted in Fig. 2.13. The specimens with smaller holes absorb more energy than the specimens with regular holes, a benefit that increases with the increase in displacements. Side-by-side comparisons were carried out at representative displacement levels to investigate the significance of this effect. Levene's test was used to check homogeneity of variances. Pooled variances t-test was used to check for equality of means in cases where homoscadasticity was confirmed, and the Satterthwaite (Welch-Aspin) t-test was used for the other cases. The nonparametric Wilcoxon rank sums tests were carried out for completeness. The series of tests, whose summary is given in Table 2.11, failed to refute the null hypothesis that absorbed energy means or medians were equal. Therefore, it can be concluded that wide tie design with smaller fastener hole has no statistically significant benefit in absorbed energy over the wide tie with regular hole.

Envelopes

Average envelopes for four specimen groups with narrow tie design are shown in Fig. 2.14. Three of them are almost indistinguishable leading to a conclusion that considering this parameter the effects of fastener type (nail vs. screw) and of tie location with respect to the head joint (no offset vs. offset) are not important. Only the effect of fastener quantity (1 nail vs. 2 nails) is pronounced. Clearly the addition of a second nail is beneficial to the behavior of the connection. It constrains tie pivoting around a single fastener, resulting in higher strengths in the leading loading direction. Consequently the envelope curve retains symmetry even for larger displacements.

The significance of tie design and bent eccentricity effects on the average envelope curves is shown in Fig. 2.15. The narrow tie connections are inferior to the wide tie connections. The connections with minimum bent eccentricity have much larger envelope values giving them a
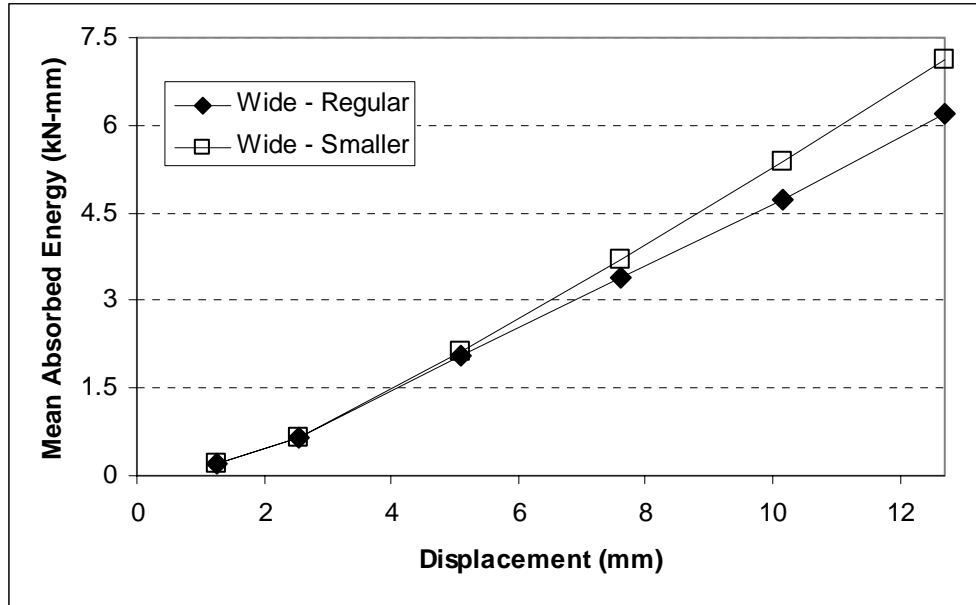
Fig. 2.13. Mean absorbed energy for fastener hole size effect in wide tie specimens

Table 2.11. Summary of statistical tests for absorbed energy considering fastener hole effect

Displ.	Parameter	Test	Statistics	p value	H_0
	variance	F	6.26	0.034	NG
1.27	mean	t_s	-0.34	0.746	OK
	median	Z	0.09	0.927	OK
	variance	F	6.60	0.030	NG
2.54	mean	t_s	-0.16	0.879	OK
	median	Z	0.64	0.523	OK
	variance	F	2.02	0.189	OK
5.08	mean	t_p	-0.15	0.885	OK
	median	Z	0.09	0.927	OK
	variance	F	0.74	0.412	OK
7.62	mean	t_p	-0.59	0.572	OK
	median	Z	0.82	0.411	OK
	variance	F	0.60	0.460	OK
10.16	mean	t_p	-0.95	0.366	OK
	median	Z	1.00	0.315	OK
	variance	F	0.23	0.641	OK
12.7	mean	t_p	-1.10	0.300	OK
	median	Z	1.19	0.235	OK
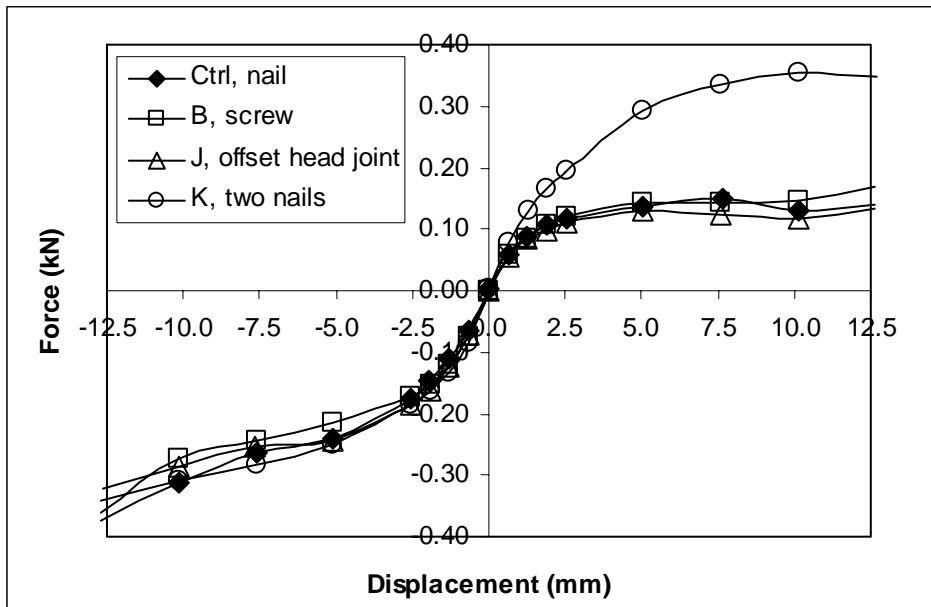
Fig. 2.14. Mean envelopes for specimen groups with narrow ties
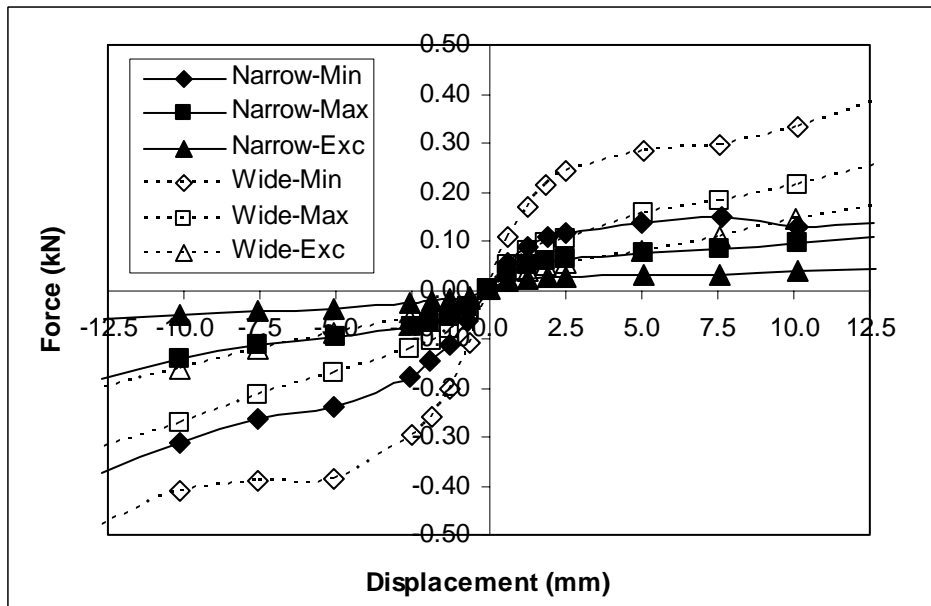
Fig. 2.15. Tie type and bent eccentricity effects on mean envelopes

distinctive advantage over the connections with the code maximum bent eccentricity. The connections with excessive bent eccentricity have by far the lowest load capacity.

It can be seen in Fig. 2.16. that the effect of tie location in the bed joint is not easily distinguishable. In the leading loading direction the flush specimens show higher envelope values, while the situation reverses in the opposite loading direction.

Loading Type Effect

The average load-displacement curve from monotonic loading of six specimens with narrow ties along with the average envelope curve from cyclic loading of a corresponding set of specimens are illustrated in Fig. 2.17. The curves are very close to one another at smaller displacements and diverge as the displacement increases and the behavior becomes distinctively nonlinear. The envelope curve at all displacement levels is below the corresponding monotonic loading curve, a fact that was expected given the damage that accumulates during cycling. The load-displacement curve from monotonic loading can serve as a good upper bound approximation to the cycling loading envelope.

General Observations and Failure Modes

From the cyclic test initiation up to the terminal stage the tie pivoted around the fastener in all cases where it was attached to the wood stud with a single fastener. The increase in displacements would then cause the tie to twist. This twist was more pronounced in the narrow ties then in the wide ones. It was also more prominent in specimens with minimum bent eccentricity compared to the ones with maximum or excessive eccentricity. In the latter cases the actual length of the tie fixed in the cavity was larger then the cavity width. The superfluous tie length resulting from the added extra bent eccentricity allowed it to straighten rather than to twist. This obviously required less amount of work to achieve a certain displacement level and resulted in notably smaller absorbed energy capacities. Further increase in displacements would cause larger tie twisting resulting in initiation of cracks and ultimately dislodgment of mortar droppings that encompassed the tie. As a consequence notable stiffness loss was observed. Near the ultimate loading stage the tie would further straighten, the fastener hole would elongate and
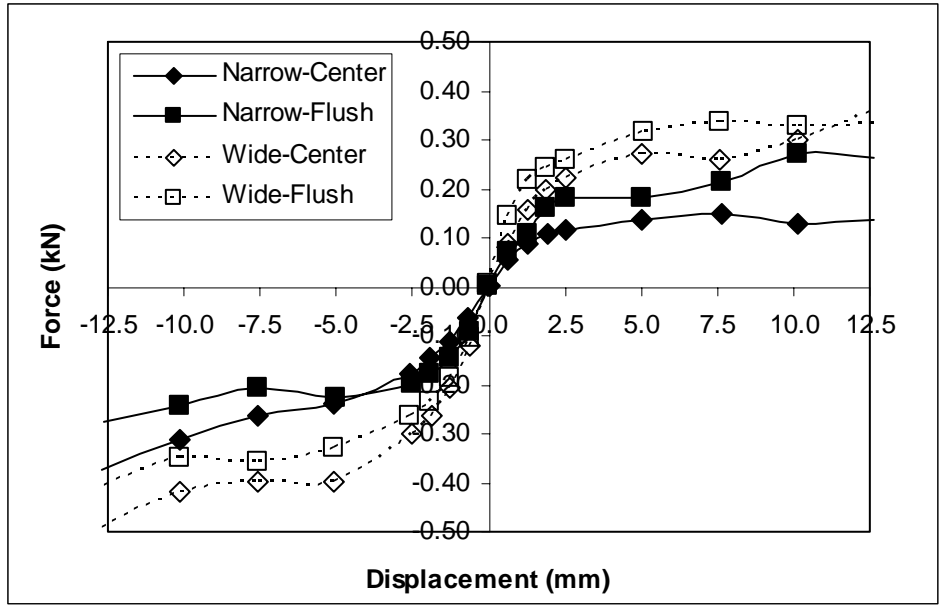
Fig. 2.16. Tie type and tie location in bed joint effects on mean envelopes
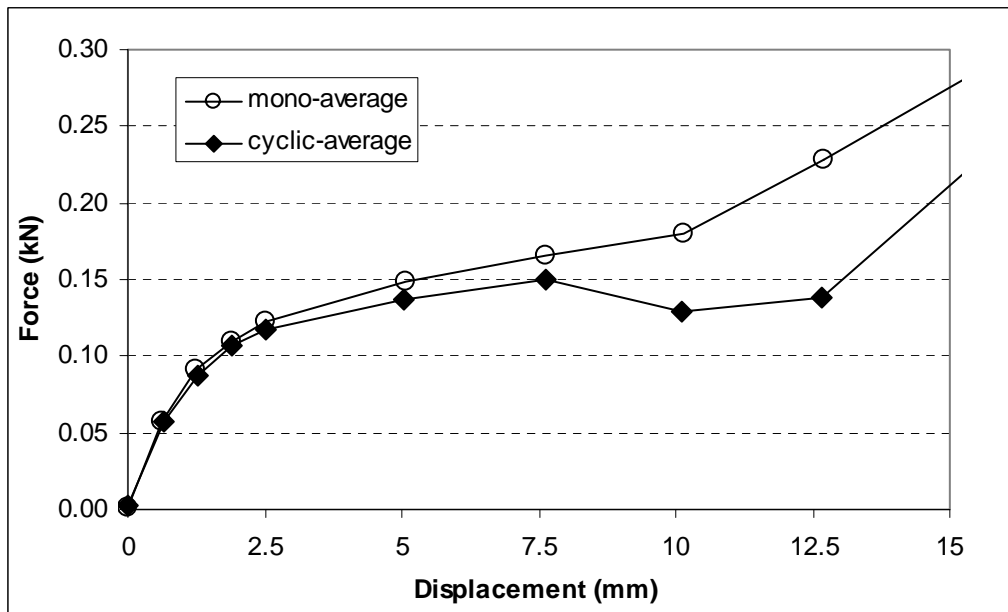
Fig. 2.17. Comparison of monotonic force-displacement relation to envelope for cyclic loading

51

fastener pullout would appear as a prevailing mode of failure in all specimens fastened with a single nail. The main behavioral difference in specimens fastened with two nails was the lack of tie pivoting. Bottom nail pullout was notably smaller compared to the single nail specimens, and large tie tear adjacent to the mortar joint was recorded in five of the six tested specimens. Just one of the five specimens fastened with a screw failed by a complete tie tear. The rest suffered corrugation straightening and severe tie twist. Because the screw wouldn't pull out, the wood piece would come closer to the brick couplet. All specimens with wide ties in which the tie was laid flush on the brick failed in nail pullout, but these were the only specimens in which the tie was completely loosened in the mortar joint. While this had some adverse effect on the shear behavior, it would have a large effect on the connection pullout stiffness and strength.

Conclusions

The following conclusions can be drawn regarding the parameters influencing the shear behavior of corrugated tie connections in brick veneer wall systems.

Effect of cyclic loading - Nonlinear hysteretic behavior was present even in small displacements. Hysteresis pinching and asymmetry became pronounced with the increase in displacements. Repetitive cycling at a certain displacement level caused strength reduction and loss in absorbed energy capacity that both attenuated as the cycling progressed. The envelope curve from cyclic loading came short of the corresponding load-displacement curve obtained from monotonic loading, a difference that increased with an increase in displacements.

Effect of tie design – Of the considered two 22 gauge tie designs the wider tie was found to be advantageous. Subassemblies constructed with wide ties had larger initial stiffness, absorbed more energy and had higher envelopes than the ones constructed with the more common narrow ties.

Effect of fastener type – Using screws for fastening ties in the wood backup was found to have no impact on initial stiffness and cyclic envelope. The absorbed energy was larger compared to the nailed connections at larger displacement levels, but the difference was statistically

insignificant. Failure modes were different. The predominant fastener pullout occurring in nailed specimens was virtually nonexistent in screwed specimens.

Effect of fastener quantity – The advantage of subassemblies with two fasteners was expressed in both larger values in initial stiffness and absorbed energy. The latter was found statistically significant at larger displacement levels. Failure modes were affected as well. Partial tie tear near the mortar joint accompanied by moderate nail pullout was a combined failure mode recorded in all subassemblies fastened with two nails and just in one case in subassemblies fastened with a single nail.

Effect of bent eccentricity – This effect was highly influential. Larger initial stiffness, more absorbed energy and higher cyclic envelopes were associated with smaller eccentricities.

Effect of tie location in bed joint – This effect had significant influence on initial stiffness, but results may be compromised by coupling with the effect of mortar droppings that was not controlled in the study. Absorbed energy values and envelope curves for subassemblies with narrow ties were indistinguishable with respect to this effect. All subassemblies with wide ties laid flush on the brick were loosened in the mortar joint, which had adverse effect on absorbed energy values.

Effect of tie location with respect to head joint – Tie offset from the head joint was found to be insignificant for all considered variables.

Effect of fastener hole size – Subassemblies with ties having smaller diameter holes had apparently better behavior considering absorbed energy, but the difference was found to be statistically insignificant.

CHAPTER III - ANALYTICAL

Analysis of Anchored Brick Veneer - Wood Frame Wall Systems Subjected to In-Plane Loads

Abstract

An analytical finite element study was carried out to investigate the in-plane behavior of wall systems composed of brick veneer anchored to light wood frame backing with corrugated metal ties. The core wall model simulated a wood frame sheathed with oriented strand board. Brick veneer was then tied to the exterior wall face, and gypsum wallboard sheathing was added on the interior wall face. Two-dimensional linear elastic beam and continuum type elements were used to model principal wall components. The fasteners connecting the sheathing to the frame backing, and the ties anchoring the veneer were modeled with pairs of orthogonal independent nonlinear inelastic springs. Gap elements were used to prevent sheathing overlap and to model panel bearing at the base. The veneer was supported on compression-only spring elements in the vertical direction and infinitely stiff elastic perfectly plastic spring elements in the horizontal direction. The effect of the interior wallboard sheathing as well as the brick veneer contribution through two different tie designs was investigated in detail. It was determined that both the interior sheathing and the brick veneer stiffen significantly the core light frame wood shear wall and alter its response. Their simultaneous presence increased racking wall strength, but diminished its ductility. The addition of anchored brick veneer limited wood shear wall displacements and reduced wall's base shear under dynamic excitation.

Introduction

Typical residential construction in North America consists of individual low rise dwellings in which a stiff core wall assembly made of dimensional lumber frames sheathed with plywood or oriented strand board (OSB) represents a major part of the overall load bearing system (Fig. 3.1).

54

Interior wallboard sheathing

Light frame wood shear wall:
- dimensional lumber frame
- exterior grade sheathing
- fasteners

Corrugated tie

Brick veneer

Flashing
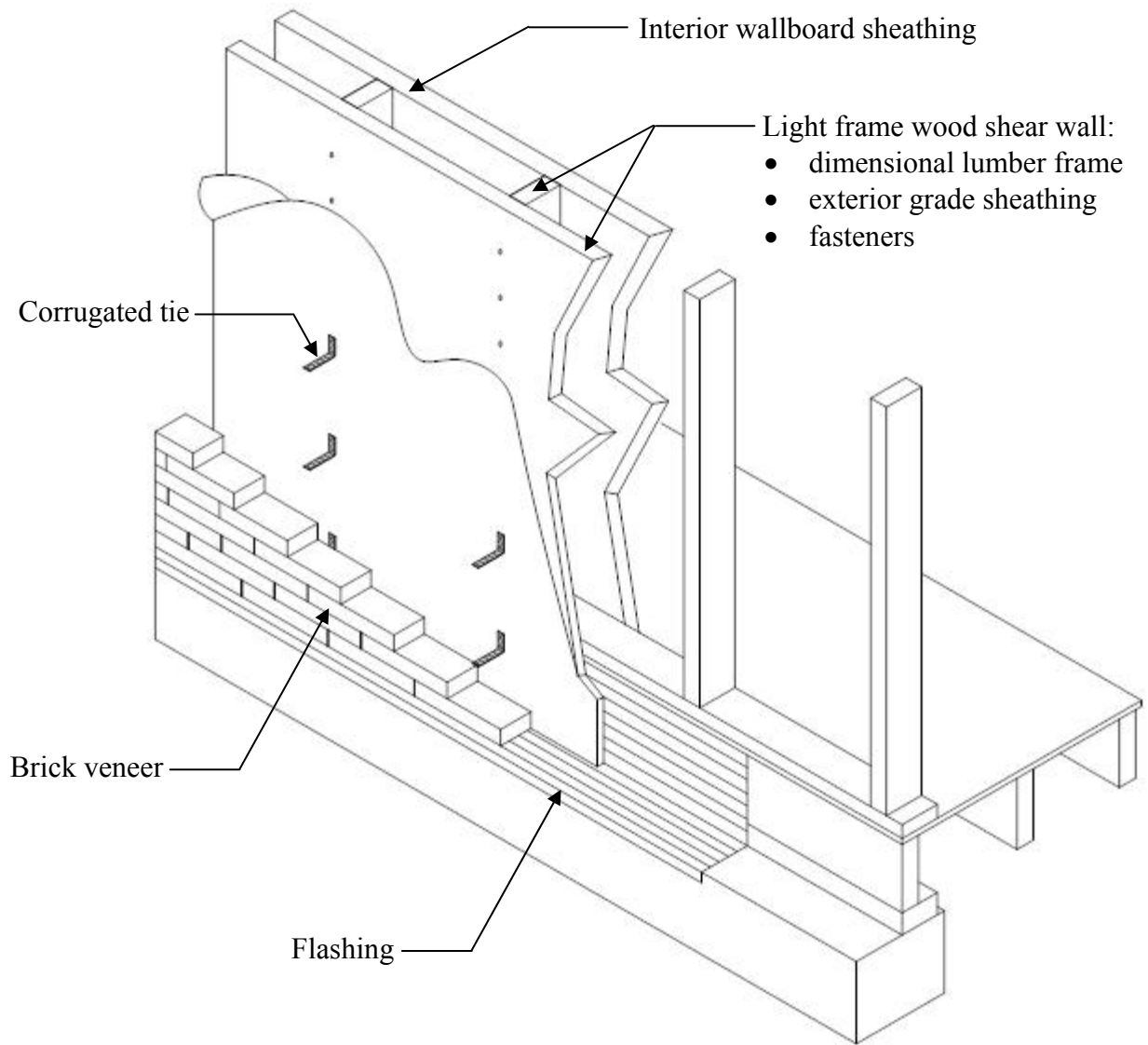
Fig. 3.1. Components of an anchored brick veneer – light frame wood shear wall

It is considered that the lumber frames transfer the vertical loads from the diaphragms to the foundations, while the lateral forces induced into the walls from winds or earthquakes are resisted by racking of the sheathing and are transferred to the framing members via nailed connections.

These walls are often sheathed from the interior with gypsum wallboard (GWB) which is considered a nonstructural component that does not contribute to the lateral wall resistance. On the exterior, the aesthetic appearance of brick makes masonry a frequent choice for a façade. In such cases the single wythe walls commonly referred to as brick veneers are anchored over an air cavity to the wood frame wall backing through various types of structural ties. The resulting integral wall system benefits from improved moisture resistance, fire resistance, resistance to heat transfer, and favorable acoustics (BIA 2002). While the brick veneer (BV) is recognized as being capable of bearing its own gravity loads, the MSJC Code (MSJC 2008) does not acknowledge its contribution to the in-plane load resistance, assuming the wood frame shear wall to bear all racking loads, although BIA Tech Notes (2002) acknowledge that brick veneers do carry a proportionate share of the lateral load.

The primary objective of the research reported here is to incorporate appropriate analytical formulations and material behavior for all constituent wall components into an integral wall model suitable for parametric analyses of in-plane wall behavior.

Background

Light Frame Wood Shear Walls

Over the years extensive experimental and analytical research has been conducted to determine the racking behavior of light frame wood shear walls and a bibliography written by van de Lindt (2004) summarizes it well. Numerous researchers have shown that these walls are capable of dissipating large amounts of energy through the summation of individual fastener deformations that are nonlinear in their nature (Foschi and Bonac 1977, Easley et al. 1982, McCutcheon 1985, Gupta and Kuo 1987). It is the behavior of the nailed sheathing-to-wall connections that governs the response of the whole shear wall assembly. The load-deformation relation of such shear walls during cyclic loading is characterized by pinched hystereses that show both stiffness degradation

and strength deterioration (Dolan and Madsen 1992 b, Shenton et al. 1998, Folz and Filiatrault 2001).

Parametric studies identified that nail spacing had the most prominent effect on wall stiffness and strength, followed by blocking, nail head penetration, panel size, panel orientation, panel thickness and nail type (Atherton 1983, Falk and Itani 1989, Lam et al. 1997, Jones and Fonseca 2002). Tests on both small and full scale wood shear walls sheathed with plywood on the outside and GWB on the inside have shown that racking strength was linearly proportional to the wall length and that the GWB significantly contributed to the shear wall performance. Its resistance was additive to the resistance provided by the plywood sheathing (Patton-Mallory et al. 1985). This finding was corroborated on a shaking table test of a two story residential house (Filiatrault et al. 2002). The installation of wall finish materials on both wall faces increased markedly the lateral stiffness of the structure and caused considerable reduction in its displacement response.

Anchored Brick Veneer - Light Frame Wood Shear Walls

Focused research on in-plane anchored brick veneer-light frame wood shear wall behavior and load distribution between its constitutive parts is quite scarce. An early experimental study of entire wall assemblies conducted by Allen and Lapish (1986) reported that stiff strip metal ties nailed to the backing could transfer a substantial racking load component from the wood frame into the brick veneer. The transferred force was sufficient to break the brick mortar bond at the base beam. At higher deflections, the strength of the tested ties was sufficient to rock the brick veneer in unison with the racking of the timber frame, yet the brick veneer sustained its integrity up to the final stages. The presence of brick veneer markedly increased the racking strength of the brick-wood wall assembly over the strength of a comparable light frame wood shear wall, while adversely effecting wall ductility.

A similar investigation carried out by Shelton and King (1994) on complete veneer wall systems utilizing mild steel strip ties revealed that at an intermediate loading stage the frame and the veneer were each resisting about half the applied in-plane load. Johnson and McGinley (2003) experimented with small wall specimens loaded in uniform double shear throughout the wall height and determined that properly spaced standard 22 gauge corrugated metal ties, the type

most commonly used in North America, have considerable capacity to transfer racking loads from the wood wall to the brick veneer. The shear transfer was greatly enhanced when additional truss type horizontal joint reinforcement was laid into the veneer and fastened to the backing wall.

A comprehensive behavioral study conducted by Choi and LaFave (2004) on brick veneer-wood frame subassemblies anchored with corrugated metal ties addressed among other things in-plane wall loading. Idealized force-displacement relations for monotonic shear loading and envelope curves for cyclic shear loading were published demonstrating the tie thickness, fastener type and bent eccentricity effects.

The experimental study reported in Chapter 2 broadened the in-plane loading part of Choi and LaFave's (2004) research. The significance of multiple effects on the shear behavior of corrugated metal tie connections was statistically investigated, and it was determined that tie design and bent eccentricity were the most important factors, while tie location in the bed joint, fastener type and fastener quantity were influential to a lesser degree. The research revealed that force-displacement curves of tie connections obtained under monotonic loading can be considered an upper bound for the hysteresis loop envelopes. Fastener slippage during cyclic shear loading enabled by the localized damage of the surrounding wood fibers diminished the energy absorption capacity of the connection and caused pronounced pinching in the hystereses.

Flashing at Brick Veneer Base

Proper brick veneer design mandates the use of continuous through-wall flashing at wall base just above grade to drain the moisture out of the wall cavity and to prevent water from rising up into the wall system due to capillary action. (BIA 2002, 2005). The flashing acts as a bond breaker between the brick veneer and its concrete foundation, allowing some slippage to occur and hence controls their susceptibility to cracking due to moisture and thermal movements. However, breaking the bond has an adverse effect on the shear strength of the veneer wall (McGinley and Borchelt 1990). Under these conditions frictional forces arising from vertical compressive loads above the plane of the flashing provide the shear resistance at the joint. The bond strength and coefficient of friction values were determined experimentally for various

combinations of flashing, mortar and masonry materials (Thrischuk and Suter 1996, Rajakaruna 1997, Zhuge and Mills 1998, Griffith and Page 1998). Cyclic shear tests on concrete brick triplets with incorporated flushing revealed very stable hystereses that closely follow an elastic-perfectly plastic shear load-displacement skeleton curve and show no joint degradation with repeated cycling. An increase in the precompression level shifted the skeleton curve towards higher shear resistance values, and the subsequent hysteresis encompassed a larger area (Griffith and Page 1998).

Modeling

Benchmark Wall Sample

A benchmark wall sample 2.44×2.44 m in size that complied with the standard codes of practice was used as a representative wall system for analysis. The dimensional lumber frame in the wall core had all components made with nominal 2×4 studs (38×89 mm) of Standard Grade Pine. The vertical studs were placed 406 mm apart. Two vertically oriented 11.1 mm thick, 1.22×2.44 m Southern pine OSB panels were nailed with 8d (63.5 mm long) common nails to the frame. Nail spacing was 152 mm at the edge studs, 304 mm at the interior studs and 135 mm at the header and sill, resulting with 64 nails per panel. The brick veneer was made of standard size ASTM C216 bricks (100×67×200 mm) and type N masonry cement mortar. The veneer rested on the foundation over a plastic type membrane flashing. It was anchored to the frame with corrugated ties fastened to the studs at 406 mm long vertical intervals. This pattern required a total of 42 ties for the entire wall sample. The interior wall side was sheathed with two vertically oriented 12.7 mm thick, 1.22×2.44 m GWB panels. They were screwed to the studs with 32 mm long drywall screws spaced at 406 mm in vertical direction. This pattern consumed 28 screws per panel.

Element and Boundary Condition Definitions

The element and boundary condition definitions utilized in the composition of a finite element (FE) model of the wall adhered to the variety of elements and sophisticated material models available in the OpenSees software framework used in the numerical analysis process.

Frame members were modeled with two-dimensional linear elastic beam elements (Fig. 3.2). The common formulation with a linear displacement field in the axial direction and a cubic displacement field for the deflections perpendicular to the beam axis resulted in three degrees-of-freedom (DOF) per node. Master and slave nodes constrained to equal displacements in both orthogonal directions were utilized to simulate the lack of bending stiffness at the header-to-stud and sill-to-stud connections. All sill nodes at the intersections with the studs were restrained in the vertical direction, and in addition the two corner nodes were restrained in the horizontal direction as well.

Both sheathings and brick veneer were modeled with four node quadrilateral elements (Figs. 3.3 - 3.5). A bilinear isoparametric formulation was used resulting in two translational DOF per node. Homogenous isotropic linear elastic material behavior and plane stress idealization were assumed in the formulation. Pertinent material properties are shown in Table 3.1.

Zero-length elements constrained to two-dimensions were used to simulate sheathing-to-frame fasteners and structural ties anchoring the veneer wall to the wood frame. These elements connected two corresponding nodes with common initial location, one belonging to the frame and the other belonging to the sheathing or brick veneer. Their stiffness in each of the two orthogonal directions was determined from material models with nonlinear inelastic behavior approximated from experimental investigations. The two-dimensional application and lack of drilling stiffness resulted in two translational DOF per node. In essence, each of these elements shown in Fig. 3.6 performed like a pair of orthogonal independent nonlinear inelastic springs, a modeling approach that had been used to approximate individual fasteners (Itani and Cheung 1984, Gutkowski and Castillo 1988, Dolan and Foschi 1991, White and Dolan 1995).

Commonly used constitutive relations for pullout of discrete fasteners due to unidirectional shearing of adjoining wood members ascend as exponential (Foschi and Bonac 1977, Easley et al. 1982), power (McCutcheon 1985, Gupta and Kuo 1987, Cheung et al. 1988) or logarithmic (McCutcheon 1985) functions whose parameters were determined from fits to experimental data (Fig. 3.7). Depending on the level of sophistication and the achieved deformation interval length the relation may continue asymptotically to certain cap on the force, or have a linear descending
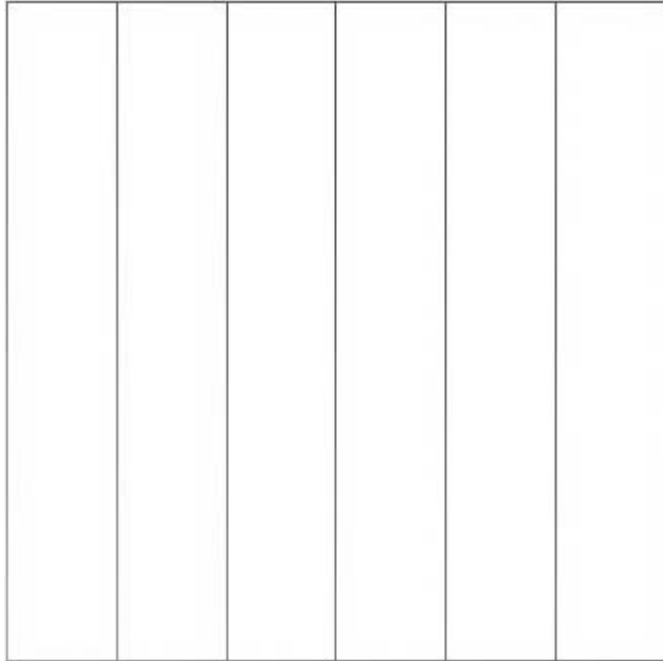
Fig. 3.2. Beam elements in the FE mesh of the benchmark wall sample
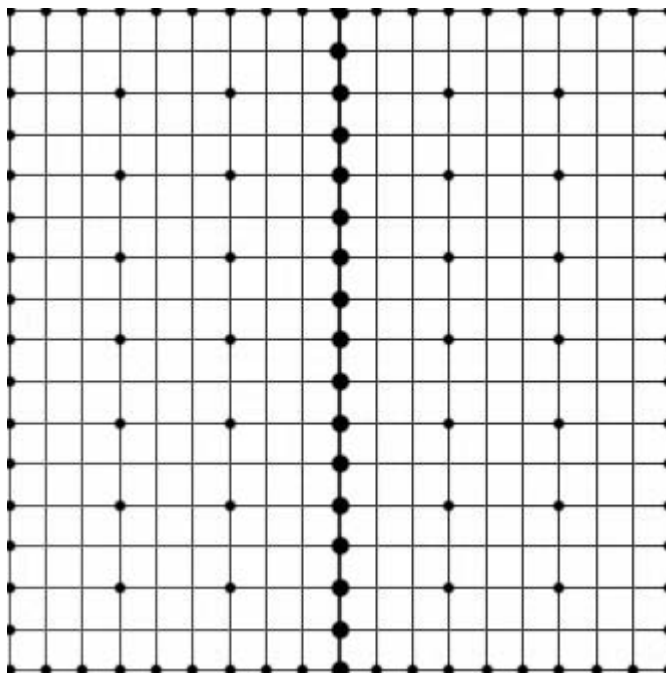
Fig. 3.3. FE discretization of the OSB sheathing in the benchmark wall sample with denoted fastener locations
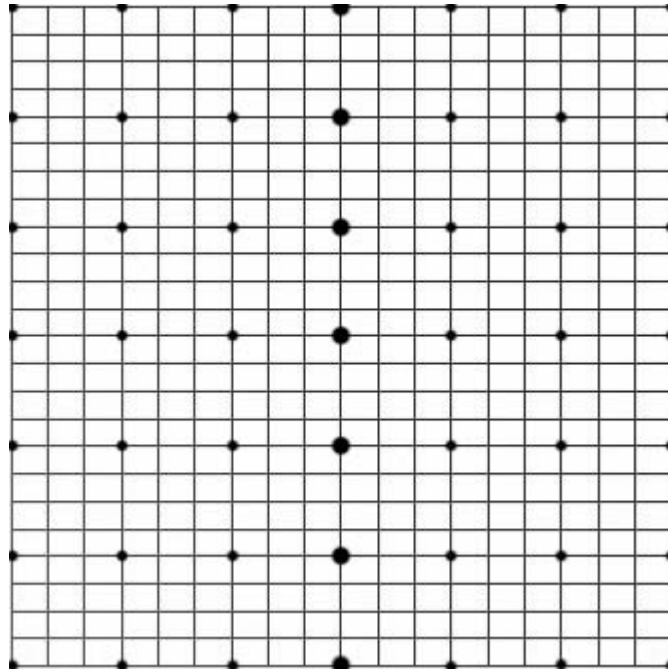
Fig. 3.4. FE discretization of the GWB sheathing in the benchmark wall sample with denoted
fastener locations
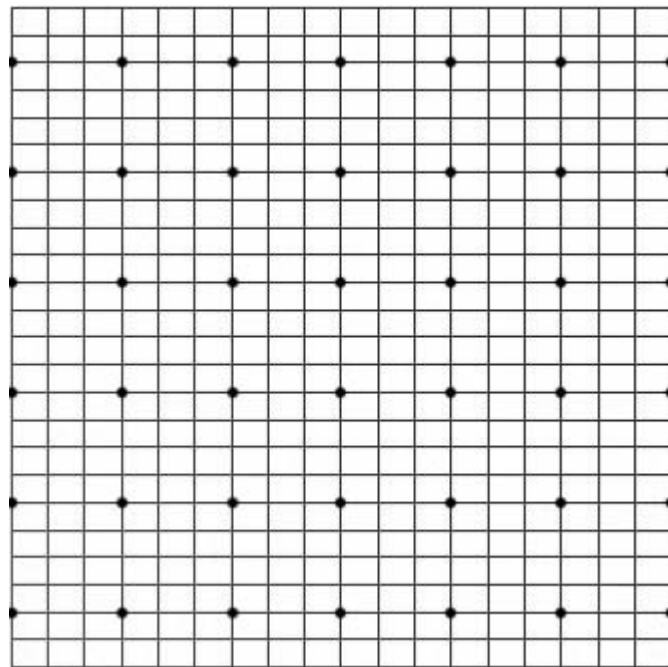
Fig. 3.5. FE discretization of the brick veneer in the benchmark wall sample with denoted tie
locations

Table 3.1. Material properties for wall components

Component	Material	Weight (kN/m^3)	Young's Modulus (GPa)	Poisson's ratio	Source
Frame	Wood, pine	5.81	9.31	-	ASCE 7-98 (1998), Forest Products Laboratory (1999)
Exterior sheathing	OSB	6.28	3.00	0.20	Structural Board Association (2004), Thomas (2001)
Interior sheathing	GWB	7.86	1.75	0.17	ASCE 7-98 (1998), Patton-Mallory & McCutcheon (1987)
Brick Veneer	Masonry	18.85	11.78	0.25	ASCE 7-98 (1998), MSJC (2008)
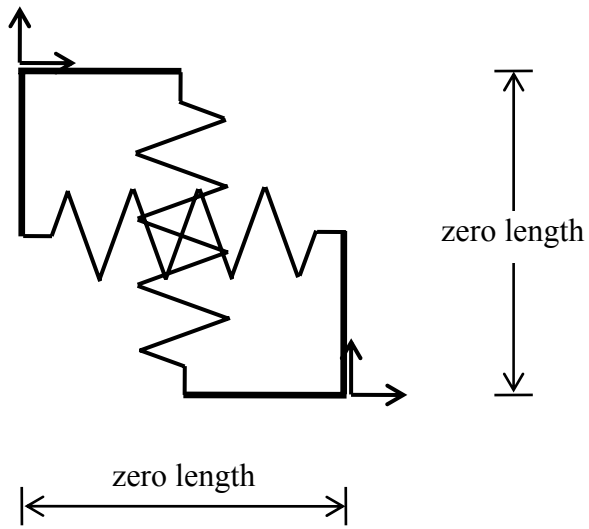
Fig. 3.6. Zero-length element with stiffness in two orthogonal directions
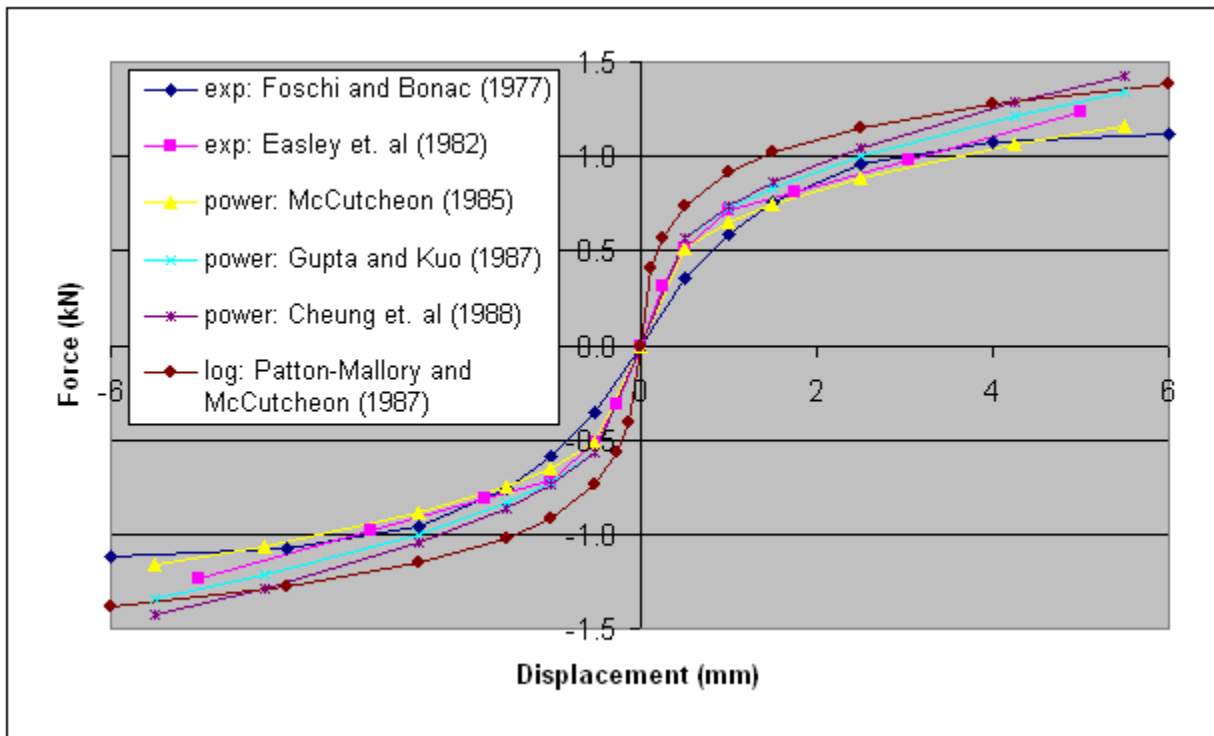
Fig. 3.7. Unidirectional constitutive relations for 8d nails fastening wood sheathing to frame

path towards ultimate failure (Dolan and Foschi 1991). These early unidirecti[conal relations served as backbone curves for developing successive hysteretic relations appropriate for cyclic lading. The hystereses are characterized by stiffness degradation, strength deterioration and pronounced pinching under subsequent reloading and unloading (Filiatrault 1990, Dolan and Madsen 1992 a, White and Dolan 1995, Folz and Filiatrault 2001). Such a hysteretic constitutive relation with a backbone curve composed of a tri-linear ascending part up to the connection strength followed by a linear descending part was applied in the analyses (Fig. 3.8). The parameters that governed the hysteretic response are given in Table A.1. They were determined as an appropriate fit to data available in the literature.

A hysteretic relation with identical behavioral parameters and a backbone curve that was fitted to data from Patton-Mallory and McCutcheon (1987) was used to approximate the behavior of screw type fasteners in GWB to wood connections subjected to shearing (Fig. 3.9, Table A.2). Due to the weaker bearing stiffness and strength of the paper lined gypsum near the panel edges, the connection strength and achieved deformation interval are considerably smaller than the corresponding values for discrete fasteners connecting OSB to wood.

The same approach was implemented for developing constitutive relations used to approximate the shear behavior of tied connections that anchor the veneer to the wood backing. In order to investigate the tie type effect, backbone curves for two tie designs were fitted to experimental data described in Chapter 2 (Fig. 3.10, Tables A.3 and A.4).

Overlap between adjacent panels and between the panels and their base was prevented by implementing discrete uniaxial spring type elements. They connected corresponding nodes on the adjacent surfaces and utilized a discontinuous constitutive relation that accounted for the width of the existing gap (Fig. 3.11). Frictional sliding was neglected. This element formulation resulted with one DOF per node, acting along the axis that connects the nodes.

Brick veneer bearing at the base was modeled with zero-length elements that connected two overlapping nodes, one belonging to the veneer and the other belonging to the fixed base. Their discontinuous constitutive relation provided for unlimited, infinitely stiff, no-tension vertical support (Fig. 3.12). The same type of elements oriented horizontally and having limited
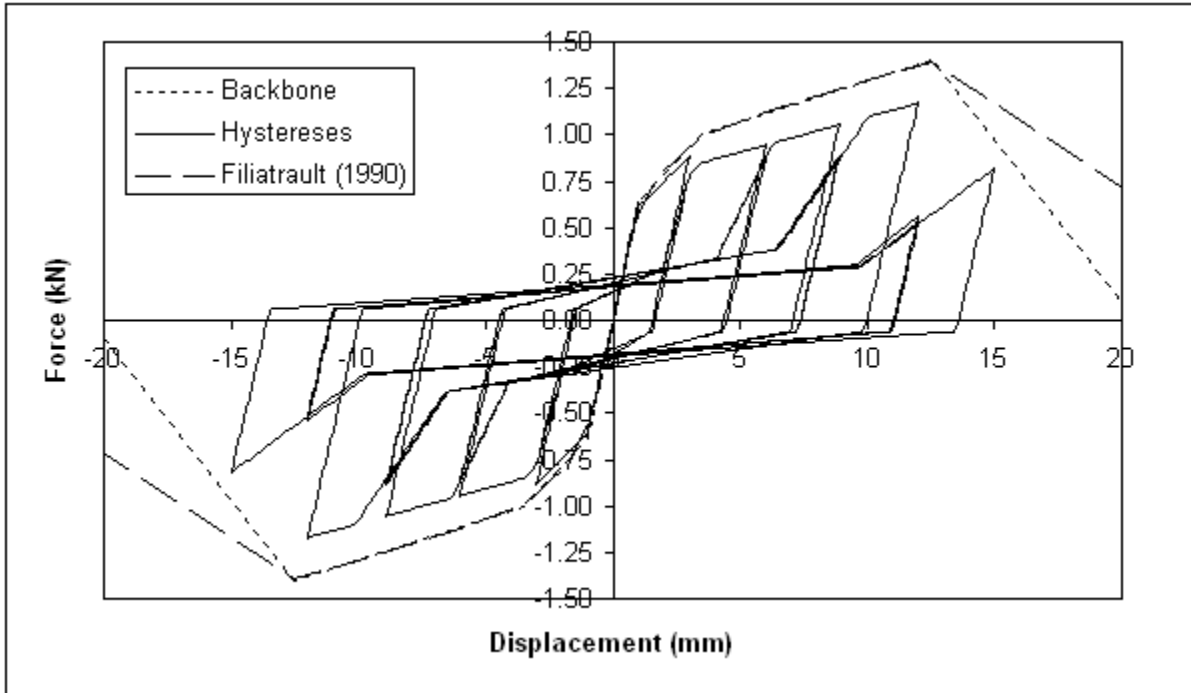
Fig. 3.8. Hysteretic constitutive relation for 8d nails fastening wood based sheathing to frame
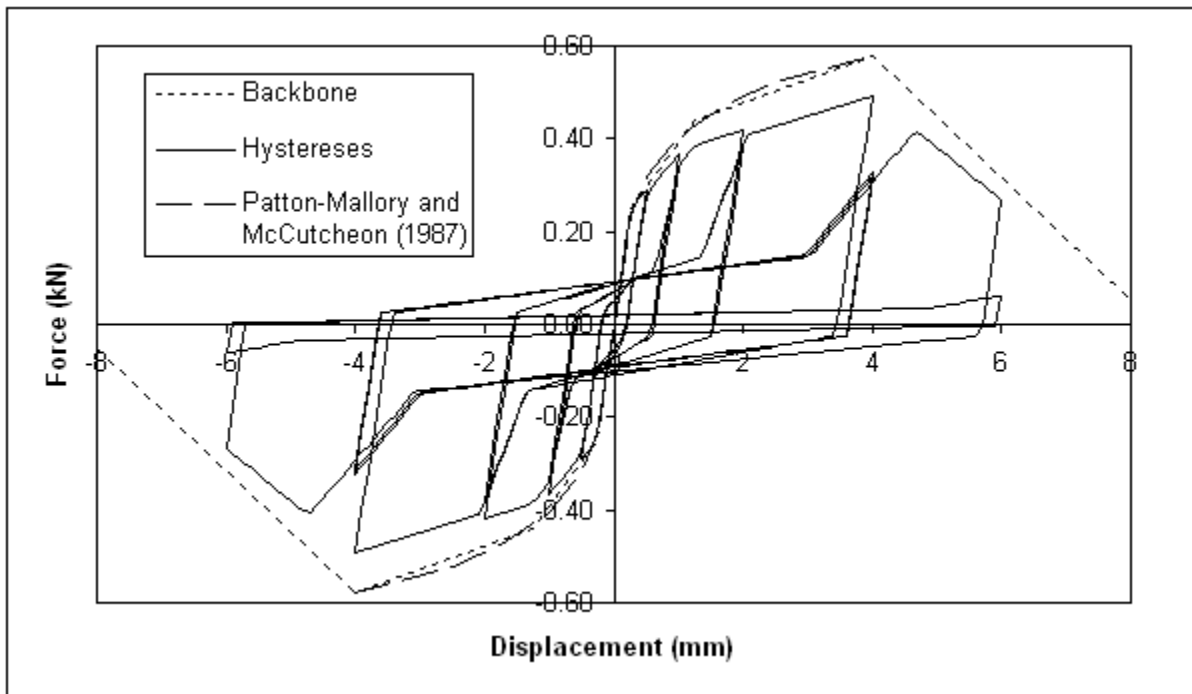
Fig. 3.9. Hysteretic constitutive relation for 32 mm drywall screws fastening 13 mm GWB
          sheathing to frame

(a)
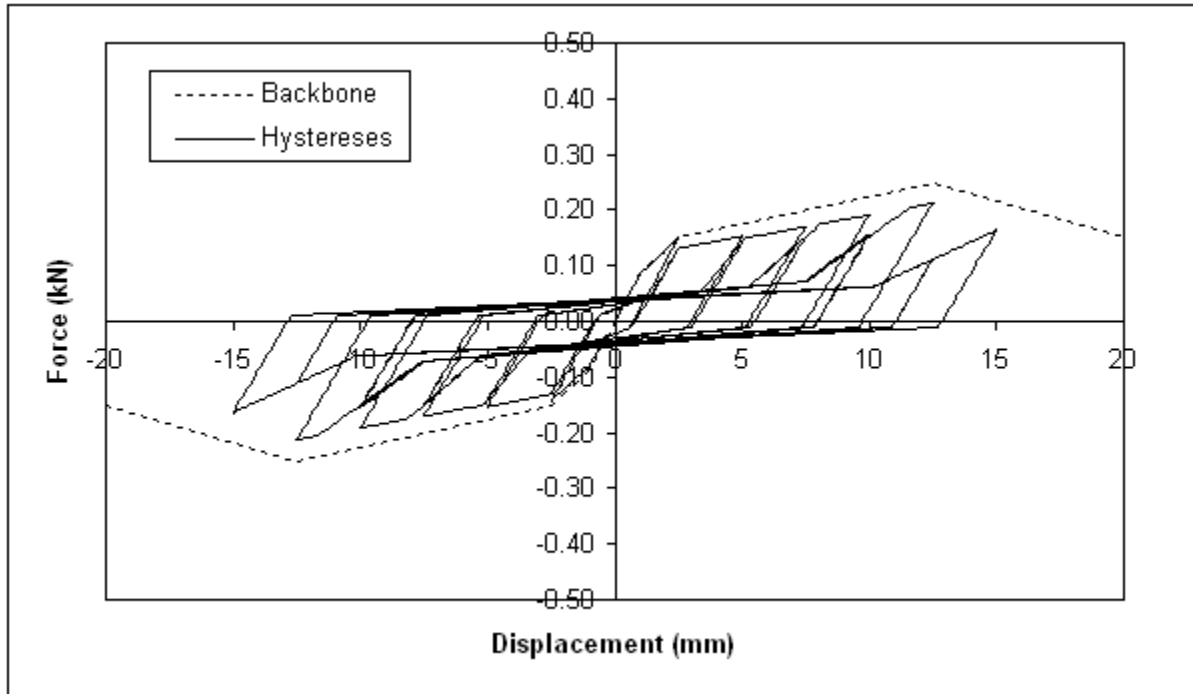
(b)
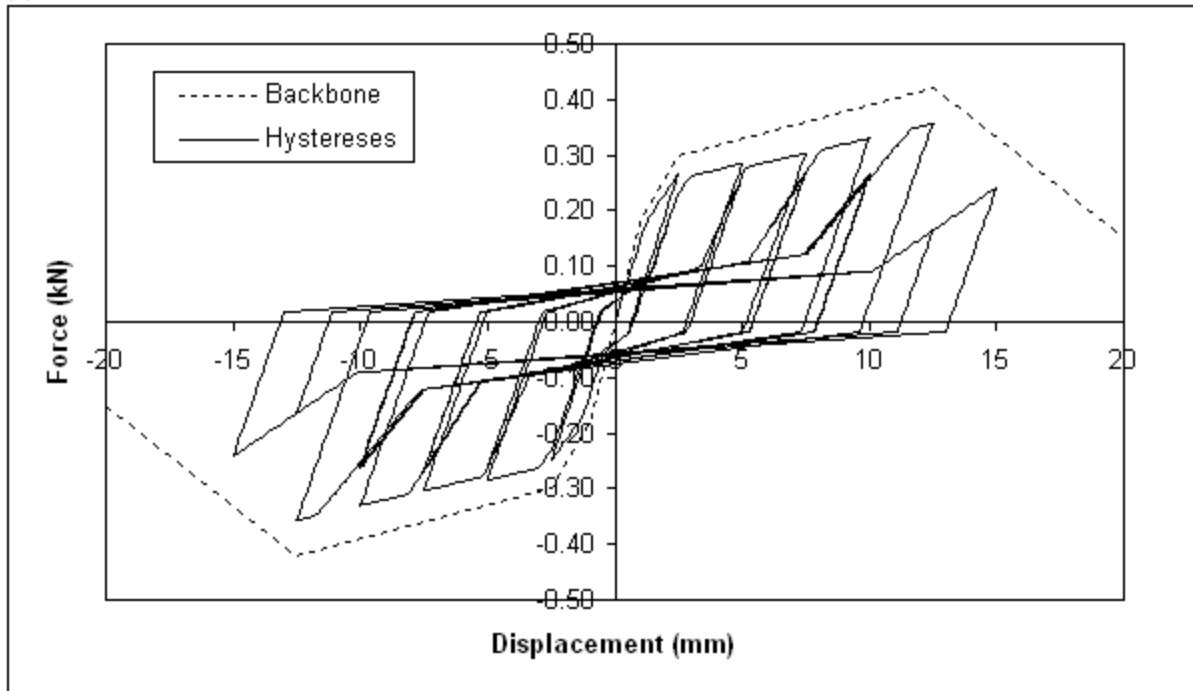
Fig. 3.10. Hysteretic constitutive relations for 22 ga corrugated ties fastened to frame backing with 8d nails. (a) Narrow ties, (b) Wide ties

(a)

gap width, w_g
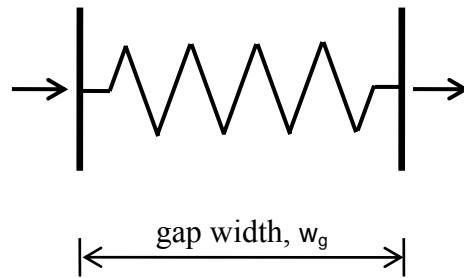
(b)
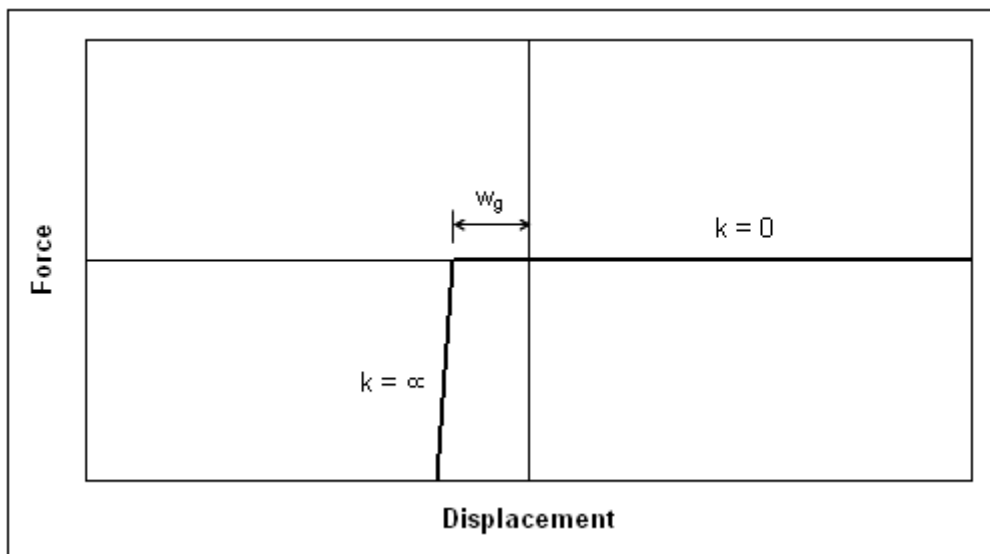
Fig. 3.11. Discrete spring type element spanning the gap between adjacent surfaces. (a) Element schematic, (b) Constitutive relation

compression capacity provided for support in the horizontal direction (Fig. 3.13). One such element with infinitely stiff elastic ideally plastic behavior in compression and no tension was incorporated at each wall bottom corner in all cases of static type loading. Its yielding force equaled the weight of the wall multiplied by a coefficient of friction whose value of 0.36 was conservatively taken as the lowest reported in literature (Fig. 3.14). Bottom node fixity in horizontal direction was enforced in cases of earthquake type dynamic loading.

Static Pushover Analysis

Light Frame Wood Shear Wall

The FE model for the light frame wood shear wall consisted of elements that approximated the wood frame, OSB sheathing and adjoining fasteners. It was created to fit into the OpenSees framework (OpenSees 2009). A progressively increasing uniform horizontal displacement applied to all frame nodes at the header level constituted the loading for this and all subsequent models. Model validation was performed by comparing calculated results from a displacement controlled analysis of two wall designs to existing experimental data and solutions ranging from simple racking equations (Tuomi and McCutcheon 1978) to sophisticated nonlinear analytical models (Filiatrault 1990). The wall size of 2.44×2.44 m, sheathing panel size of 1.22×2.44 m, its vertical orientation, as well as fastener type (8d nail) were common for both wall designs, while fastener spacing and number of studs varied. Sample wall parameters are given in Table 3.2, while Table 3.3 summarizes data for racking strength, corresponding displacement, and strength per unit wall length. The analytical results for the second wall sample obtained with the OpenSees model are shown in Fig. 3.15 superimposed on experimental data from Dolan (1989) and model predictions from Filiatrault (1990). The initial stiffness calculated with the OpenSees model was 2.223 kN/mm, and the figure shows that it closely predicted the actual value. The force-displacement relation was correctly matched well into the nonlinear range, while closer to the ultimate the model over predicted the strength by 18 %.

The force-displacement relation for the core wall part of the benchmark model is shown in Fig. 3.16. The relation was nonlinear, and it resembled the corresponding tri-linear backbone relation for the fasteners which were the principal contributor of nonlinearities in the model. The

(a)
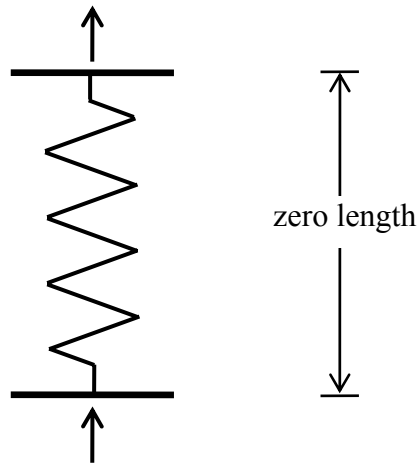
zero length

(b)
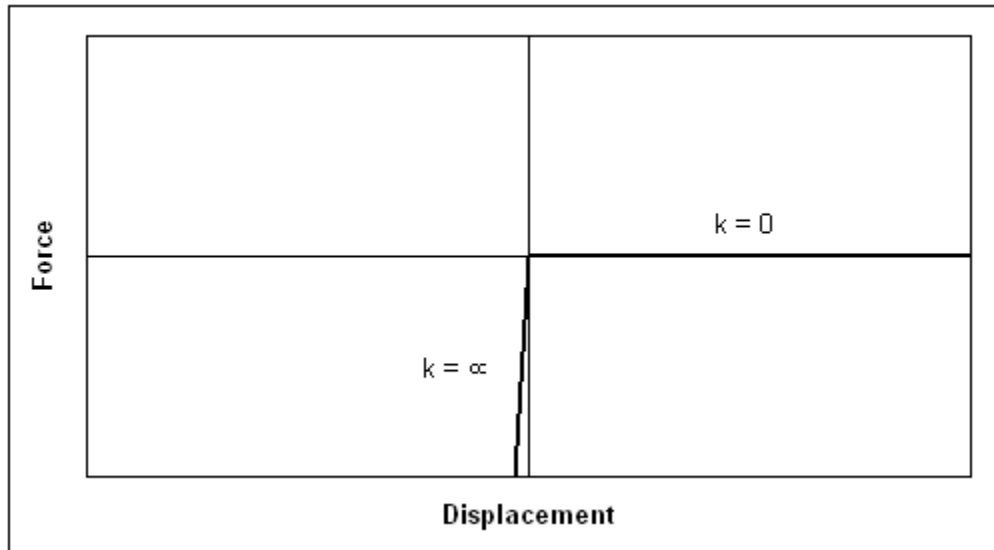
Fig. 3.12. Zero-length element for supporting veneer in vertical direction. (a) Element schematic, (b) Constitutive relation

(a)
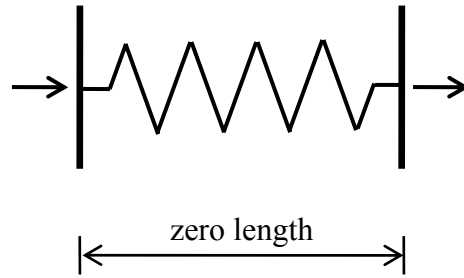
zero length

(b)
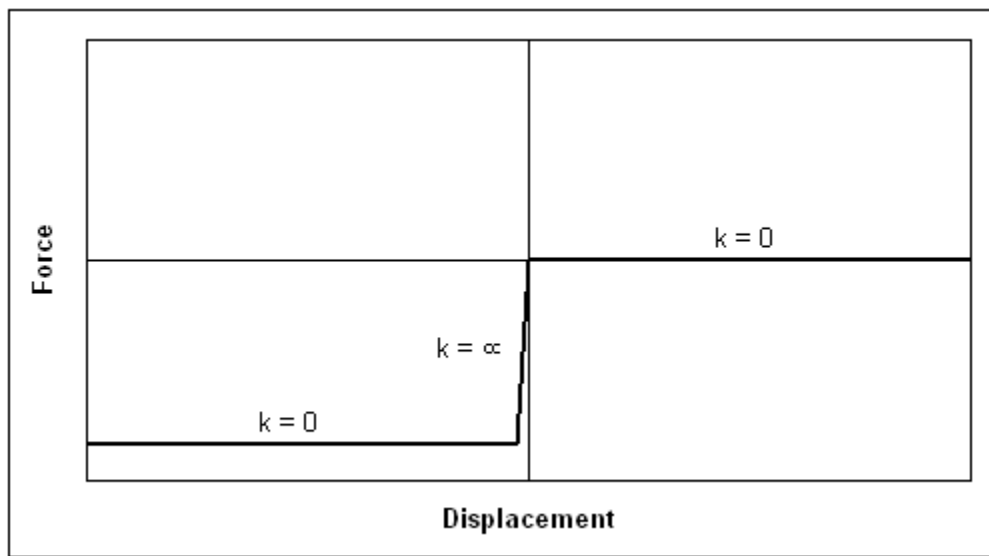
Fig. 3.13. Zero-length element for supporting veneer in horizontal direction. (a) Element schematic, (b) Constitutive relation

71
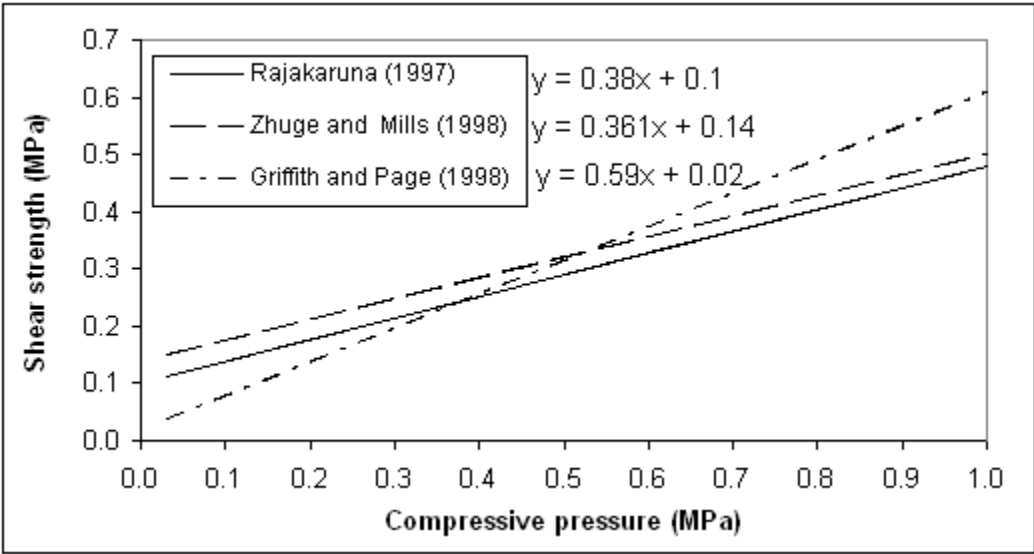
Fig. 3.14. Shear strength in bed joints with embossed polyethylene flashing

Table 3.2. Parameters of sample walls used for model validation under pushover load condition

Wall sample	Wall length (m)	Wall height (m)	Stud spacing (m)	Sheathing type	Sheathing length (m)	Sheathing height (m)	Sheathing thickn. (mm)	Sheathing orient.	Fastener type	Fastener spacing edge (mm)	Fastener spacing field (mm)
1	2.44	2.44	0.406	OSB	1.22	2.44	12.7	vertical	8d nail	152.4	304.8
2	2.44	2.44	0.610	Wafer Board	1.22	2.44	9.5	vertical	8d nail	101.6	152.4

Table 3.3. Summary of analytical predictions and experimental results for pushover loading

Wall sample	Racking strength (kN)	Corresp. displ. (mm)	Unit strength (kN/m)	Result type	Source
1	22.35	–	9.17	experimental	Price and Gromala (1980)
	25.95	–	10.64	analytical	Tuomi and McCutcheon (1978)
	28.58	66.6	11.72	analytical	OpenSees model
2	31.85	73.5	13.06	experimental	Dolan (1989), Dolan and Madsen (1992 b)
	39.56	–	16.22	analytical	Tuomi and McCutcheon (1978)
	33.73	62.3	13.83	analytical	Filiatrault (1990)
	37.65	67.8	15.44	analytical	OpenSees model

73

(a)

(b)
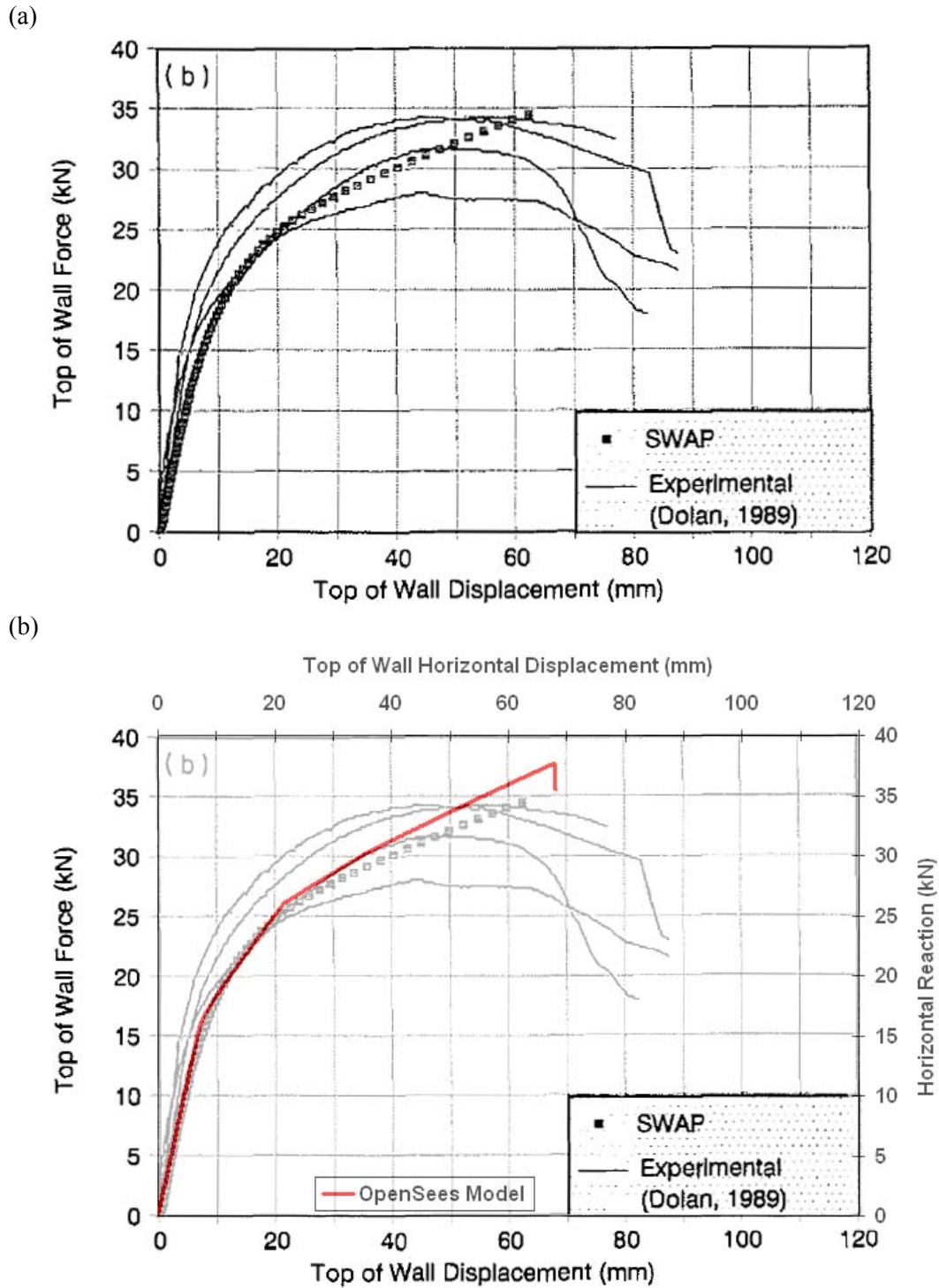
Fig. 3.15. Comparison of analytical predictions and full-scale pushover test results: (a) Filiatrault (1990)[1], (b) OpenSees model overlay

---

prediction for the initial stiffness of 1.775 kN/mm represented a 20 % decrease from the stiffness of the second wall sample with denser nail spacing. The racking strength was estimated at 28.58 kN, which constituted a 24% decrease compared to the second wall sample. The core wall model was also analyzed for the case when the OSB sheathing was allowed to bear against the base foundation. The initial part of the force-displacement relation remained exactly the same since the gap between the sheathing and the base stayed open. Once it closed and the appropriate discrete elements engaged, the wall stiffness markedly increased and its racking strength reached the value of 34.63 kN, a 21 % increase. However, this was accompanied with a decrease in wall ductility.

Anchored Brick Veneer - Light Frame Wood Shear Wall

The FE model for this wall was composed of the core wall model augmented with elements that approximated the brick veneer and the ties spanning the cavity. Both 22 ga narrow and wide tie designs were considered by incorporating appropriate constitutive relations based on backbone curves obtained from experimental investigations. Calculated force-displacement relations for this wall are shown in Fig. 3.17.a. They were nonlinear in nature and bore resemblance to the tri-linear backbone relations used to envelop the behavior of fasteners and ties which were the principal source of model nonlinearities. The predictions for initial stiffness values were 2.509 kN/mm in the case with narrow ties, and 2.844 kN/mm in the case with wide ties. These values amounted to a 41 % and 60 % increase over the initial stiffness of the core wall. The obtained racking strengths were 31.53 kN and 32.42 kN, respectively and they were reached at displacements of approximately 67 mm in both cases. These strength estimates represented a 10 % and 13 % increase over the strength of the core wall.

The strengthening effect resulting from adding anchored brick veneer to the core wall was also notable in cases when OSB sheathing was allowed to bear against the base foundation (Fig. 3.17.b). As expected, the incorporation of stronger, wider ties had a more prominent influence. Interestingly, the racking strength reached with both tie designs was nearly identical at 36.20 kN, a small 5% increase over the core wall. Notably the racking strength was being reached at displacement levels that were decreasing as the ties became stronger.
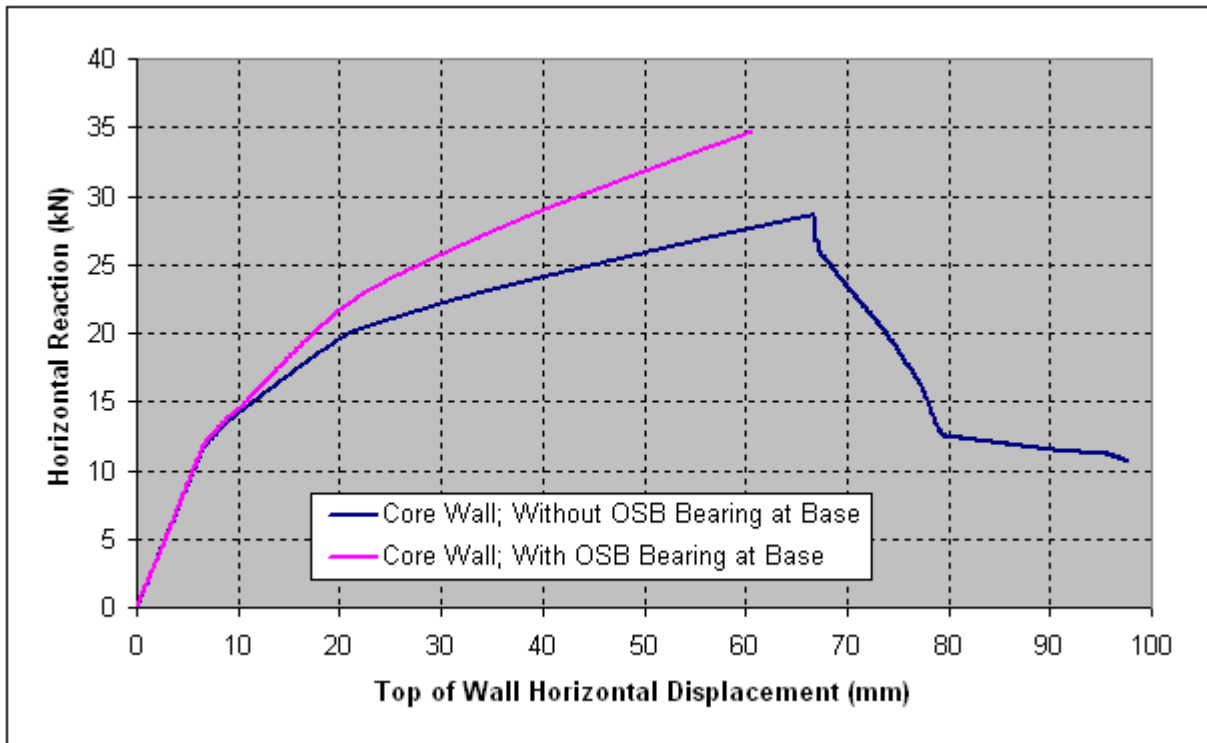
Fig. 3.16. Force vs. displacement relation for light frame wood shear walls
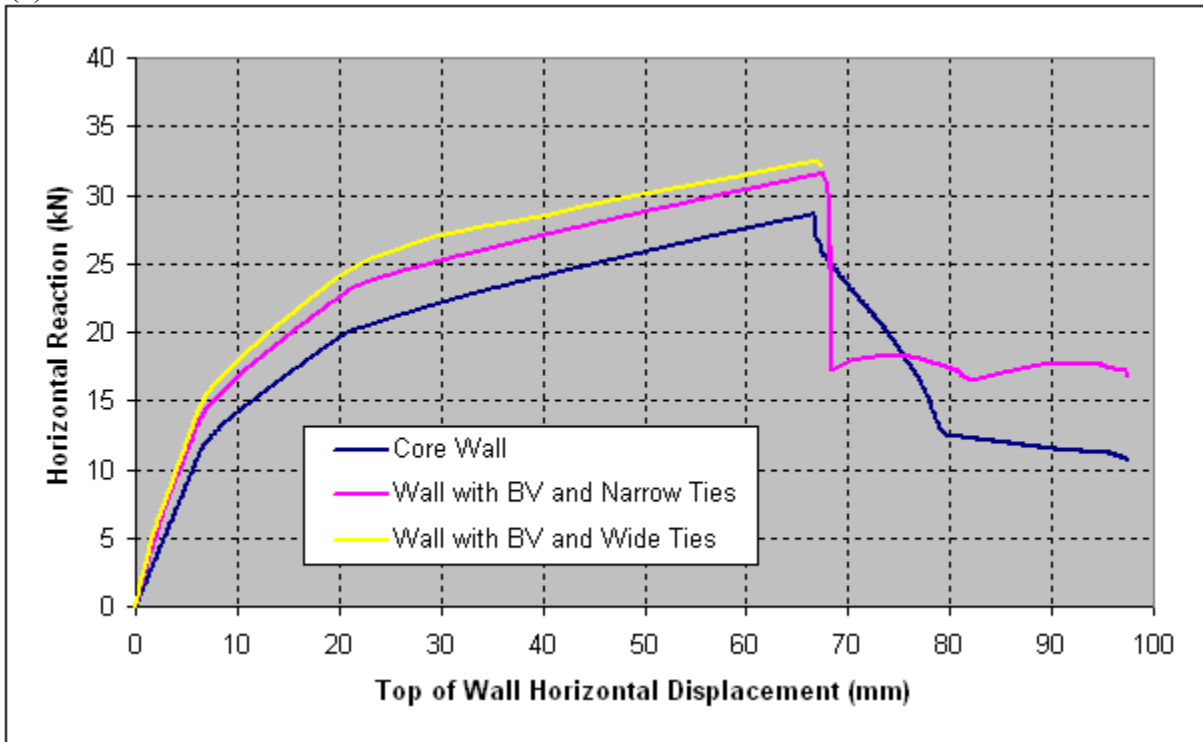
Fig. 3.17. Force vs. displacement relations for anchored brick veneer - light frame wood shear walls. (a) Without OSB bearing at base, (b) With OSB bearing at base

Light Frame Wood Shear Wall with Gypsum Wallboard Sheathing

An expansion of the core wall model with elements that approximated the GWB sheathing and corresponding screw type fasteners yielded the FE model used in the subsequent analyses. Calculated force-displacement relations for this wall in the cases when the OSB sheathing was allowed to deform freely, and when it was constrained to bear against the foundation base once the prescribed gap would close are shown in Fig. 3.18. The initial stiffness prediction of 2.368 kN/mm was identical in both considered cases. It represented a 33% improvement over the initial stiffness of the core wall. The strengthening effect of the GWB sheathing extended into the nonlinear range up to displacements of 22.6 mm and 25.5 mm, respectively. At these displacement levels the wallboard fasteners at the panel edges passed their strength limit and crossed into the descending part of their constitutive relations. Consequently, local peaks in the absorbed wall force were established at 25.21 kN and 28.92 kN, respectively. The subsequent sharp drop in the absorbed force was followed by a prolonged gradual recovery that exceeded the preceding local maximums. However, the reached racking strengths of 26.28 kN and 32.04 kN, respectively were lower then the corresponding values for the core walls by about 8%. Notably, a slight decrease in wall ductility ensued in both cases.

Anchored Brick Veneer - Light Frame Wood Shear Wall with Gypsum Wallboard Sheathing

The FE model for this wall encompassed all constituent wall components and boundary conditions deemed pertinent in analyzing wall behavior. Two 22 ga tie designs, designated as narrow type and wide type, were considered in each of the two cases of OSB sheathing bearing against the foundation base (unconstrained and constrained). Calculated force-displacement relations for these wall models are shown in Fig. 3.19. While they followed the general shape of the corresponding relations for the core wall, they were highly influenced by the presence of GWB sheathing as evidenced by the appearance of local maximums in the curves occurring when the GWB fastener connections started to fail. The predictions for initial stiffness values were 3.254 kN/mm in the case with narrow ties, and 3.764 kN/mm in the case with wide ties. These values amounted to 83 % and 112 % increase over the initial stiffness of the core wall, or an equivalent 37 % and 59 % increase over the initial stiffness of the wall with added GWB

sheathing. A comparison of initial stiffness values for all considered wall cases as given in Table 3.4 revealed that the simultaneous addition of GWB sheathing on the interior wall face and anchored BV on the exterior wall face was not just additive to the initial stiffness of the integral wall, but that there was also some minor synergy.

The wall models in which the brick veneer was anchored to the wood backing with the wider, stronger ties had larger load carrying capabilities compared with the ones in which the ties were narrower and weaker. This effect was more pronounced in the case when the OSB sheathing was allowed to bear on the base foundation. Interestingly, the local maximums of absorbed wall forces for both tie designs in both cases of OSB base boundary conditions formed a narrow range between 28.24 kN and 29.32 kN, as if a common cap on the force existed that was set by the failing of the GWB fastener connections. Having this in mind and considering the fact that the addition of brick veneer had a stiffening effect on the integral wall, these local maximums appeared at smaller displacement levels. The stiffer the wall was, the smaller the wall displacement level at which the GWB fasteners started to fail. In all cases a sharp drop in the absorbed forced ensued, followed by a gradual recovery that exceeded the preceding local maximums. The achieved racking strengths in the cases when the OSB bearing was unconstrained at its base were around 29 kN for both considered tie designs, a slight increase of 2 % – 3 % over the strength of the core wall, but a more prominent increase over the strength of a wall with added GWB sheathing (10 % – 12 %). A different look on the same numbers revealed that the addition of GWB sheathing to a wood shear wall with anchored brick veneer decreased the racking strength by 8 % – 9 %. In the cases when the OSB was allowed to bear on its base, the wall racking strengths were estimated at 33.21 kN and 37.92 kN for the narrow and wide ties, respectively. A comprehensive comparison of racking strength values for all wall designs is given in Table 3.5. Notably, the wall model with the narrow ties appeared more ductile regardless of the considered OSB boundary conditions at its base.

(a)
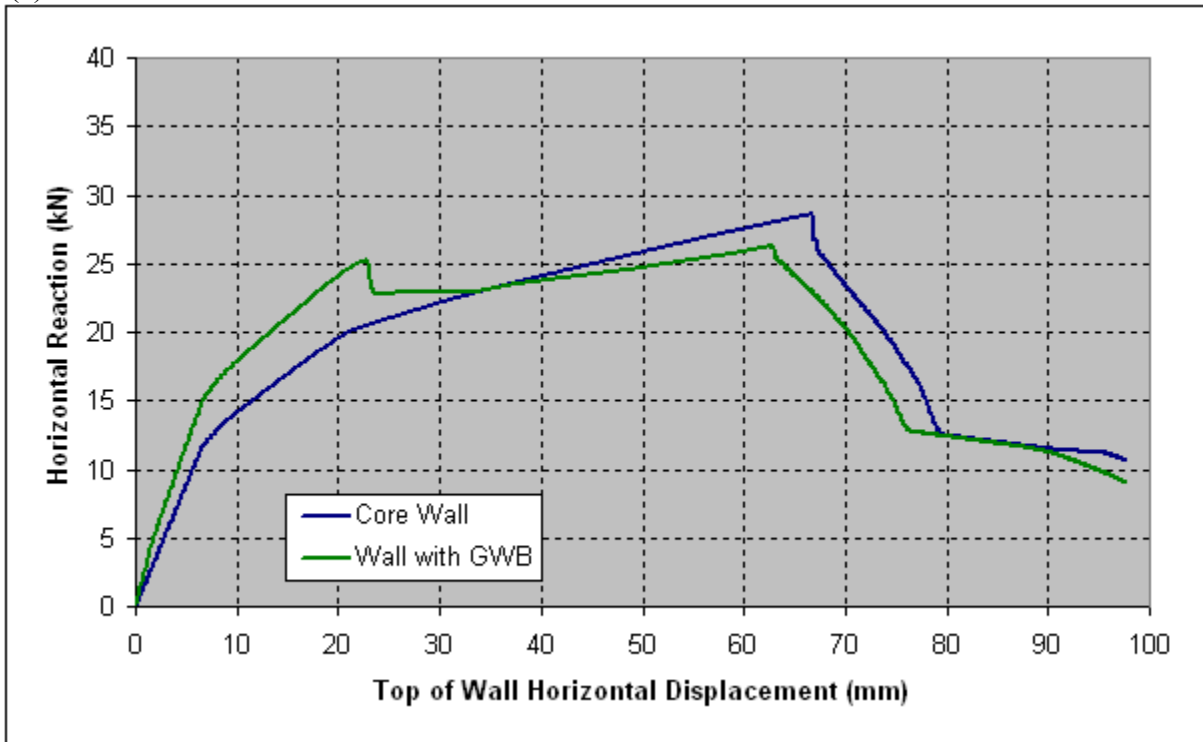
(b)
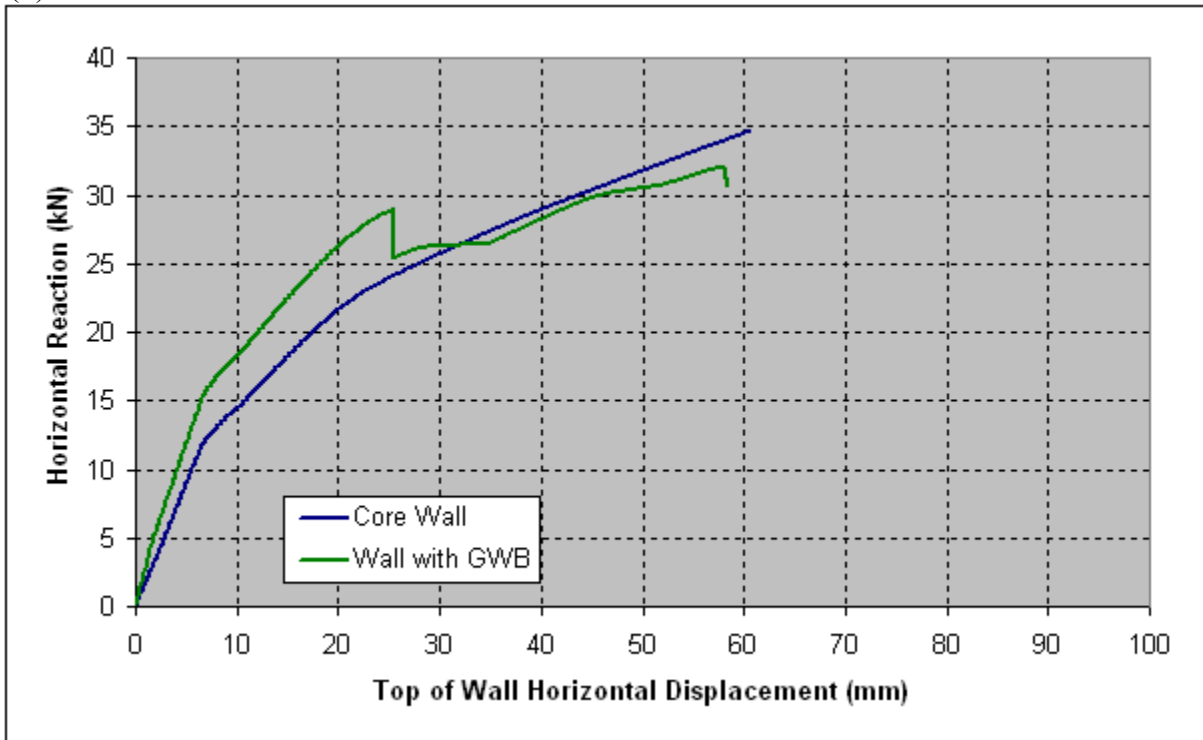
Fig. 3.18. Force vs. displacement relations for light frame wood shear walls with gypsum
wallboard sheathing. (a) Without OSB bearing at base, (b) With OSB bearing at base
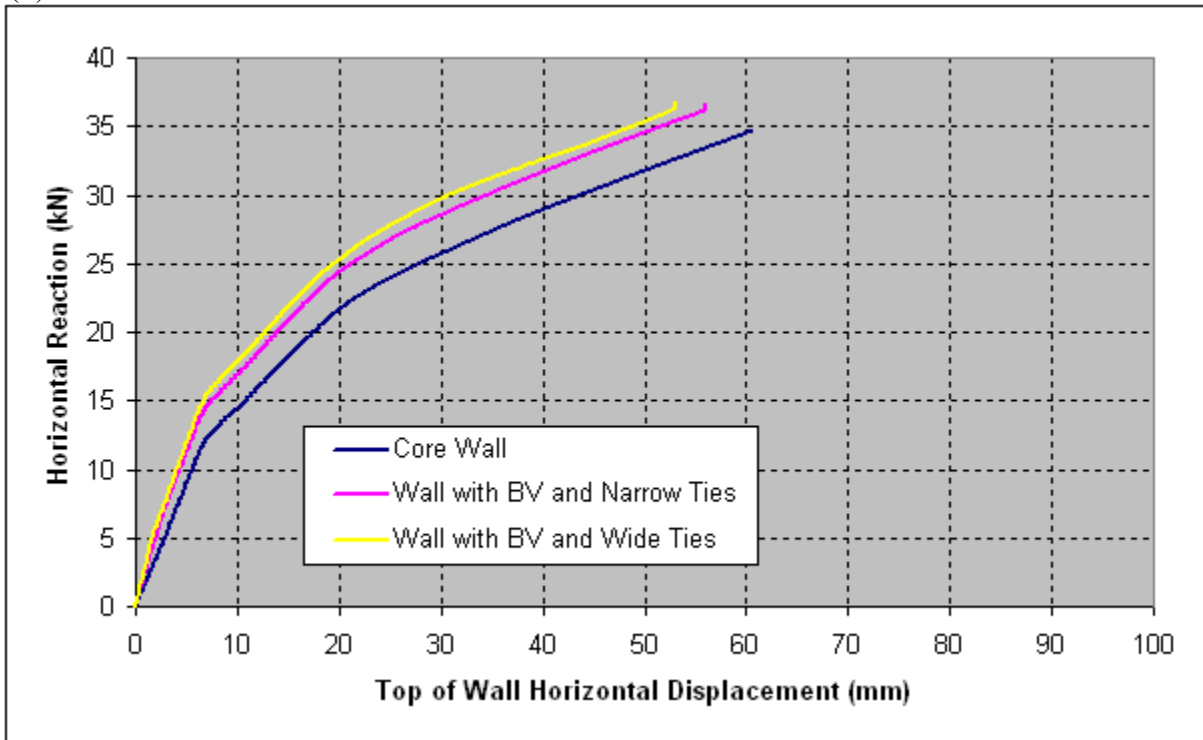
(a)
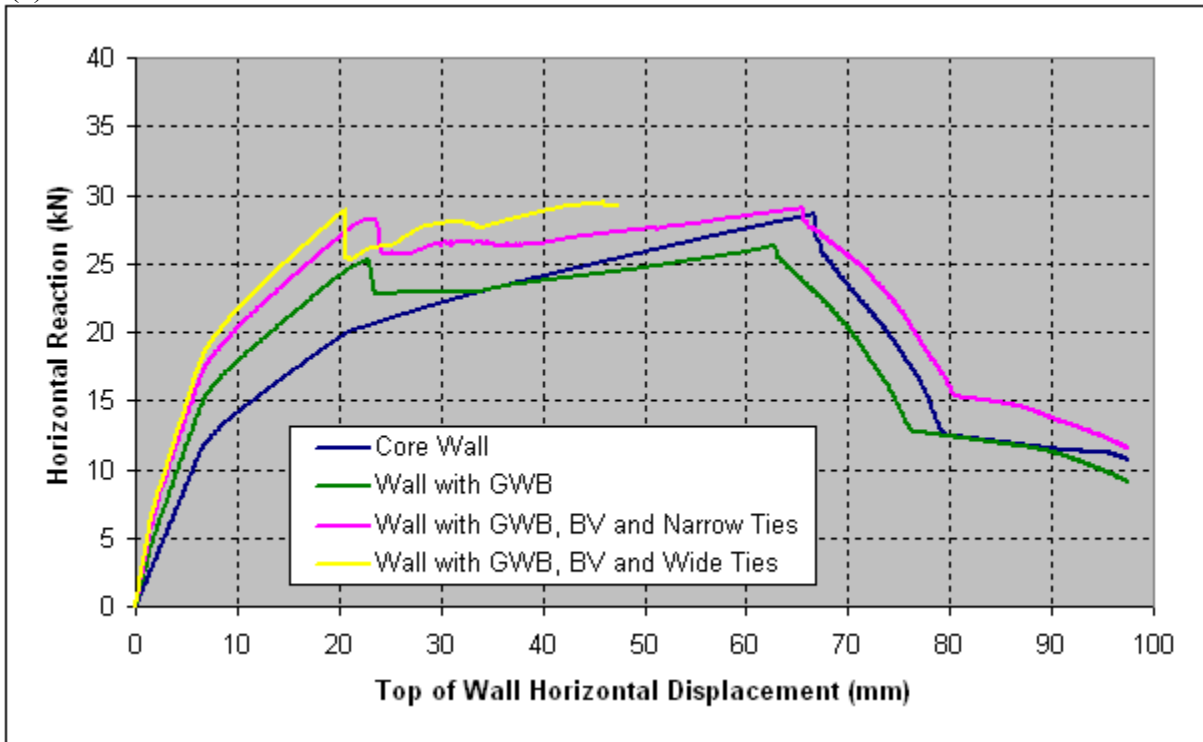
(b)
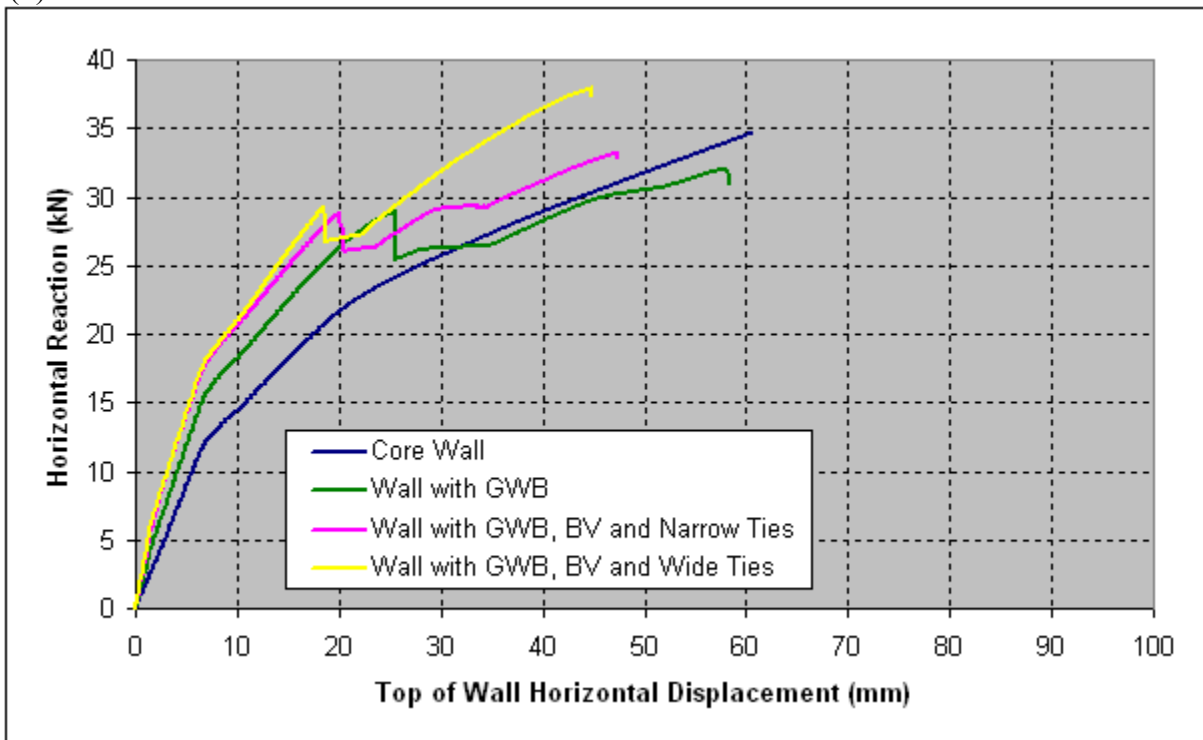
Fig. 3.19. Force vs. displacement relations for anchored brick veneer - light frame wood shear walls with GWB sheathing. (a) Without OSB bearing, (b) With OSB bearing at base

81

Table 3.4. Comparison of initial stiffness values for considered wall compositions

Wall Composition	OSB	OSB GWB	OSB BVnt	OSB BVwt	OSB GWB BVnt	OSB GWB BVwt
OSB	**1.775**	33.38%	41.33%	60.21%	83.29%	112.00%
OSB GWB		**2.368**	5.96%	20.11%	37.42%	58.95%
OSB BVnt			**2.509**	13.36%	29.70%	50.01%
OSB BVwt				**2.844**	14.41%	32.33%
OSB GWB BVnt					**3.254**	15.66%
OSB GWB BVwt						**3.764**

(Initial stiffness values are given in units of kN/mm and displayed in boldface.)

Table 3.5. Comparison of racking strength values for considered wall compositions

	Wall Composition	OSB	OSB GWB	OSB BVnt	OSB BVwt	OSB GWB BVnt	OSB GWB BVwt
Without OSB Bearing at Base	OSB	**28.58**	-8.06%	10.33%	13.43%	1.52%	2.95%
	OSB GWB		**26.28**	20.00%	23.37%	10.41%	11.97%
	OSB BVnt			**31.53**	2.81%	-7.99%	-6.69%
	OSB BVwt				**32.42**	-10.51%	-9.24%
	OSB GWB BVnt					**29.01**	1.41%
	OSB GWB BVwt						**29.42**
With OSB Bearing at Base	OSB	**34.63**	-7.46%	4.53%	4.64%	-4.09%	9.49%
	OSB GWB		**32.04**	12.96%	13.07%	3.64%	18.32%
	OSB BVnt			**36.20**	0.10%	-8.25%	4.74%
	OSB BVwt				**36.23**	-8.34%	4.64%
	OSB GWB BVnt					**33.21**	14.16%
	OSB GWB BVwt						**37.92**

(Racking strength values are given in units of kN and displayed in boldface.)

Cyclic Analysis

Light Frame Wood Shear Wall

Validation of the cyclic analysis procedure was performed by comparing calculated results from cyclic analysis of a model wall to existing experimental data from Dinehart and Shenton (1998). This sample model differed from the core wall part of the benchmark model implemented in the pushover analyses in regard to utilizing denser, 102 mm, fastener spacing on the edges of the frame. The sample wall parameters are given in Table 3.6, while Table 3.7 summarizes data for peak force, corresponding displacement, and force per unit wall length in each of the three consecutive loading half-cycles that constituted the loading history (Fig. 3.20) applied proportionally to all frame nodes at the header level. The first half-cycle limited the force to the design load, the second one doubled the previous, and the third reached for the ultimate. The force-displacement relation for this validation wall sample assessed with the OpenSees model is shown in Fig. 3.21 superimposed on experimental data from Dinehart and Shenton (1998). The initial stiffness calculated with the model was 2.23 kN/mm, and it under predicted the actual value of 2.35 kN/mm by 5 %. In the first half-cycle the model behavior was entirely linear, a minor difference from the experimental results. The nonlinearities became evident in the second half-cycle. The model slightly over predicted the stiffness in the nonlinear range and reached the limiting value of twice the design force at smaller displacement level. The unloading that went with the initial stiffness left a permanent displacement of 9 mm that reasonably matched the recorded value. The prediction for the final half-cycle was fair up to a displacement of about 50 mm, when the model continued to gain strength, while the actual wall yielded.

The loading history implemented in the cyclic analysis of all stages of the benchmark model is shown in Fig. 3.22. It consisted of six full cycles with progressively increasing displacement amplitudes in increments of 12.2 mm (0.5 % of the wall height). The loading was applied as a uniform horizontal displacement to all frame nodes at the header level. The resulting force-displacement relation for the core wall model without the OSB bearing on the foundation base is shown in Fig. 3.23 along with the corresponding relation obtained from the static pushover analysis. The response under the cyclic loading was characterized with pinched hystereses and

Table 3.6. Parameters of the sample wall used for model validation under cyclic load condition

Wall sample	Wall length (m)	height (m)	Stud spacing (m)	type	Sheathing length (m)	height (m)	thickn. (mm)	orient.	Fastener type	Fastener spacing edge (mm)	field (mm)
1	2.44	2.44	0.406	OSB	1.22	2.44	12.7	vertical	8d nail	101.6	304.8
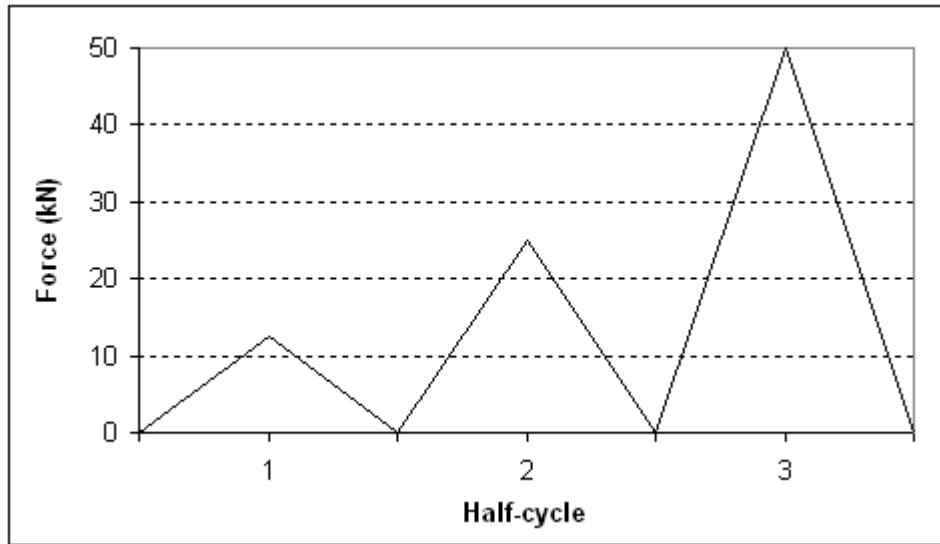
Fig. 3.20. Load history implemented in the model validation procedure

Table 3.7. Summary of analytical predictions and experimental results for cyclic loading

Wall sample	Cycle numb.	descrip.	Peak load (kN)	Corresp. displ. (mm)	Unit load (kN/m)	Result type	Source
	1	design load	12.28	5.2	5.04	experimental	Dinehart and Shenton (1998)
			12.24	5.5	5.02	analytical	OpenSees model
1	2	2×design load	25.37	25.8	10.40	experimental	Dinehart and Shenton (1998)
			25.33	21.5	10.39	analytical	OpenSees model
	3	ultimate	31.90	79.2	13.08	experimental	Dinehart and Shenton (1998)
			34.64	72.5	14.21	analytical	OpenSees model
			36.37	–	14.92	analytical	Tuomi and McCutcheon (1978)

(a)
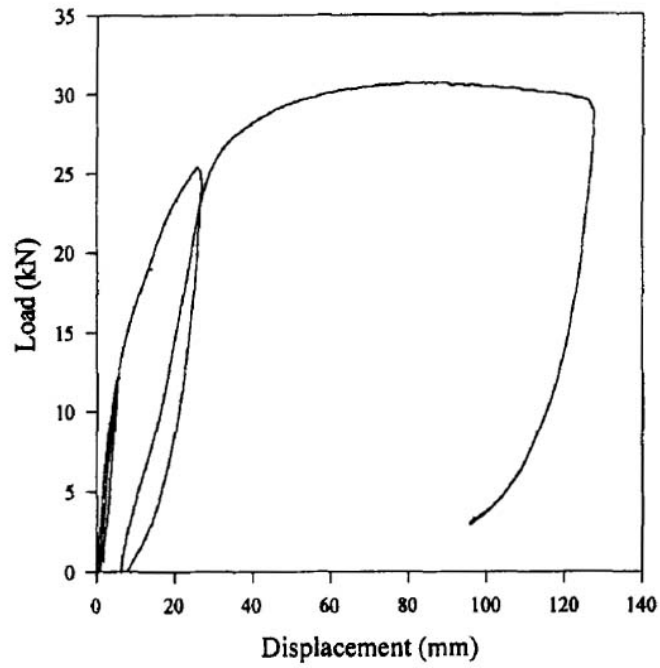
(b)
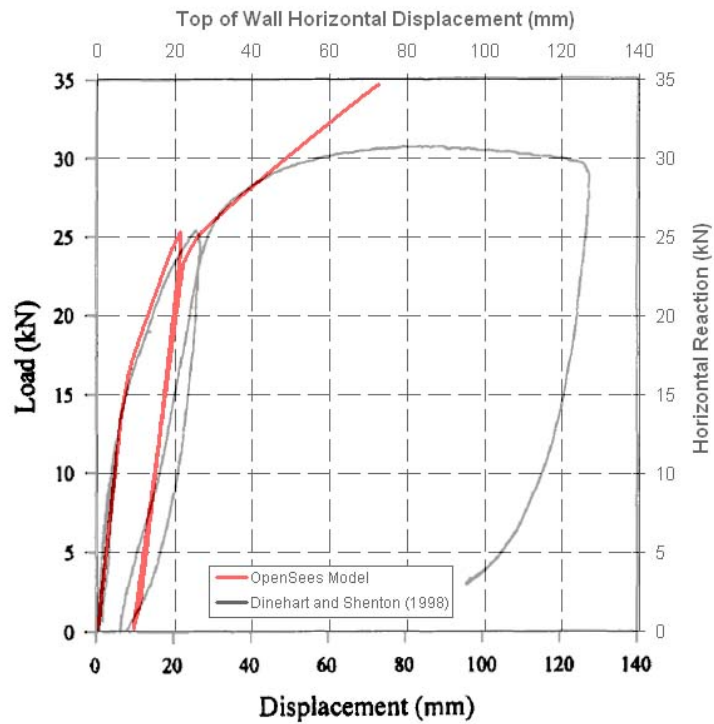
Fig. 3.21. Comparison of analytical predictions and full-scale cyclic test results: (a) Dinehart and Shenton (1998)[1], (b) OpenSees model overlay

---

progressively increasing strength, although at a considerably smaller rate compared to the pushover loading case. The maximum force of 24.94 kN was reached in the fifth cycle at a displacement of 61 mm. It constituted a 13 % decrease from the strength estimate obtained in the pushover loading case. The response in the last cycle was stable, but the obtained maximum force was in the post ultimate zone.

Anchored Brick Veneer - Light Frame Wood Shear Wall

An attempt was made to verify under cyclic loading conditions the beneficial effects resulting from the addition of brick veneer anchored to the wood shear wall that were revealed under the pushover loading case. Calculated force-displacement relations for a model wall utilizing narrow type ties and unconstrained OSB sheathing at its base under both loading conditions are shown in Fig. 3.24. Although the cyclic analysis failed prematurely in the midst of the third cycle it was sufficient to expose that the repetitive nature of the loading in the post yielding phase had the potential to reduce the achieved wall strength. It also appeared that the rate of gradual strength increase at larger displacement levels had a diminishing tendency.

The nonlinear response of the integral wall was characterized with pinched hystereses up to the abrupt simulation failure. A comparison with the corresponding behavior of the core wall as shown in Fig. 3.25, led to a conclusion that the addition of anchored brick veneer increased markedly the integral wall stiffness, strength and energy absorption capacity in the initial loading cycles. These benefits seemed to mitigate as the repetitions progressed toward larger displacement intervals. Clearly, the core wall appeared much more ductile since its simulation went successfully through the whole cyclic loading regime.

Light Frame Wood Shear Wall with Gypsum Wallboard Sheathing

A comparison of calculated force-displacement relations under cyclic and pushover loading conditions for a wall model with interior GWB sheathing in which the OSB sheathing was unconstrained at its base is shown in Fig. 3.26. The repetitive nature of the loading seemed to moderately soften the wall in the initial loading cycles as manifested with a slight decrease in the intensity of the absorbed force. However, after the force drop caused by the failure in the wallboard fasteners, the envelope of the cyclic force-displacement relation reverted to the

corresponding relation under pushover loading and reached a maximum of 25.71 kN. The analysis progressed successfully for four loading cycles and failed prematurely near the completion of the first half of the fifth cycle. Up to that point the nonlinear response of the wall was characterized with pinched hystereses. When compared to the corresponding behavior of the core wall as shown in Fig. 3.27, a conclusion could be made that the addition of interior GWB sheathing increased significantly the stiffness, strength and energy absorption capacity in the initial loading cycles. These benefits diminished as the repetitions progressed toward larger displacement intervals. Notably, the core wall model appeared to be more ductile as it was able to sustain the whole simulated cyclic loading regime and venture into the post ultimate region.

Dynamic Analysis

In order to model the mass from actual dwelling conditions realistically, in addition to the wall component weight, a surface load of 1.92 kN/m^2 acting on a 3.66 m tributary length was spread to all frame nodes at the header level. Appropriate masses were assigned accordingly. These additional masses totaling 1.74 tons accounted for the adjoining diaphragm.

The acceleration time history recorded at the El Centro station from the May 19, 1940 Imperial Valley earthquake was chosen as a representative load for dynamic analysis. The record shown in Fig. 3.28 had a peak ground acceleration of 0.313 g and it was applied in the in-plane horizontal direction.

The dynamic analysis advanced the solution in 0.01 sec time increments utilizing the Newmark's direct integration method with parameters γ and β set to 0.5 and 0.25, respectively. A Rayleigh damping matrix was calculated from the stiffness matrix at the last-committed state assuming a 2 % damping ratio.

Light Frame Wood Shear Wall

Time histories of the horizontal displacement at the top left corner of the frame, and the base shear obtained from the analysis of the core wall part of the benchmark model without OSB bearing at the base are shown in Figs. 3.29 and 3.30, respectively. The displacements were within 10 mm in either direction, while the prediction for the extreme base shear of 13.93 kN

87
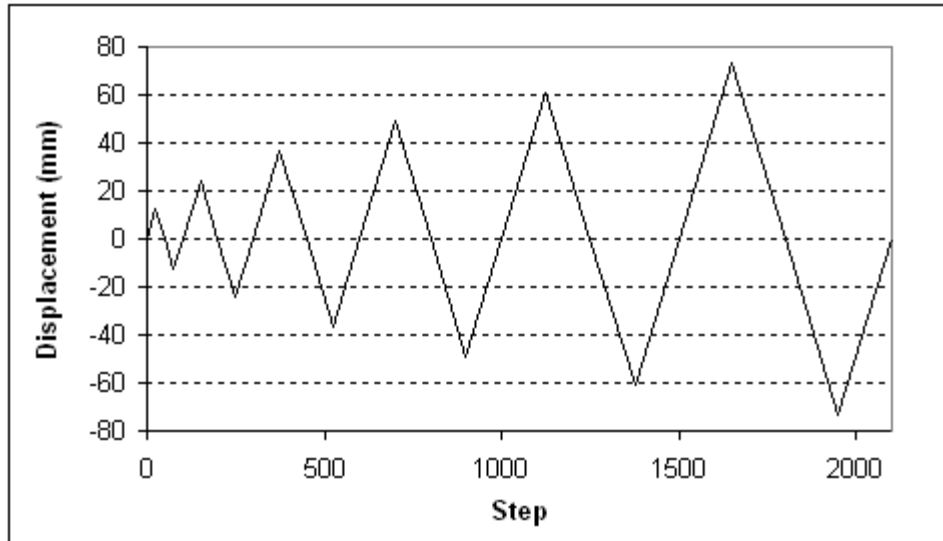
Fig. 3.22. Load history implemented in the cyclic analysis
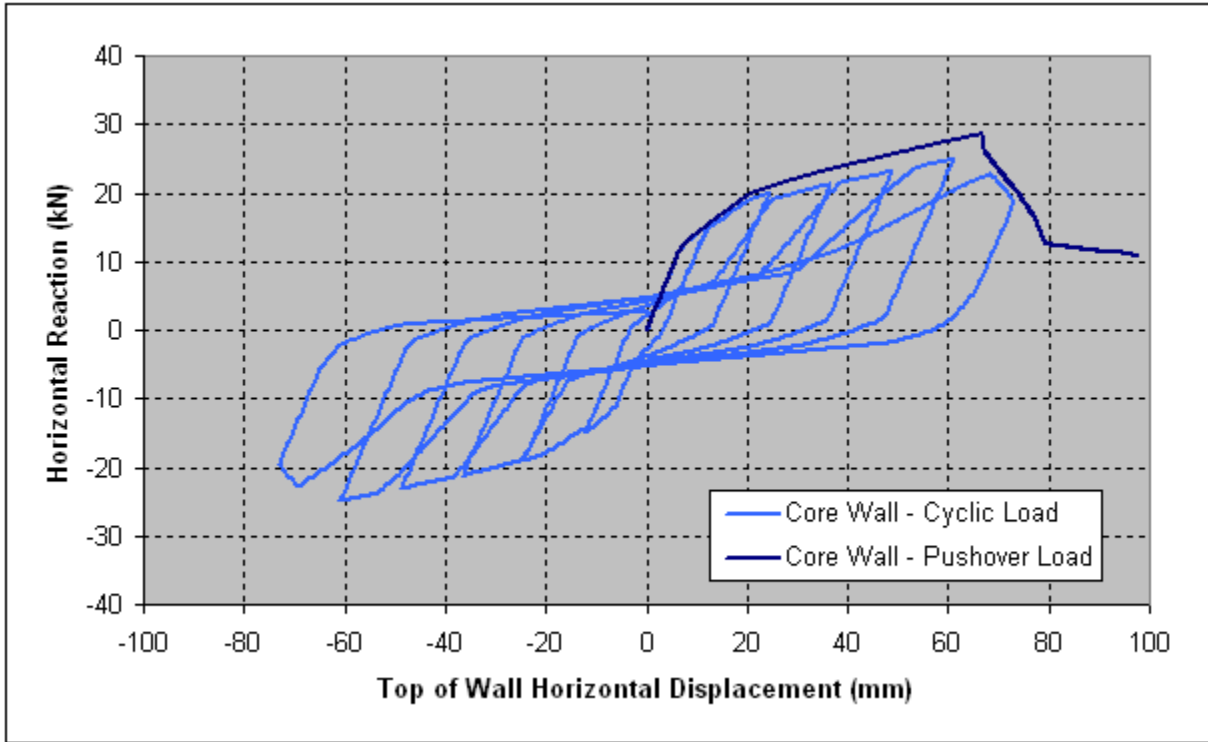
Fig. 3.23. Force vs. displacement relations for the light frame wood shear wall under cyclic and pushover loading
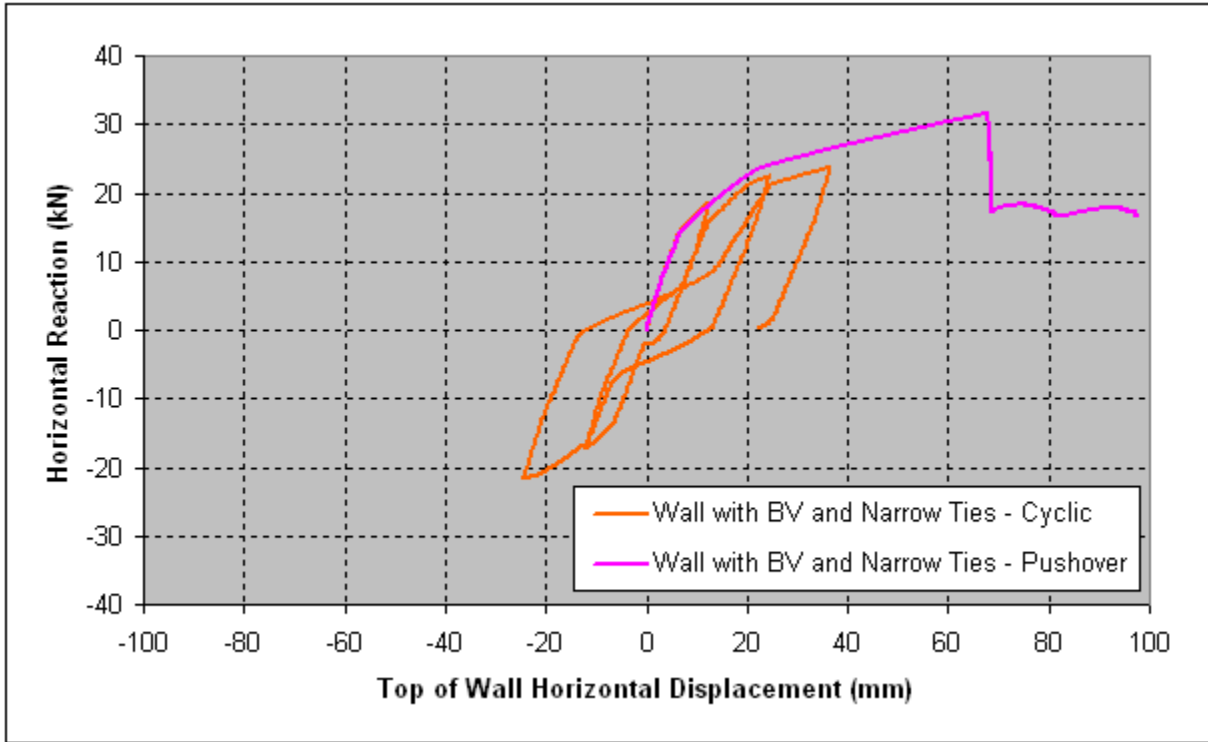
Fig. 3.24. Force vs. displacement relations for the anchored brick veneer - light frame wood shear wall under cyclic and pushover loading
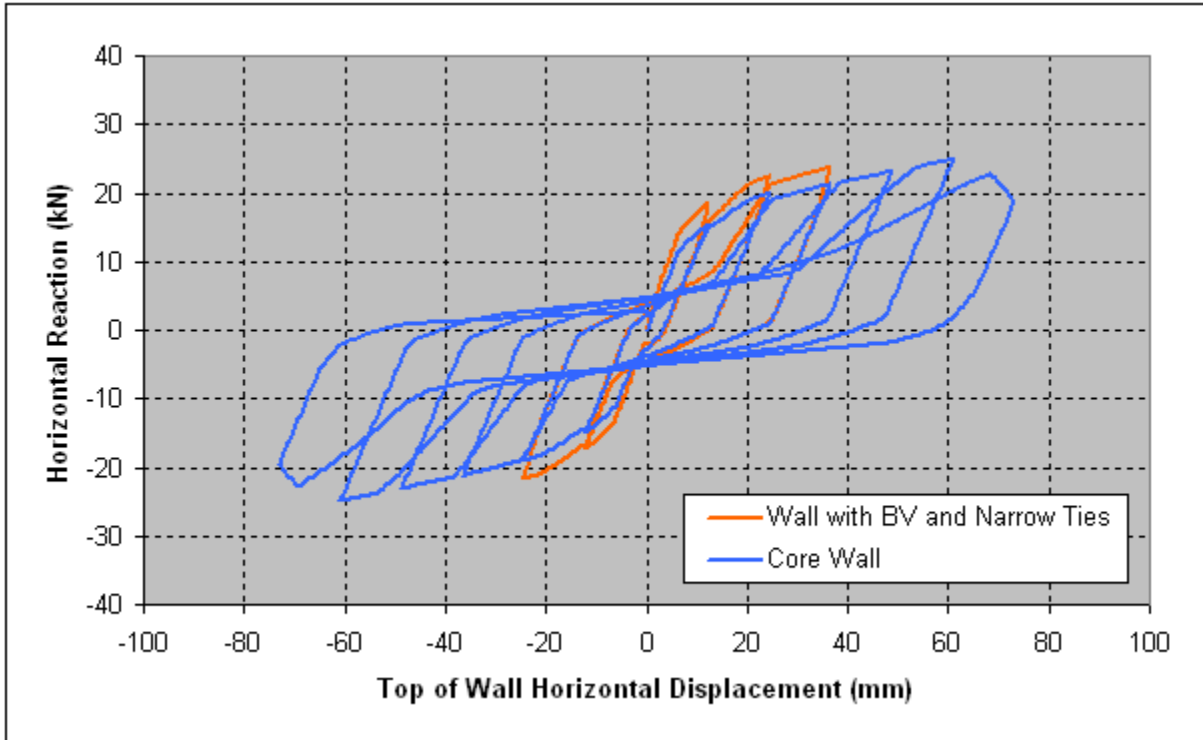
Fig. 3.25. Effect of exterior brick veneer on the behavior of light frame wood shear walls under cyclic loading
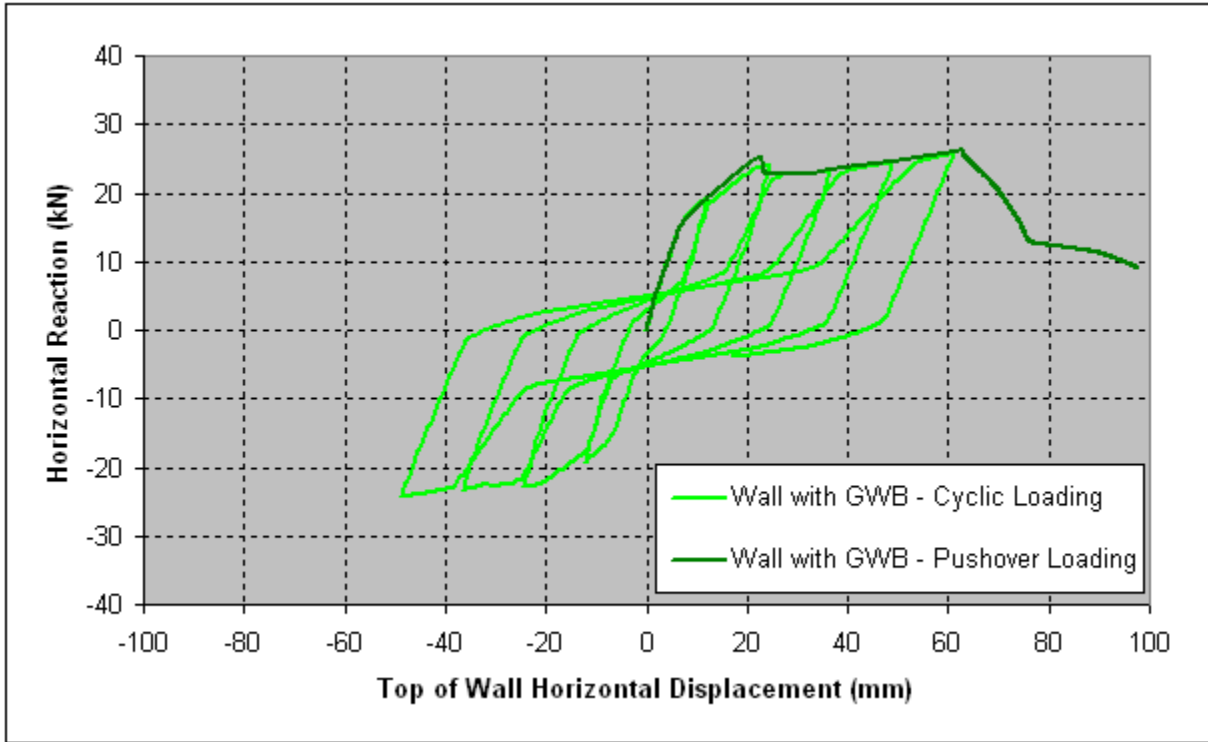
Fig. 3.26. Force vs. displacement relations of the light frame wood shear wall with interior GWB sheathing under cyclic and pushover loading
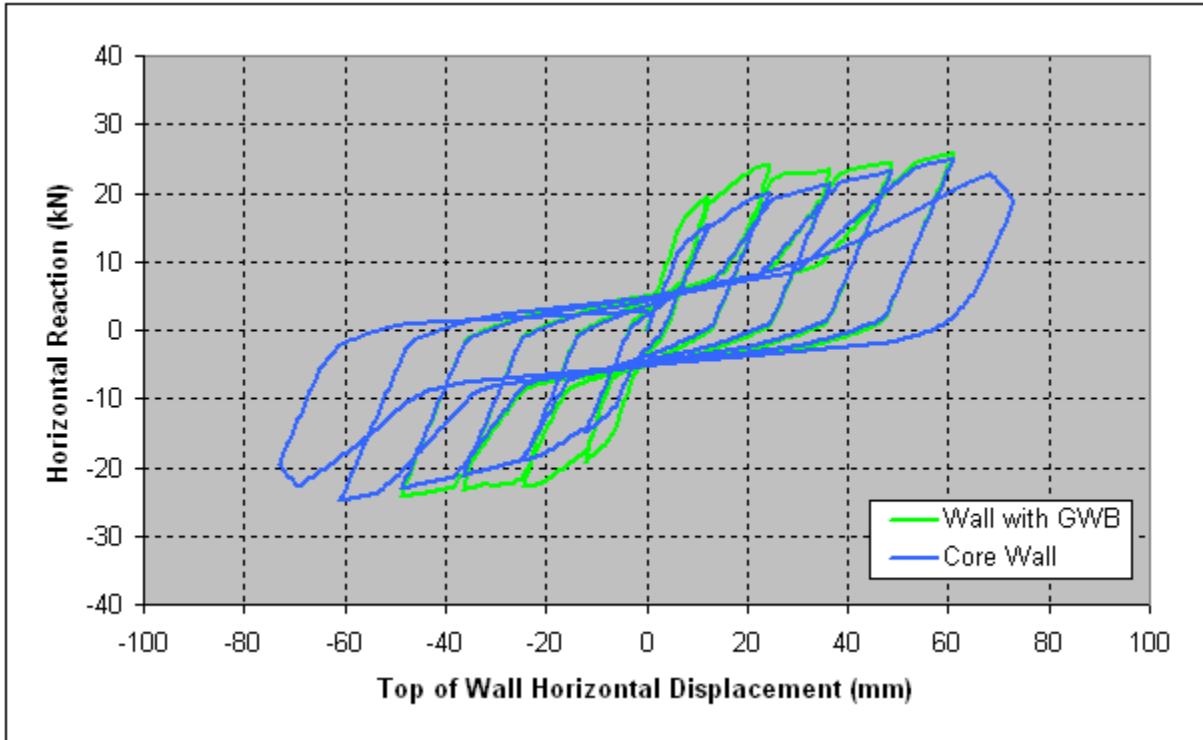
Fig. 3.27. Effect of interior GWB sheathing on the behavior of light frame wood shear walls under cyclic loading

represented 78 % of the total vertical load (Table 3.10). This value amounted to 49 % of the estimated racking strength under unidirectional pushover loading.

Brick Veneer Wall

The FE model for the brick veneer wall was extracted from the existing integral wall model in order to obtain the response under dynamic loading that would serve as a base for comparison with the anchored brick veneer component of the integral wall. The OpenSees model simulation under representative dynamic loading yielded time histories of horizontal displacements at the top left wall corner, and base shear shown in Figs. 3.31 and 3.22, respectively. The wall being quite stiff had very small predicted displacements at the top, while the estimates for the base shear were around the 3 kN range which represented 31 % of its self weight.

Anchored Brick Veneer - Light Frame Wood Shear Wall

The dynamic analysis of the integral wall model under representative earthquake loading revealed that the addition of anchored brick veneer to the core wood shear wall with narrow type ties had considerable beneficial effects on wall behavior. It appeared that an interaction occurred between the anchored brick veneer and its wood wall backing that went beyond the obvious increase in overall wall racking stiffness. This interaction was manifested with simultaneous diminishing of core wall response, and intensifying of brick veneer response. A comparison of horizontal displacement time histories at constituent wall component's tops shown in Fig. 3.33 with corresponding histories obtained from individual wall analyses shown in Figs. 3.29 and 3.31 revealed that the change in response intensity was much more prevalent then the change in response frequency. The addition of anchored brick veneer reduced the core wall displacements at the top from the 10 mm to the 6 mm range, a 37 % decrease, while corresponding displacements at the brick veneer top increased about three fold (Tables 3.8 and 3.9). This significant change in intensity of the displacement response was accompanied with adequate change in base shear as shown in Fig. 3.34. The core wall component absorbed much less force. The prediction for base shear it attracted fell to the 9 kN range, a 35 % drop. At the same time the base shear attracted by the anchored brick veneer more than doubled from the previous 3 kN to the 7 kN range (Tables 3.11 and 3.12). Interestingly, there was no noticeable change in the

integral wall total base shear range compared to the adequate range of the core wall, despite the added veneer mass equaling 55 % of the mass of the core wall (Table 3.10).

Light Frame Wood Shear Wall with Gypsum Wallboard Sheathing

The FE analysis of the wall model approximating a light wood frame sheathed with OSB on the exterior side, and GWB on the interior side under the selected earthquake loading showed that the addition of GWB sheathing stiffened the core wall and altered the intensity of the response. The horizontal displacements at the top of the wall shown in Fig. 3.35 peaked at 6.9 mm, which represented a 29 % drop from the 10 mm range predicted for the core wall (Table 3.8). While the drop in displacements caused by the added GWB sheathing was comparative in magnitude to the case of anchoring brick veneer to the core wall, there was no accompanying decrease in base shear. As Fig. 3.36 shows, the demand in base shear from the representative earthquake loading actually increased by 11 % to 15.39 kN (Table 3.11).

Anchored Brick Veneer - Light Frame Wood Shear Wall with Gypsum Wallboard Sheathing

Results from the predicted dynamic response of the integral wall model composed of all constituent wall components under representative earthquake loading revealed that the benefits from adding anchored brick veneer intensified once the interior GWB sheathing was taken into consideration as a contributing structural component. The predicted horizontal displacements of the top of the individual wall components are shown in Fig. 3.37. In the wood shear wall component they decreased to the 4.0 mm range, a 60 % drop compared to the core wall, or an equivalent 44 % drop compared to the core wall sheathed with GWB. The displacements in the brick veneer component increased considerably, but still remained very small.

At the same time the predicted demand for base shear in the wood wall component peaked at 8.25 kN, a significant reduction of about 37 % compared to the core wall (Fig. 3.38 and Table 3.11). The estimates for the base shear in the brick were in the 6.00 kN range, an increase of 93 % over the corresponding value for the core wall, or an equivalent decrease of 11 % from the corresponding value for the anchored brick veneer wall without GWB sheathing (Table 3.12). Again, there was only a minor change in integral wall total base shear range compared to the range of the core wall.
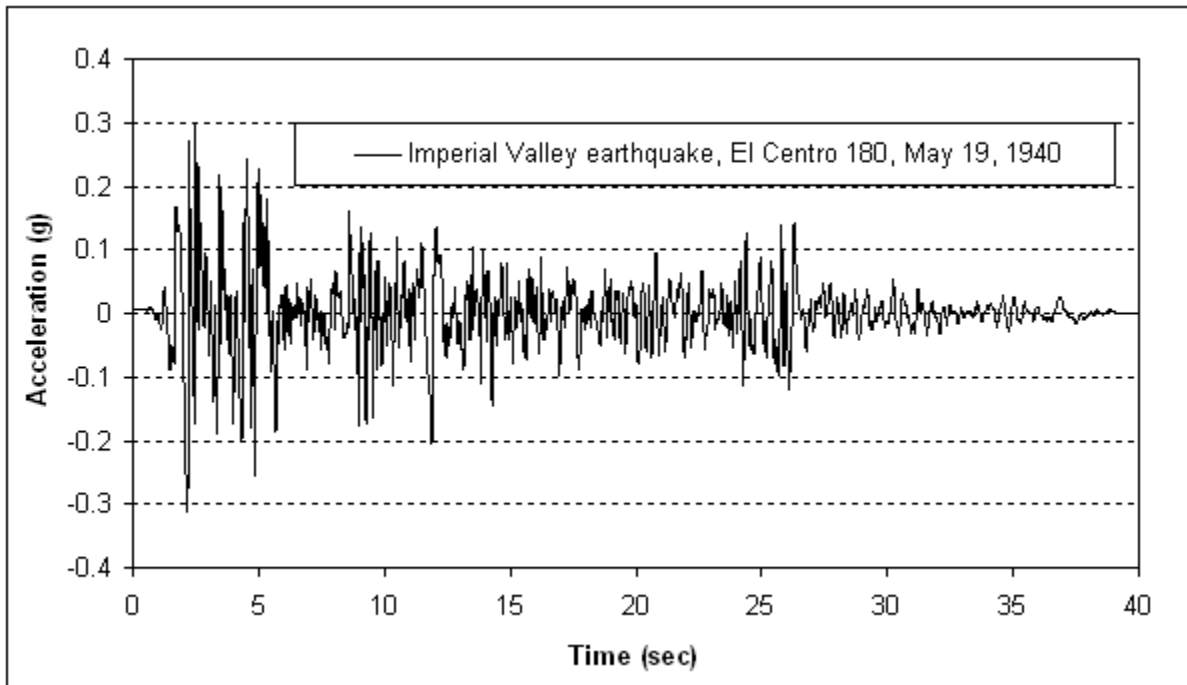
Fig. 3.28. Acceleration record of the 1940 Imperial Valley, California earthquake implemented in the dynamic analysis
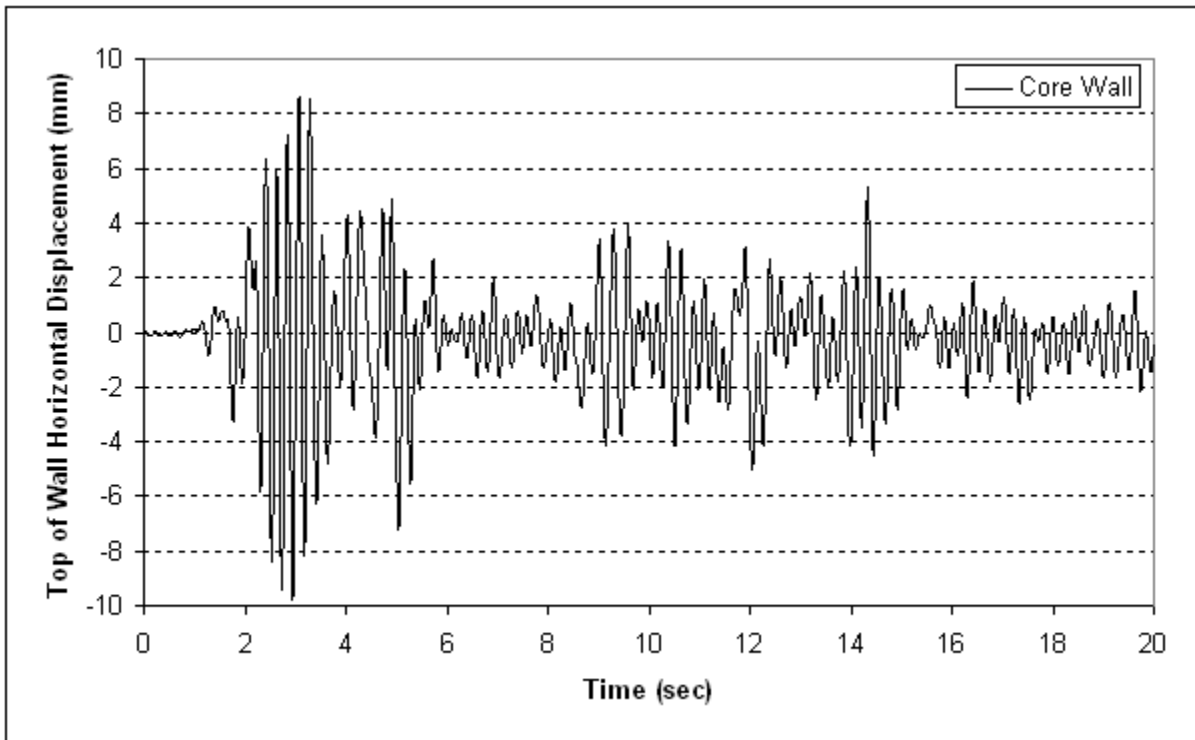
Fig. 3.29. Horizontal displacement time history of the top left corner of the frame for a light frame wood shear wall
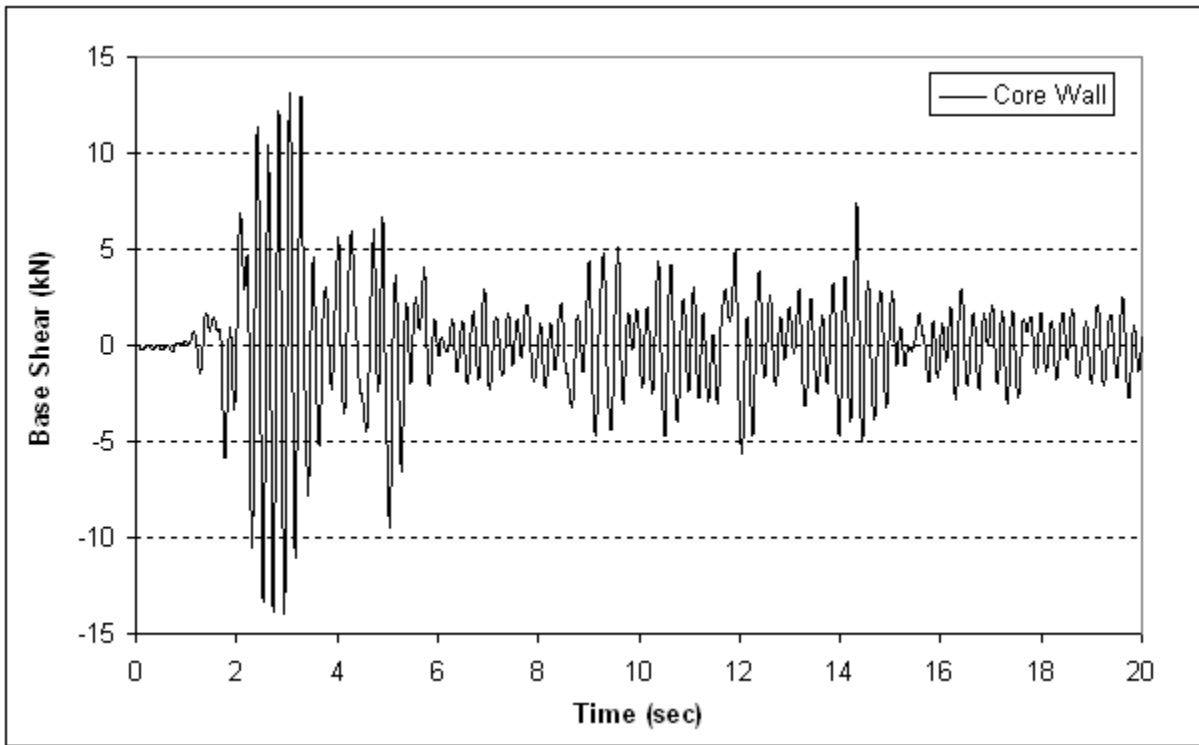
Fig. 3.30.   Base shear time history for the light frame wood shear wall
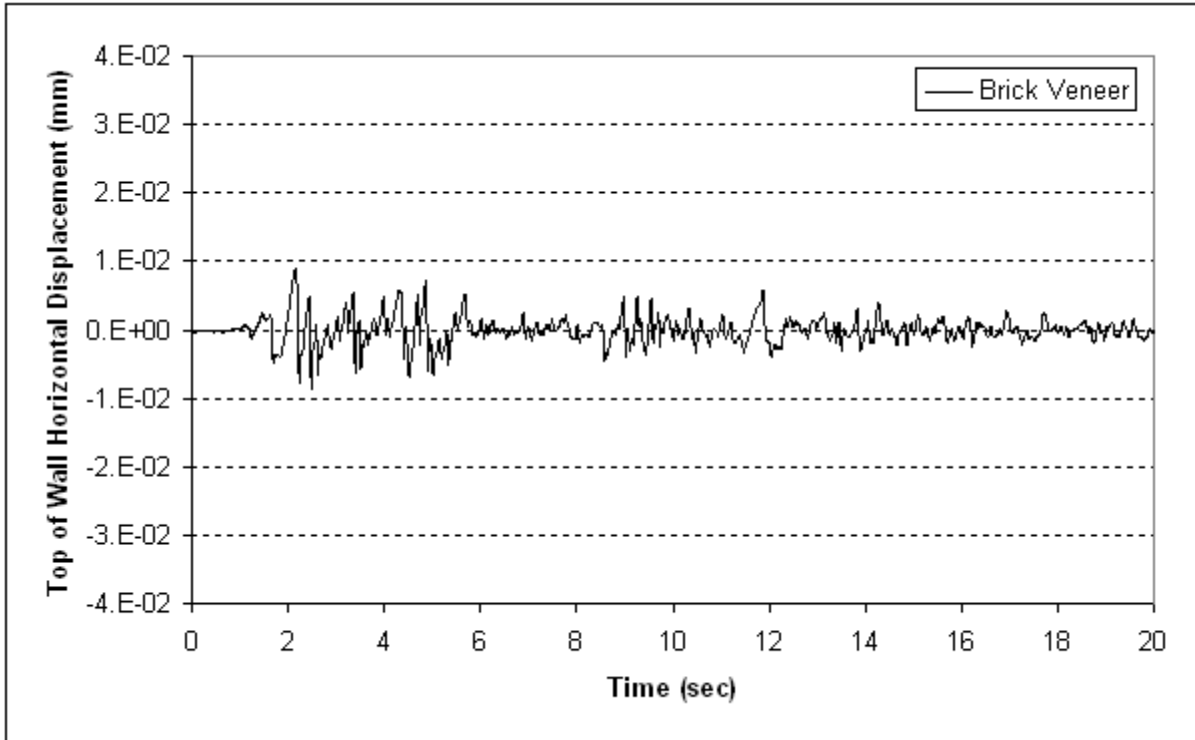
Fig. 3.31. Horizontal displacement time history of the top left corner of the brick veneer wall
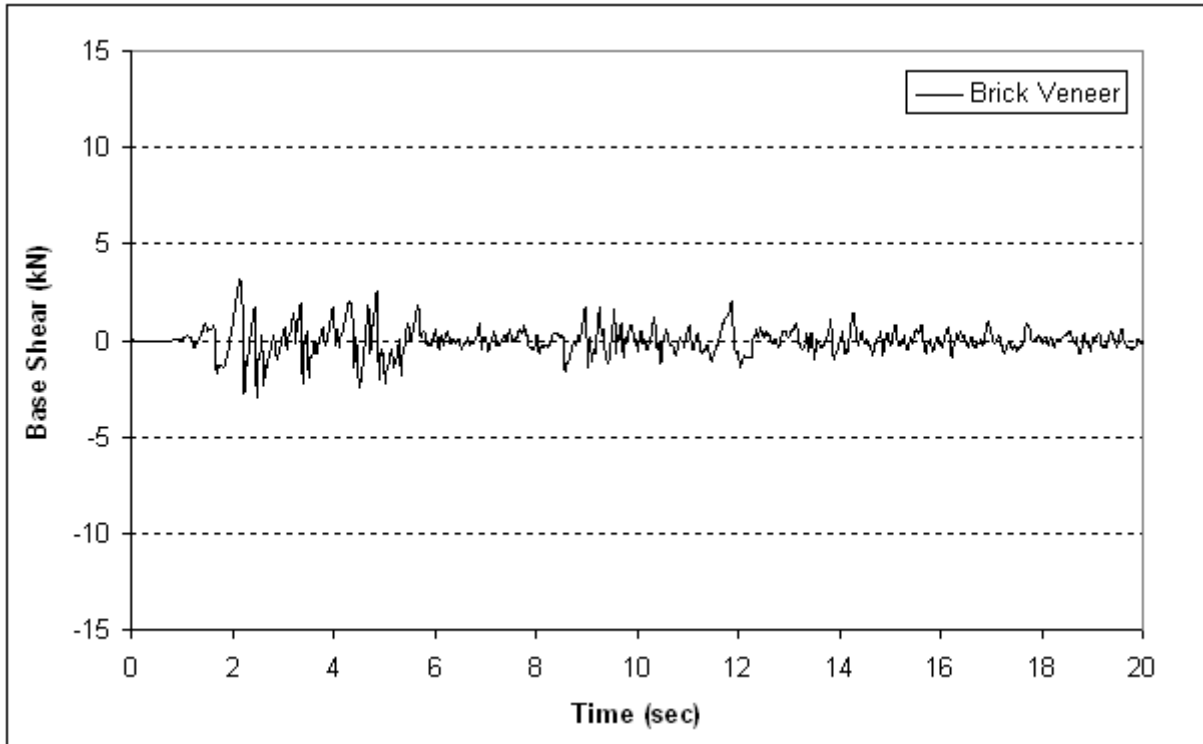
Fig. 3.32.   Base shear time history for the brick veneer wall

(a)

(b)
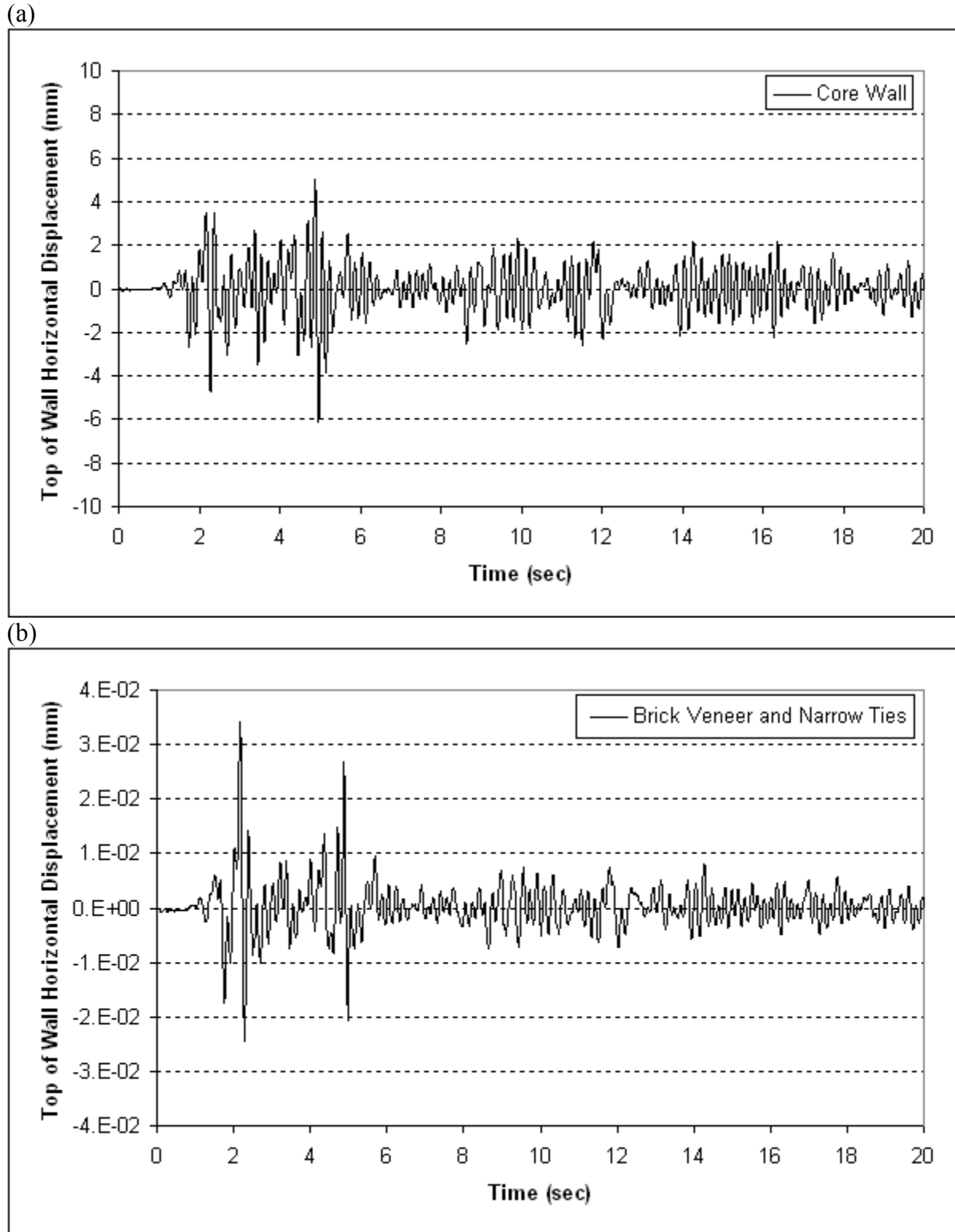
Fig. 3.33. Horizontal displacement time history of the top left corner of the (a) frame, and (b) brick veneer of the anchored brick veneer – light frame wood shear wall

101
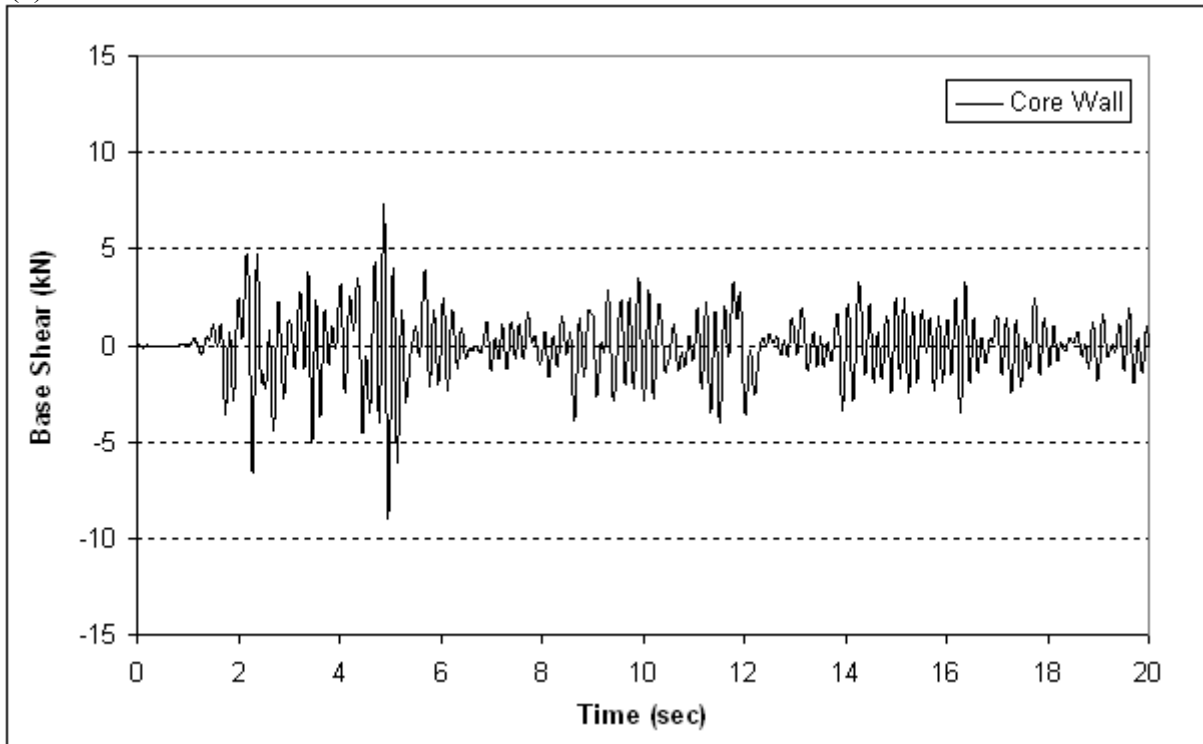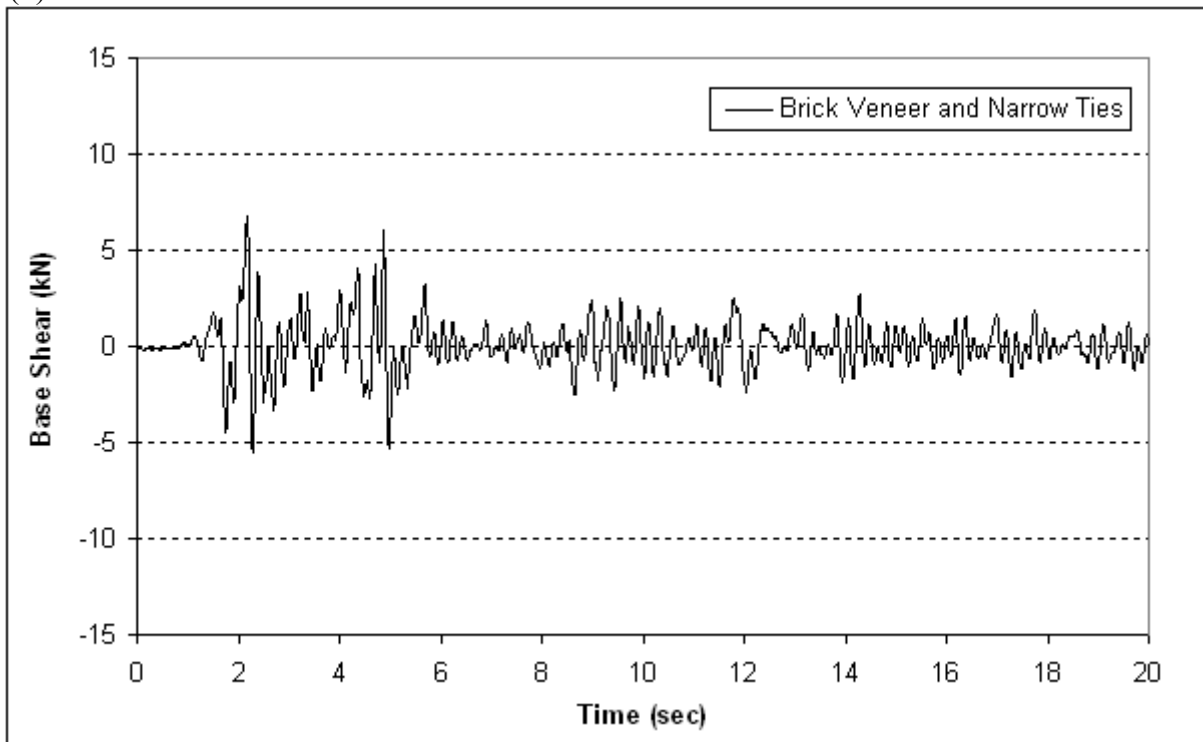
Fig. 3.34. Base shear time history for the (a) core wall, and (b) brick veneer of the anchored brick veneer – light frame wood shear wall
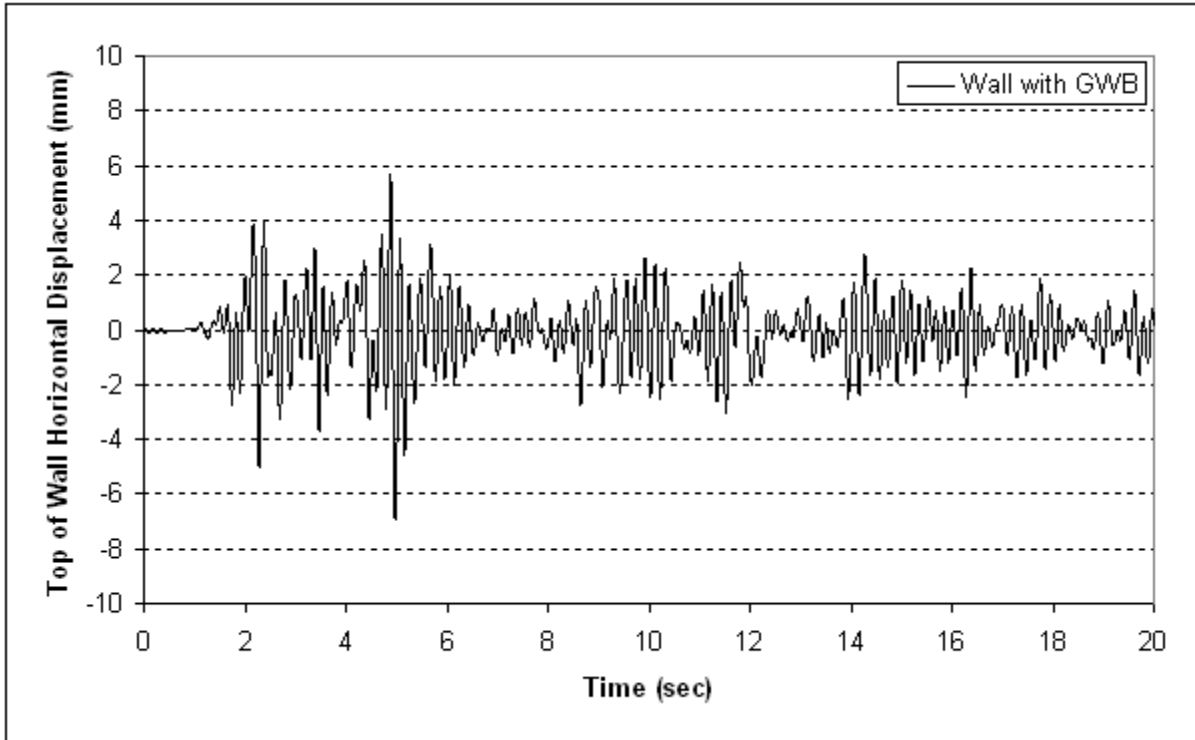
Fig. 3.35. Horizontal displacement time history of the top left corner of the frame for a light frame wood shear wall with gypsum wallboard sheathing

103
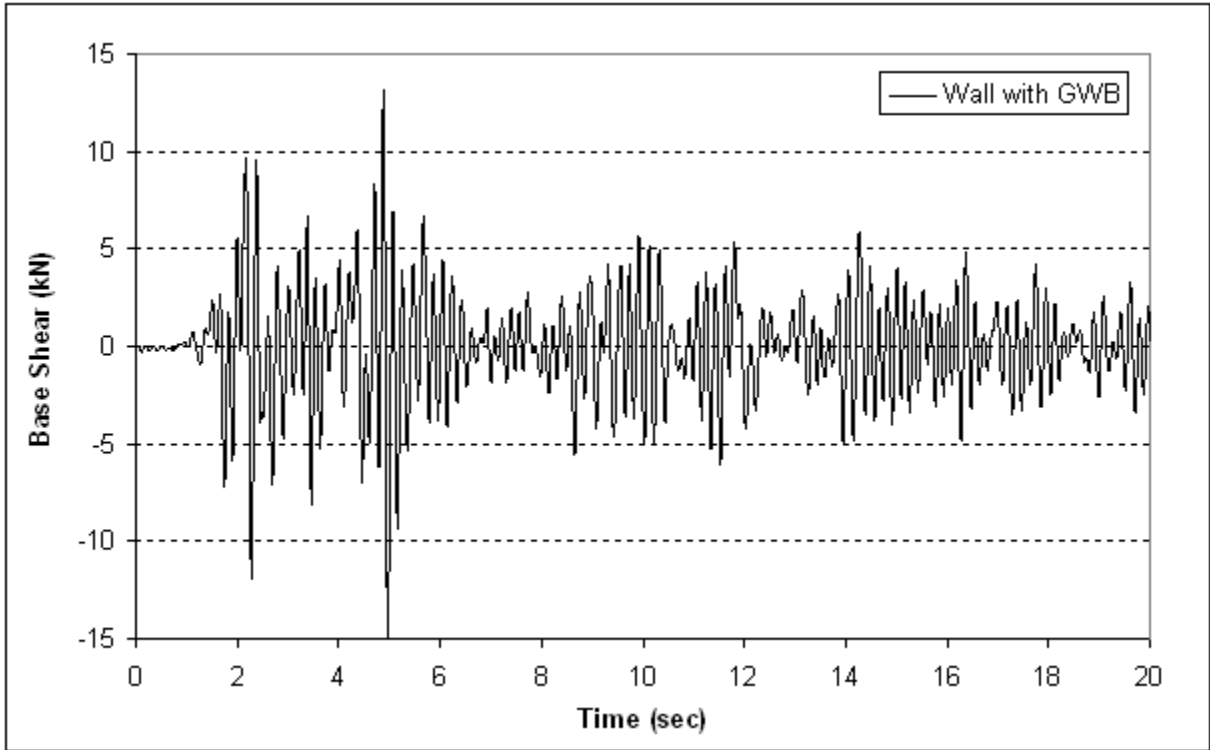
Fig. 3.36.   Base shear time history for the light frame wood shear wall with GWB sheathing

(a)
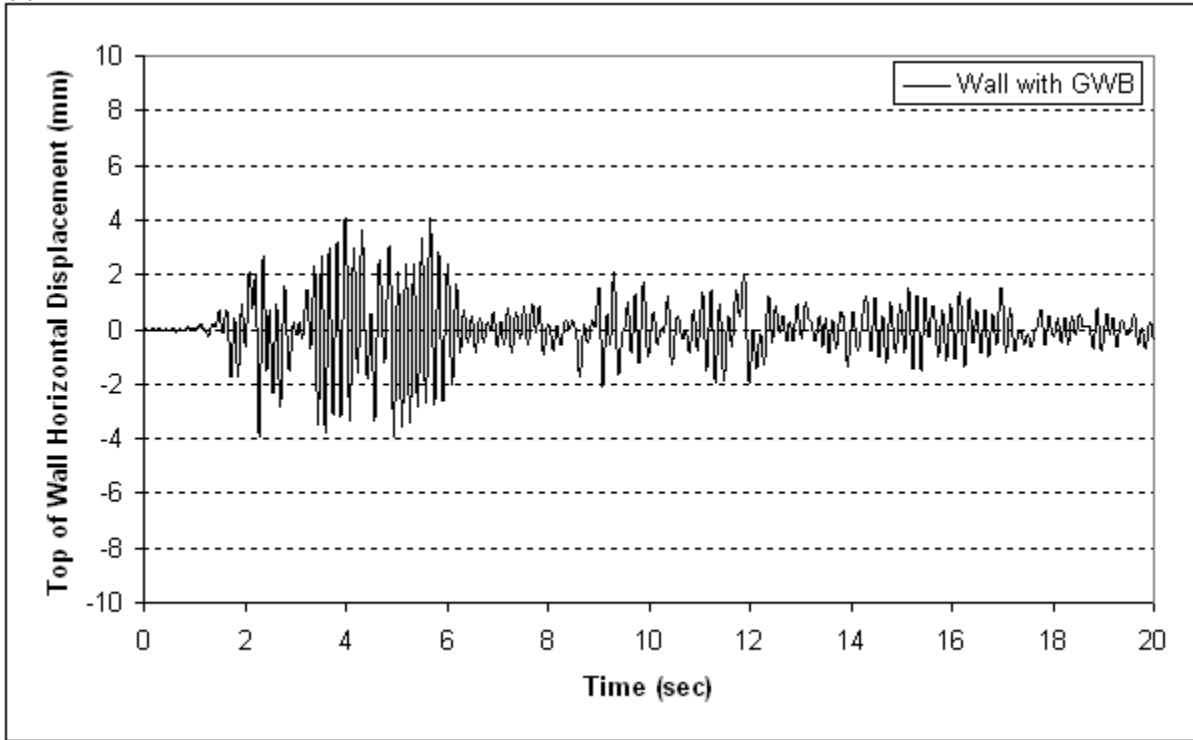
(b)
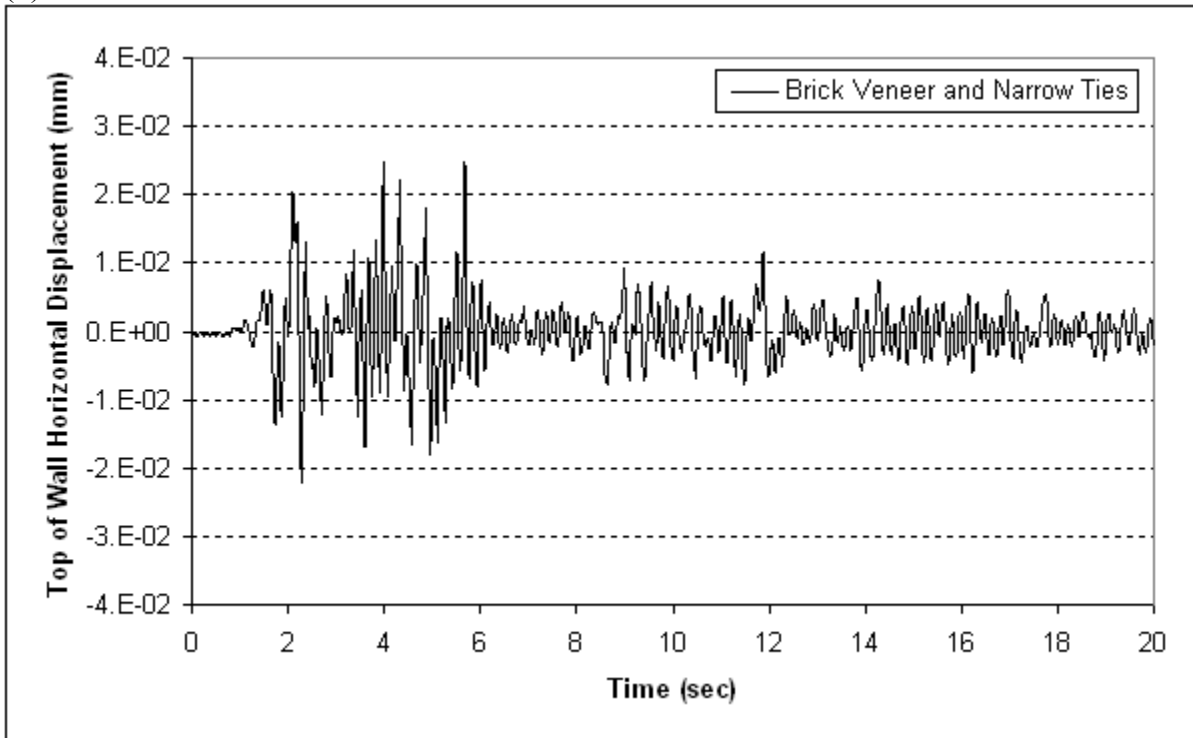
Fig. 3.37. Horizontal displacement time history of the top left corner of the (a) frame, and (b) brick veneer of the brick veneer – wood frame shear wall with GWB sheathing
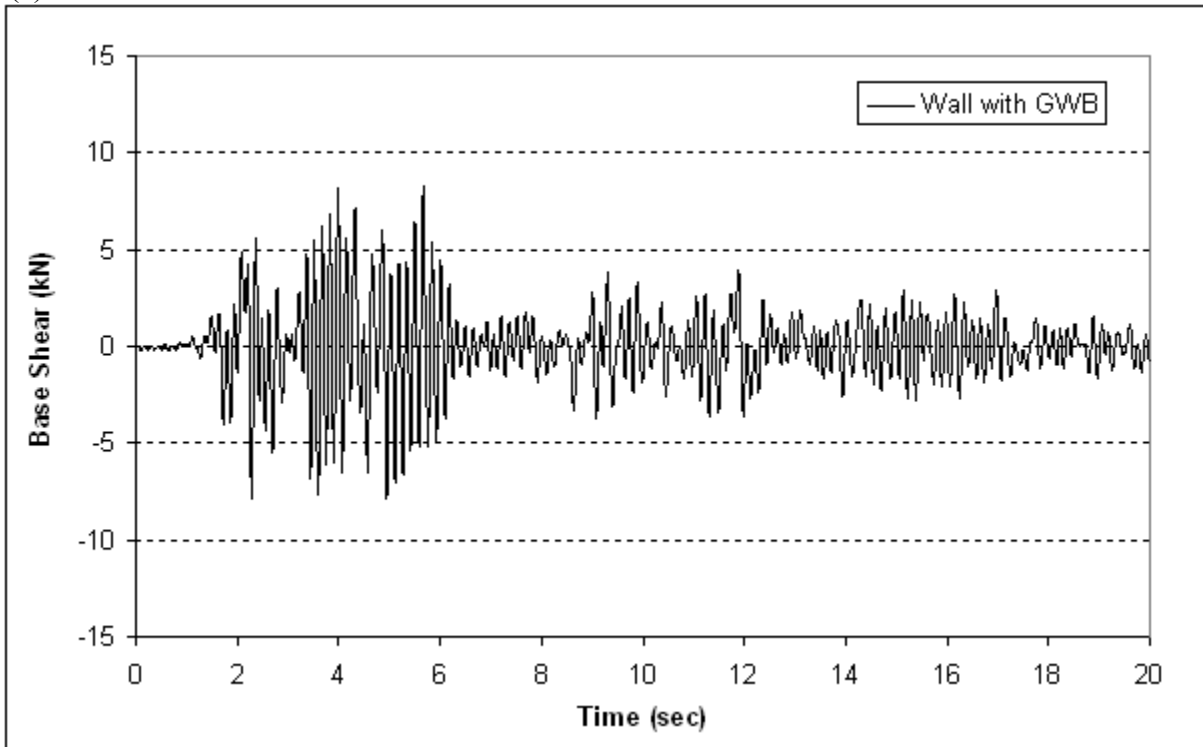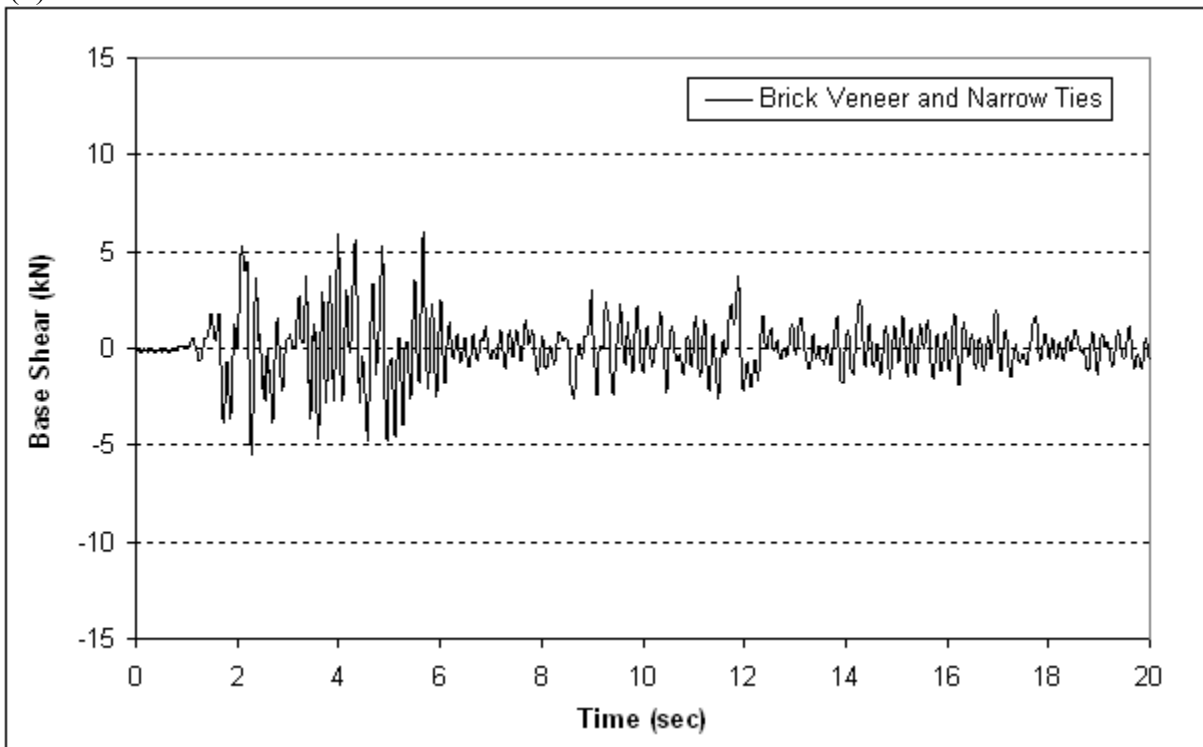
Fig. 3.38. Base shear time history for the (a) wall with GWB, and (b) brick veneer of the anchored brick veneer – light frame wood shear wall with GWB sheathing

106

Table 3.8. Comparison of wood wall extreme displacements in the frame's top left corner for considered wall compositions

		Wall Composition	OSB	OSB GWB	OSB BVnt	OSB GWB BVnt
Without OSB Bearing at Base	Minimum	OSB	**-9.753**	-28.99%	-37.40%	-59.98%
		OSB GWB		**-6.925**	-11.84%	-43.64%
		OSB BVnt			**-6.105**	-36.07%
		OSB GWB BVnt				**-3.903**
	Maximum	OSB	**8.575**	-33.60%	-41.06%	-52.85%
		OSB GWB		**5.693**	-11.24%	-28.99%
		OSB BVnt			**5.054**	-20.00%
		OSB GWB BVnt				**4.043**

(Displacement values are given in units of mm and displayed in boldface.)

Table 3.9. Comparison of brick veneer extreme displacements in the top left corner for considered wall compositions

		Wall Composition	BV	OSB BVnt	OSB GWB BVnt
Without OSB Bearing at Base	Min	BV	**-0.009**	187.59%	159.74%
		OSB BVnt		**-0.025**	-9.68%
		OSB GWB BVnt			**-0.022**
	Max	BV	**0.009**	284.36%	177.22%
		OSB BVnt		**0.034**	-27.88%
		OSB GWB BVnt			**0.025**

(Displacement values are given in units of mm and displayed in boldface.)

Table 3.10. Base shear and wall component weights comparison

Wall Composition	Weight (kN)				Base Shear (kN)						
	wood wall	veneer	total		wood wall	weight percent		veneer	weight percent		total
						wall	total		veneer	total	
OSB	17.93	–	17.93	min	-13.93	77.67%	77.67%	–	–	–	-13.93
				max	13.14	73.29%	73.29%	–	–	–	13.14
OSB GWB	18.52	–	18.52	min	-15.39	83.09%	83.09%	–	–	–	-15.39
				max	13.13	70.91%	70.91%	–	–	–	13.13
BV	–	9.96	9.96	min	–	–	–	-2.97	29.76%	29.76%	-2.97
				max	–	–	–	3.12	31.29%	31.29%	3.12
OSB BVnt	17.93	9.96	27.89	min	-8.99	50.14%	32.23%	-5.57	55.90%	19.97%	-14.02
				max	7.27	40.55%	26.06%	6.73	67.56%	24.13%	13.27
OSB GWB BVnt	18.52	9.96	28.49	min	-7.90	42.66%	27.74%	-5.43	54.54%	19.08%	-13.26
				max	8.25	44.56%	28.97%	6.00	60.25%	21.08%	14.26

Table 3.11. Comparison of base shear in the wood wall for considered wall compositions

		Wall Composition	OSB	OSB GWB	OSB BVnt	OSB GWB BVnt
Without OSB Bearing at Base	Minimum	OSB	**-13.93**	10.51%	-35.44%	-43.25%
		OSB GWB		**-15.39**	-41.58%	-48.65%
		OSB BVnt			**-8.99**	-12.10%
		OSB GWB BVwt				**-7.90**
	Maximum	OSB	**13.14**	-0.05%	-44.68%	-37.19%
		OSB GWB		**13.13**	-44.65%	-37.16%
		OSB BVnt			**7.27**	13.53%
		OSB GWB BVnt				**8.25**

(Base shear values are given in units of kN and displayed in boldface.)

Table 3.12. Comparison of base shear in the brick veneer for considered wall compositions

		Wall Composition	BV	OSB BVnt	OSB GWB BVnt
Without OSB Bearing at Base	Min	BV	**-2.97**	87.84%	83.27%
		OSB BVnt		**-5.57**	-2.43%
		OSB GWB BVnt			**-5.43**
	Max	BV	**3.12**	115.92%	92.59%
		OSB BVnt		**6.73**	-10.81%
		OSB GWB BVnt			**6.00**

(Base shear values are given in units of kN and displayed in boldface.)

Conclusions

An analytical investigation was carried out to determine the racking behavior of an anchored brick veneer-light frame wood shear wall. Of particular interest were the effects resulting from the inclusion of tied brick veneer to the outer wall face and/or addition of gypsum wallboard sheathing on the interior wall face, as well as the viability of the created integral wall system.

The effects from tying brick veneer to the wood shear wall were dependent on the tie design and installation. All else being equal, the stronger the tie was the more prominent were the benefits. The initial wall stiffness increased between 41 % and 60 % when optimal installation practice had been utilized. The gain in wall strength was estimated to be rather small and amounted up to 5 %. The inclusion of anchored brick veneer resulted in a slight decrease in wall ductility.

Considering the existing gypsum wallboard sheathing as a contributing structural component had a significant effect on the in-plane behavior of the wood shear wall. When maximum Code permitted wallboard fastener spacing was implemented, the initial wall stiffness increased by 33 %. However, this strengthening effect was limited by the relatively small deformation capacity of the screwed wallboard-to-wood connections. Once these connections started to fail the gains quickly diminished and weren't sustained at larger displacement intervals. As a result, the estimated wall strength decreased by about 8 %. An accompanying consequence of the addition of gypsum wallboard sheathing was a slight decrease in wall ductility.

The simultaneous inclusion of anchored brick veneer and gypsum wallboard sheathing to the wood shear wall resulted with an integral wall system whose in-plane response was influenced by all constituent components. Depending on the tie type, the gain in initial stiffness ranged between 83 % and 112 % over the stiffness of the wood shear wall. The earlier failure of the screwed wallboard-to-wood connections put limits on the initial gains in wall stiffness and strength, and caused a drawback in absorbed force. However, the benefits from the added anchored brick veneer were prevalent and sustained deep into the nonlinear range. The estimated ultimate strength of an integral wall was at least equal to the corresponding strength of the core wood shear wall.

Regardless of the considered contributing wall components, the response of the wood shear wall under cyclic in-plane loading was characterized with pinched hystereses and progressively increasing strength as the displacements became larger. However, the rate at which the strength increased was considerably smaller than the corresponding rate obtained under static pushover loading. This was due to the repetitive nature of the loading at intensities above the yielding point that caused damage accrual in the wall fastener connections.

Dynamic analyses of wall models under representative earthquake loading confirmed that both the addition of gypsum wallboard and anchored brick veneer stiffen the core wood shear wall and alter its response. Favorable reduction in wall displacements was common for both cases. However, only the addition of anchored brick veneer resulted with subsequent beneficial reduction in base shear absorbed by the core wall. This decrease was counterbalanced with an increase in base shear absorbed by the veneer wall, pointing to an existence of interaction between the anchored brick veneer and its wood wall backing.

CHAPTER IV - CONCLUSIONS

An analytical investigation was carried out to determine the racking behavior of anchored brick veneer-light frame wood shear walls. Of particular interest were the effects resulting from the inclusion of tied brick veneer to the outer wall face and/or addition of gypsum wallboard sheathing on the interior wall face, as well as the viability of the created integral wall system.

A precursor experimental study looked into the shear behavior of corrugated tie connections in brick veneer wall systems. Connection subassemblies were tested under monotonic and cyclic shear loading to obtain constitutive relations necessary for analytical modeling. It was found that force-displacement curves obtained under monotonic loading can be considered an upper bound for the hysteresis loop envelopes. Fastener slippage during cyclic loading enabled by the localized damage of the surrounding wood fibers diminished the energy absorption capacity of the connection and caused pronounced pinching in the hystereses. Statistical analyses were then conducted to identify and quantify the parameters influencing the shear behavior of the connections. Considering corrugated ties with minimum thickness permitted by the MSJC Code, tie design and bent eccentricity were found to be the most important factors, while tie location in the bed joint, fastener type and fastener quantity were influential to a lesser degree.

Analytical simulations showed that the effects from tying brick veneer to the wood shear wall were dependent on the tie design and installation. All else being equal, the stronger the tie was the more prominent were the benefits. The initial wall stiffness increased between 41 % and 60 % when optimal installation practice had been utilized. The gain in wall strength was estimated to be rather small and amounted up to 5 %. The inclusion of anchored brick veneer resulted in a slight decrease in wall ductility.

Considering the existing gypsum wallboard sheathing as a contributing structural component had significant effect on the in-plane behavior of the wood shear wall. When maximum Code permitted wallboard fastener spacing was implemented, the initial wall stiffness increased by 33

%. However, this strengthening effect was limited by the relatively small deformation capacity of the screwed wallboard-to-wood connections. Once these connections started to fail the gains quickly diminished and weren't sustained at larger displacement intervals. As a result, the estimated wall strength decreased by about 8 %. An accompanying consequence of the addition of gypsum wallboard sheathing was a slight decrease in wall ductility.

The simultaneous inclusion of anchored brick veneer and gypsum wallboard sheathing to the wood shear wall resulted with an integral wall system whose in-plane response was influenced by all constituent components. Depending on the tie type, the gain in initial stiffness ranged between 83 % and 112 % over the stiffness of the wood shear wall. The earlier failure of the screwed wallboard-to-wood connections put limits on the initial gains in wall stiffness and strength, and caused a drawback in absorbed force. However, the benefits from the added anchored brick veneer were prevalent and sustained deep into the nonlinear range. The estimated ultimate strength of an integral wall was at least equal to the corresponding strength of the core wood shear wall.

Regardless of the considered contributing wall components, the response of the wood shear wall under cyclic in-plane loading was characterized with pinched hystereses and progressively increasing strength as the displacements became larger. However, the rate at which the strength increased was considerably smaller than the corresponding rate obtained under static pushover loading. This was due to the repetitive nature of the loading at intensities above the yielding point that caused damage accrual in the wall fastener connections.

Dynamic analyses of wall models under representative earthquake loading confirmed that both the addition of gypsum wallboard and anchored brick veneer stiffen the core wood shear wall and alter its response. Favorable reduction in wall displacements was common for both cases. However, only the addition of anchored brick veneer resulted with subsequent beneficial reduction in base shear absorbed by the core wall. This decrease was counterbalanced with an increase in base shear absorbed by the veneer wall, pointing to an existence of interaction between the anchored brick veneer and its wood wall backing.

LIST OF REFERENCES

LIST OF REFERENCES

Ali, S., Page, A. W. and Kleeman, P. W. (1986). "Non-linear finite element model for concrete masonry with particular reference to concentrated loads." *Proceedings of the 4th Canadian Masonry Symposium*, Vol. 1, 137–148.

Allen, D., and Lapish, E. B. (1986). "The interaction of timber framed walls with a tied masonry veneer under cyclic racking loads." *Proceedings of the 4th Canadian Masonry Symposium*, Fredericton, Canada, Vol. 2, 702–715.

American Society of Civil Engineers (ASCE). (1998) "Minimum Design Loads for Buildings and Other Structures (ASCE 7-98)." American Society of Civil Engineers, Reston, VA.

Andreaus, U. (1996). "Failure criteria for masonry panels under in-plane loading." *Journal of Structural Engineering*, 122(1), 37–46.

APA – The Engineered Wood Association (2001) "Diaphragms and Shear Walls." Design/Construction Guide, (L350G), Tacoma, WA.

Asteris, P.G., and Tzamtzis, A. D. (2003). "On the use of a regular yield surface for the analysis of unreinforced masonry walls." *Electronic Journal of Structural Engineering*, 3, 23–42.

Atherton, G. H. (1983). "Ultimate strength of structural particleboard diaphragms." *Forest Products Journal*, 33(5), 22–26.

Brick Industry Association (BIA) (2002). "Anchored Brick Veneer, Wood Frame Construction." *Tech. Notes,* (28), Reston, VA.

Brick Industry Association (BIA) (2005). "Water Penetration Resistance – Design and Detailing." *Tech. Notes,* (7), Reston, VA.

Cheung, C. K., Itani, R. Y., and Polansek A. (1988). "Characteristics of wood diaphragms: Experimental and parametric studies." *Wood and Fiber Science*, 20(4), 438–456.

Choi, Y-H., and LaFave J. M. (2004). "Performance of corrugated metal ties for brick veneer wall systems." *Journal of Materials in Civil Engineering*, 16(3), 202–211.

Dinehart, D. W., and Shenton, H. W. III. (2000). "Model for dynamic analysis of wood frame shear walls." *Journal of Engineering Mechanics*, 126(9), 899–908.

Dolan, J. D. (1989). "The dynamic response of timber shear walls." Ph.D. thesis, University of British Columbia, Vancouver, B.C.

Dolan, J. D., and Foschi, R. O. (1991). "Structural analysis model for static loads on timber shear walls." *Journal of Structural Engineering*, 117(3), 851–861.

Dolan, J. D., and Madsen, B. (1992 a). "Monotonic and cyclic nail connection tests." *Canadian Journal of Civil Engineering*, 19(1), 97–104.

Dolan, J. D., and Madsen, B. (1992 b). "Monotonic and cyclic tests of timber shear walls." *Canadian Journal of Civil Engineering*, 19(3), 415–422.

Easley, J. T., Foomani, M., and Dodds, R. H. (1982). "Formulas for wood shear walls." *Journal of the Structural Division, ASCE*, 108(11), 2460–2478.

Falk, R. H., and Itani, R. Y. (1989). "Finite element modeling of wood diaphragms." *Journal of Structural Engineering*, 115(3), 543–559.

Filiatrault, A. (1990). "Static and dynamic analysis of timber shear walls." *Canadian Journal of Civil Engineering*, 17(4), 643–651.

Filiatrault, A., Fischer, D., Folz, B., and Uang, C.-M. (2002). "Seismic testing of two-story woodframe house: Influence of wall finish materials." *Journal of Structural Engineering*, 128(10), 1337–1345.

Folz, B., and Filiatrault, A. (2001). "Cyclic analysis of wood shear walls." *Journal of Structural Engineering*, 127(4), 433–441.

Forest Products Laboratory. (1999). "Wood handbook—Wood as an engineering material." Gen. Tech. Rep. FPL–GTR–113. Madison, WI: U.S. Department of Agriculture, Forest Service, Forest Products Laboratory. 463 p.

Foschi, R. O., and Bonac, T. (1977). "Load-slip characteristics for connections with common nails." *Wood Science*, 9(3), 118–123.

Gambarotta, L., and Lagomarsino, S. (1997 a). "Damage models for the seismic response of brick masonry shear walls. Part I: The mortar joint model and its application." *Earthquake Engineering and Structural Dynamics*, 26(4), 423–439.

Gambarotta, L., and Lagomarsino, S. (1997 b). "Damage models for the seismic response of brick masonry shear walls. Part II: The continuum model and its application." *Earthquake Engineering and Structural Dynamics*, 26(4), 441–462.

Ghosh, A. K., Amde, A. M., and Colville, J. (1994). "Finite element modeling of unreinforced masonry." *Proceedings of the 10th International Brick/Block Masonry Conference*, Calgary, Canada, Vol. 1, 61-69.

Griffith, M. C., and Page, A. W. (1998). "On the seismic capacity of typical DPC and slip joints in unreinforced masonry structures." *Australian Journal of Structural Engineering*, The Institution of Engineers Australia, 1(2), 133–140.

Gupta, A. K., and Kuo, G. P. (1987). "Wood-framed shear walls with uplifting." *Journal of Structural Engineering*, 113(2), 241–259.

Gutkowski, R. M., and Castillo, A. L. (1988). "Single- and double-sheathed wood shear wall study." *Journal of Structural Engineering*, 114(6), 1268–1284.

Itani, R. Y., and Cheung, C. K. (1984). "Nonlinear analysis of sheathed wood diaphragms." *Journal of Structural Engineering*, 110(9), 2137–2147.

Johnson, E. N., and McGinley, W. M. (2003). "The in plane shear performance of brick veneer and wood stud walls." *Proceedings of the 9th North American Masonry Conference*, Clemson, SC, USA, CD-ROM, 226–237.

Jones, S. N., and Fonseca, F. S. (2002). "Capacity of oriented strand board shear walls with overdriven sheathing nails." *Journal of Structural Engineering*, 128(7), 898–907.

Lam, F., Prion, H. G. L., and He, M. (1997). "Lateral resistance of wood shear walls with large sheathing panels." *Journal of Structural Engineering*, 123(12), 1666–1673.

Lotfi, H. R., and Shing, P. B. (1994). "Interface model applied to fracture of masonry structures." *Journal of Structural Engineering*, 120(1), 63–80.

Lourenco, P. B., and Rots, J. G. (1997). "Multisurface interface model for analysis of masonry structures." *Journal of Engineering Mechanics*, 123(7), 660–668.

Lourenco, P. B., Rots, J. G., and Blaauwendraad J. (1998). "Continuum model for masonry: Parameter estimation and validation." *Journal of Structural Engineering*, 124(6), 642–652.

Lowes, L. N., Mitra, N., and Altoontash, A. (2004). "A beam-column joint model for simulating the earthquake response of reinforced concrete frames." Pacific Earthquake Engineering Research Center, Report 2003/10, University of California, Berkeley, CA.

Masonry Standards Joint Committee (MSJC) (2008). "Building Code Requirements for Masonry Structures (ACI 530-08/ASCE 5-08/TMS 402-08)." American Concrete Institute, Structural Engineering Institute, The Masonry Society.

Mazzoni, S., McKenna, F., Scott, M. H., Gregory L. Fenves, G. L., et al. (2007). "OpenSees Command Language Manual." University of California, Berkeley, CA

McCutcheon, W. J. (1985). "Racking deformations in wood shear walls." *Journal of Structural Engineering*, 111(2), 257–269.

McGinley, W. M., and Borchelt, J. G. (1990). "Friction at supports of clay brick walls." *Proceedings of the 5th North American Masonry Conference*, Urbana-Champaign, IL, USA, Vol. 3, 1053–1066.

"OpenSees." *OpenSees*. University of California at Berkeley, n.d. Web. 1 May 2009.

Page, A. W. (1978) "Finite element model for masonry." *Journal of the Structural Division, ASCE*, 104(8), 1267–1285.

Page, A. W., Kleeman, P. W., and Dhanasekar, M. (1985). "An in-plane finite element model for brick masonry." *Proceedings of the Structural Engineering Congress, ASCE*, Chicago, IL, USA, 1–18.

Pappa, E., and Nappi, A. (1997). "Numerical modeling of masonry: A material model accounting for damage effects and plastic strains." *Applied Mathematical Modeling*, 21(6), 319–335.

Park, Y. J. and Ang, A. H. S. (1985). "Mechanistic Seismic Damage Model for Reinforced Concrete." *Journal of Structural Engineering*, 111(4), 722-739.

Patton-Mallory, M., Wolfe, R. W., Soltis, L. A. and Gutkowski, R. M. (1985). "Light-frame shear wall length and opening effects." *Journal of Structural Engineering*, 111(10), 2227–2239.

Patton-Mallory, M. and McCutcheon, W. J. (1987). "Predicting racking performance of walls sheathed on both sides." *Forest Products Journal*, 37(9), 27–32.

Price, E. W., and Gromala, D. S. (1980). "Racking strength of walls sheathed with structural flakeboards made from Southern species." *Forest Products Journal*, 30(12), 19–23.

Rajakaruna, M. P. (1997). "Effect of damp proof course on the shear strength of masonry." *Proceedings of the 15th Australasian Conference on the Mechanics of Structures and Materials*, Melbourne, Australia, 633–637.

Shelton, R. H., and King A. B. (1994). "Seismic performance of masonry veneers on timber frame backing." *Proceedings of the 10th International Brick/Block Masonry Conference*, Calgary, Canada, Vol. 1, 215–225.

Shenton, H. W., III, Dinehart, D. W., and Elliott, T. E. (1998). "Stiffness and energy degradation of wood frame shear walls." *Canadian Journal of Civil Engineering*, 25(3), 412–423.

Structural Board Association. (2004). "Oriented Strand Board in Wood Frame Construction." TM422 Willowdale, Toronto, ON, Canada, 28p.

Tarabia, A. M., and Itani, R. Y. (1997). "Static and dynamic modeling of light-frame wood buildings." *Computers and Structures,* 63(2), 319–334.

Thomas, W. H. (2001). "Mechanical properties of structural-grade oriented strand board." *Holz als Roh- und Werkstoff*, 59, 405–410.

Thrischuk, K. and Suter, G. T. (1996). "Shear resistance of flashing materials in brick veneer-foundation wall joints." *Proceedings of the 7th North American Masonry Conference*, South Bend, Indiana, USA, Vol. 2, 836–846.

Tuomi, R. L., and McCutcheon, W. J. (1978). "Racking strength of light-frame nailed walls." *Journal of the Structural Division*, ASCE, 104(7), 1131–1140.

Tzamtzis, A. D., and Asteris P.G. (2003). "Finite element analysis of masonry structures: Part II – Proposed 3-D nonlinear microscopic model." *Proceedings of the 9ᵗʰ North American Masonry Conference*, Clemson, SC, USA, CD-ROM, 146-155.

van de Lindt J. W. (2004). "Evolution of Wood Shear Wall Testing, Modeling, and Reliability Analysis: Bibliography." *Practice Periodical on Structural Design and Construction*, 9(1), 44–53.

White, M. W., and Dolan, J. D. (1995). "Nonlinear shear-wall analysis." *Journal of Structural Engineering*, 121(11), 1629–1635.

Zhuge, Y., and Mills, J. (1998). "The behaviour of masonry walls containing a damp proof course under cyclic loads." *Proceedings of the 2ⁿᵈ Australasian Structural Engineering Conference*, Auckland, New Zealand, Vol. 2, 655–661.

Zhuge, Y., Thambiratnam, D., and Corderoy, J. (1998). "Nonlinear dynamic analysis of unreinforced masonry." *Journal of Structural Engineering*, 124(3), 270–277.

APPENDIX

Constitutive Model for Fasteners and Ties

A general one-dimensional deformation based model developed by Lowes et al. (2004) and available in the OpenSees framework as Pinching4 uniaxial material (Mazzoni et al. 2007) was used to define appropriate constitutive relations for all fasteners and ties. An idealization of a load-deformation history predicted using this model is shown in Fig. A.1. As the figure shows, and the name suggests the main characteristic of the model is its 'pinched' hysteretic response under repetitive loading. Distinctive model features enable application of unloading stiffness degradation, reloading stiffness degradation and strength degradation.

The hysteretic model is implemented by defining essential material states, the rules that control changes between states, and the rules that govern the evolution of states.

State Definition

The behavior of the model is determined from four distinctive material states shown in Fig. A.1. States 1 and 2 correspond to the response along the envelope in the positive and negative deformation ranges, respectively, while States 3 and 4 signify the two inside unloading-reloading paths. The load paths for States 1 and 2 can change during an analysis to account for the reduction in strength caused by previous load-deformation history. For States 3 and 4 the load path is defined each time the state is entered and does not change until the state is exited.

Each state is defined by the same data: the minimum and maximum deformations and associated loads that mark the beginning and end of the state, a loading direction, and a series of rules that define the load path within the state. In addition, States 3 and 4 each require establishment of two supplementary load-deformation points. One marks the end of substantial unloading, and the other denotes the beginning of substantial reloading. The former point is obtained once the unloading stiffness is calculated and the load achieved upon unloading reaches the limiting fraction of strength developed under monotonic loading in the corresponding deformation range. The coordinates of the later point are set to a fraction of the extreme historic deformation and a fraction of the load developed at the extreme deformation demand in the corresponding deformation range.
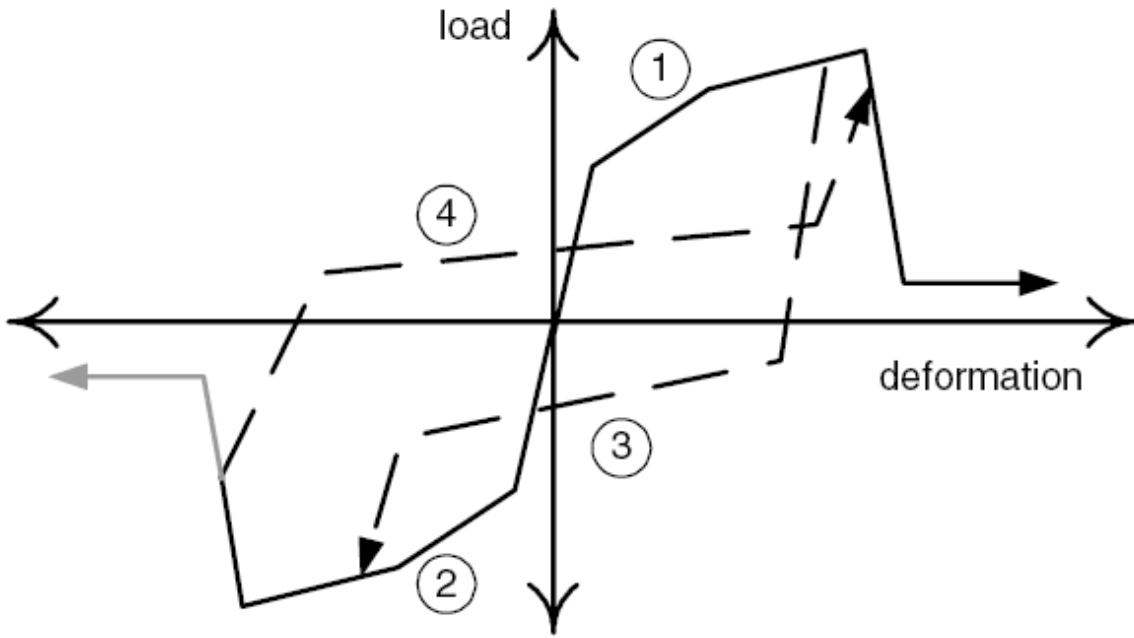
Fig. A.1. One-dimensional load-deformation response model

(source: Lowes et al. 2004)

Rules for Change in State

In a step by step numerical integration procedure the model determines the current load and instantaneous tangent to the load-deformation response based on the material state in the preceding step and an imposed deformation increment. While model outputs are straightforward when the increment is such that the response remains within the state bounds, rules must be established that trigger necessary changes between material states. A schematic displaying the connectivity between the four material states is shown in Fig. A.2.

For States 1 and 2, a change in state (CIS) occurs only if there is a reversal in the loading direction. A negative deformation increment imposed while the current state is State 1 triggers a CIS to State 3 or, if the increment is very large to State 2. Similarly, a positive deformation increment imposed while the current state is State 2 triggers a CIS to State 4 or, if the increment is very large to State 1.

For States 3 and 4, a CIS occurs either by change in the direction of loading or by loading beyond the current state bounds. If the current state is State 3 and the imposed deformation increment is positive, then there is a CIS to State 4 or, if the increment is large, to State 1. A negative deformation increment imposed while the current state is State 3 may trigger CIS to State 2. Likewise, a negative deformation increment imposed while the current state is State 4 triggers a CIS to State 3 or, if the increment is very large to State 2. A positive deformation increment imposed while the current state is State 4 may trigger CIS to State 1.

Rules for Evolution of States

In order to simulate complex nonlinear behavior the model has built-in three damage rules that define evolutions of response envelopes (States 1 and 2) and unload-reload paths (States 3 and 4) as functions of load-deformation history. Hysteretic damage is simulated through unloading stiffness degradation, reloading stiffness degradation in the vicinity of the extreme deformation demands, and envelope strength degradation (deterioration in strength at previously unachieved deformation demands). The impact of these three different damage modes on the hysteretic material response is shown in Figs. A.3 - A.5.
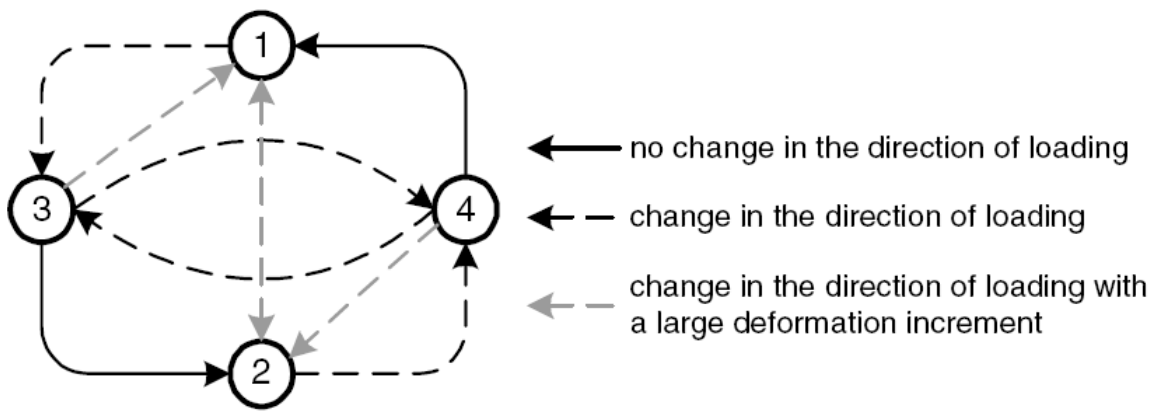
Fig. A.2. State connectivity
(source: Lowes et al. 2004)
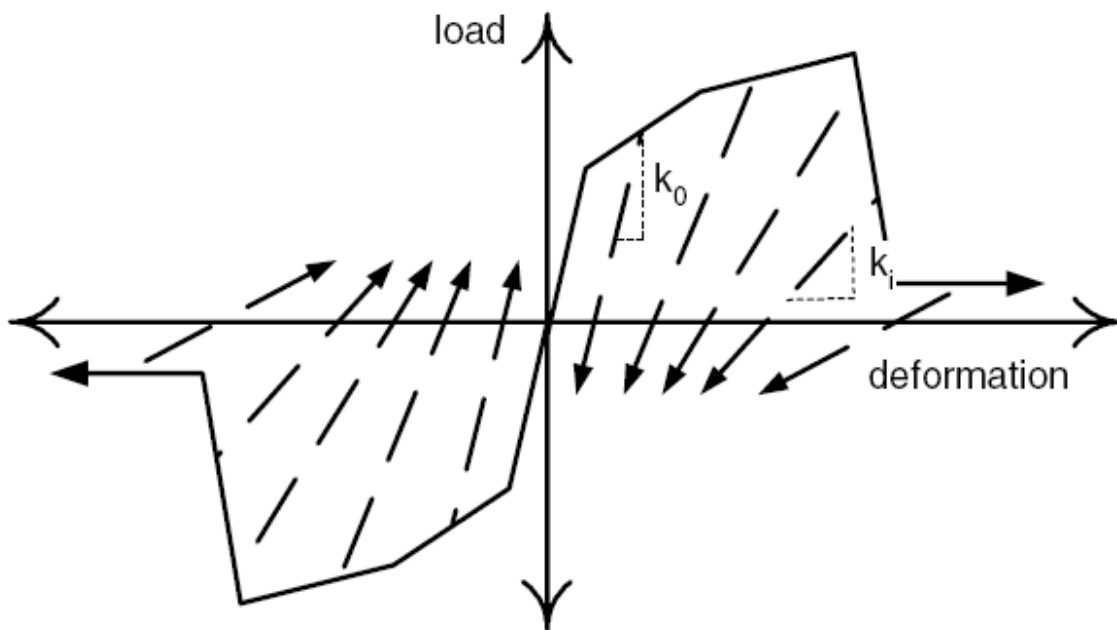
Fig. A.3. Unloading stiffness degradation
(source: Lowes et al. 2004)
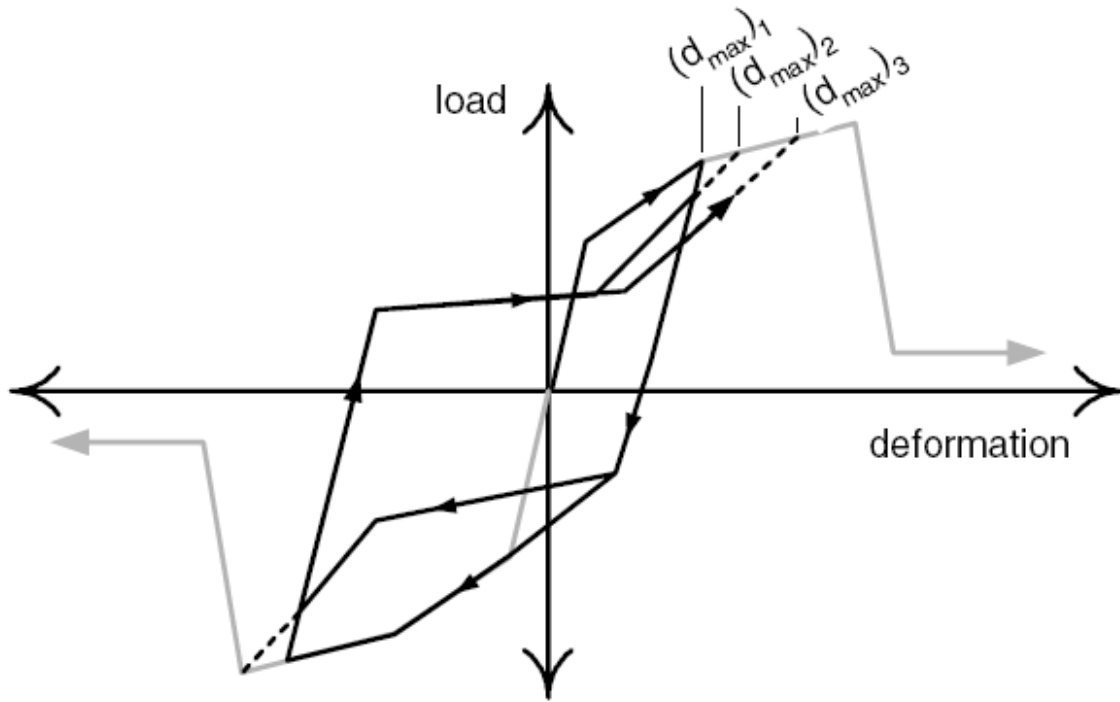
Fig. A.4. Reloading stiffness degradation
(source: Lowes et al. 2004)
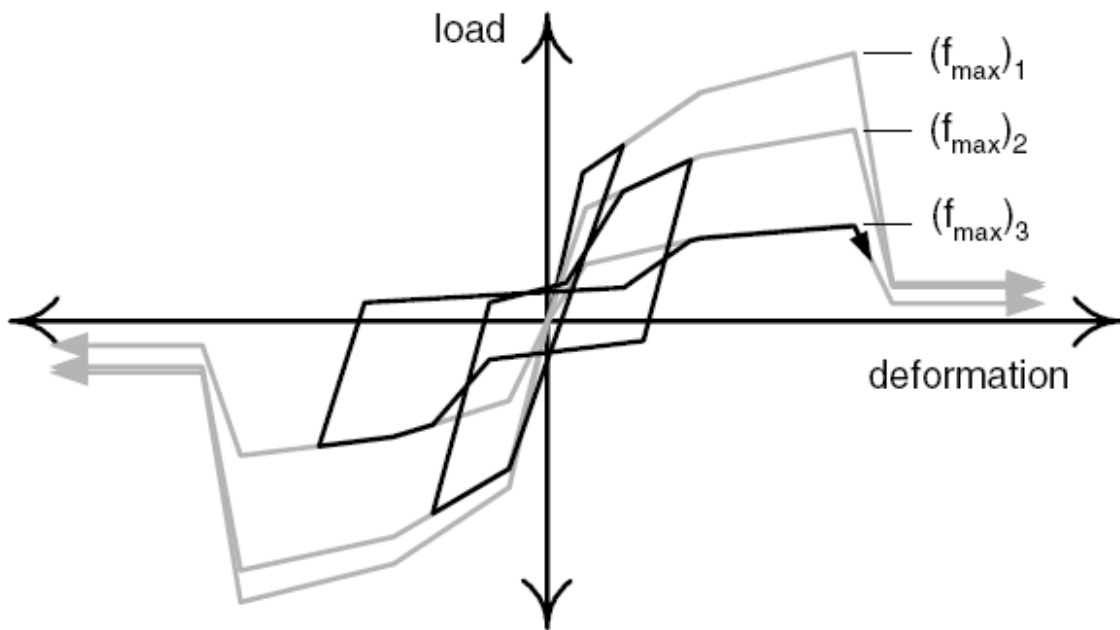
Fig. A.5. Strength degradation
(source: Lowes et al. 2004)

All three damage rules share a common form that represents a more general version of the damage index proposed by Park and Ang (1985). The damage index has two contributing components, one taking account for the extreme historic deformation demand, and the other taking into account the energy dissipated during response. It is calculated as:

$$\delta_i = \left[\alpha_1 \left(\tilde{d}_{max} \right)^{\alpha_2} + \alpha_3 \left(\frac{E_i}{\alpha_E E_{monotonic}} \right)^{\alpha_4} \right] \leq \delta_{\lim it} \qquad \text{(Eq. A.1a)}$$

$$\tilde{d}_{max} = \max \begin{cases} \dfrac{d_{max,i}}{def_{max}} \\[2ex] \dfrac{d_{min,i}}{def_{min}} \end{cases} \qquad \text{(Eq. A.1b)}$$

$$E_i = \int\limits_{load\ history} dE \qquad \text{(Eq. A.1c)}$$

$$E_{monotonic} = \int\limits_{monotonic\ load\ history} dE \qquad \text{(Eq. A.1d)}$$

where:

i denotes the current displacement increment

δ_i damage index

                    $\delta = 0$ represents a case of no damage, and

                    $\delta = 1$ represents a case of maximum damage

δ_{limit} damage index limiting value

def_{max}, def_{min} maximum (positive) and minimum (negative) deformations that define failure

$d_{max,i}, d_{min,i}$ maximum (positive) and minimum (negative) historic deformation demands

E_i hysteretic energy

$E_{monotonic}$ energy required to achieve failure deformation under monotonic loading

$\alpha_E = \dfrac{E_{cyclic}}{E_{monotonic}}$ ratio of energy dissipation capacities under cyclic and monotonic loading

α_1 - α_4 parameters used to fit the damage rule to the experimental data

For the case of unloading stiffness degradation:

$$k_i = k_0 \left(1 - \delta k_i \right) \tag{Eq. A.2}$$

where:

k_i current unloading stiffness (Fig. A.3)

k_0 initial unloading stiffness for the case of no damage (Fig. A.3)

δk_i current value of the unloading stiffness damage index

The reduction in stiffness observed upon reloading in the vicinity of the extreme deformation demand is simulated by applying the damage rule to define an increase in the maximum historic deformation if the current state is State 4, or a decrease in the minimum historic deformation if the current state is State 3:

$$\left(d_{max} \right)_i = \left(d_{max} \right)_0 \left(1 + \delta d_i \right) \tag{Eq. A.3a}$$

$$\left(d_{min} \right)_i = \left(d_{min} \right)_0 \left(1 + \delta d_i \right) \tag{Eq. A.3b}$$

where:

$(d_{max})_i$, $(d_{min})_i$ current deformation that defines the end of the reload cycle for increasing/decreasing deformation demand (Fig. A.4)

$(d_{max})_0$, $(d_{min})_0$ maximum/minimum historic deformation demand (Fig. A.4)

δd_i current value of the reloading stiffness damage index

The envelope strength degradation is computed in the same way as the unloading stiffness degradation:

$$(f_{\max})_i = (f_{\max})_0 (1 - \delta f_i) \qquad\qquad \text{(Eq. A.4a)}$$

$$(f_{\min})_i = (f_{\min})_0 (1 - \delta f_i) \qquad\qquad \text{(Eq. A.4b)}$$

where:

$(f_{max})_i$, $(f_{min})_i$ current envelope maximum/minimum strength (Fig. A.5)

$(f_{max})_0$, $(f_{min})_0$ initial envelope maximum/minimum strength for the case of no damage (Fig. A.5)

δf_i current value of the strength damage index

Model Implementation in OpenSees Framework

The one-dimensional constitutive model descried above is introduced into the OpenSees framework as the Pinching4 uniaxial material. Complete model definition requires establishment of a response envelope, unload-reload paths, and damage rules. In the current model implementation the envelope is composed of four continuous lines in each of the positive and negative displacement regions. Since four points beside the origin are needed to define the envelope in each displacement region, and with two coordinates (force, displacement) defining each point, the total number of parameters defining the envelope amounts to 16. The definition of a trilinear unload-reload path requires three parameters, one related to the unloading stiffness (uForce) and two related to the reloading stiffness (rDisp, rForce). With two such paths in existence, the number of path related parameters totals 6. A model illustration with indications of all envelope and path related parameters is shown in Fig A.6. In addition, each of the three damage rules requires four damage index calibration parameters, and a limiting value, which amounts to 15 damage parameters. The final damage related parameter is the ratio of energy

dissipation capacities under cyclic and monotonic loading, whose value is common to all damage rules. Hence, the total number of parameters defining the model totals 38.

The parameter values used to define appropriate constitutive relations for all fasteners and ties are given in Tables A.1 – A.4. Few of the damage related parameters were kept at their recommended default values, while the rest were adjusted in order to obtain best visual match between the hysteresis model predictions and recorded experimental data. Each connector type (fastener or tie) had unique envelope defining parameters, while the parameters governing the unload-reload paths and the damage rules were kept identical among connector types. This was justified with the fact that all connector types expressed common hysteretic behavior caused by the irreversible damage in the wood fibers surrounding the fastener that resulted with slippage in the elongated hole under reversed type loading.
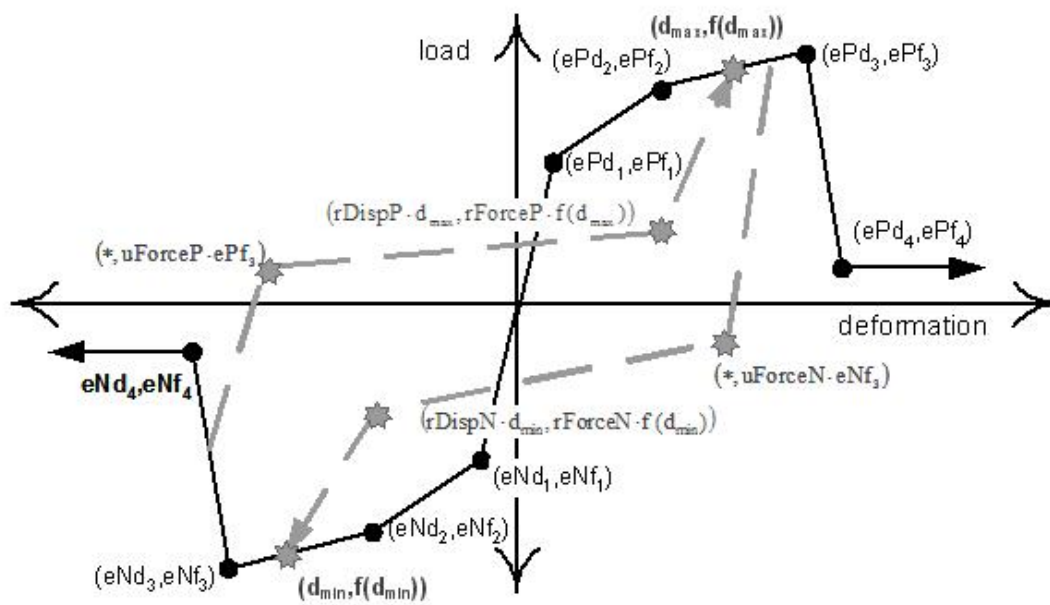
Fig. A.6. Definition of the Pinching4 uniaxial material model

(source: Mazzoni et al. 2007)

Table A.1. Model parameters for 8d nails fastening wood based sheathing to frame

envelope in positive displacement range (State 1)				
	1	2	3	4
ePf (kN)	0.640	1.000	1.400	0.100
ePd (mm)	1.0	3.5	12.5	20.0
envelope in negative displacement range (State 2)				
	1	2	3	4
eNf (kN)	-0.640	-1.000	-1.400	-0.100
eNd (mm)	-1.0	-3.5	-12.5	-20.0
unloading-reloading path (State 4)				
	rDispP	rForceP	uForceP	
	0.65	0.35	0.05	
unloading-reloading path (State 3)				
	rDispN	rForceN	uForceN	
	0.65	0.35	0.05	
unloading stiffness degradation					
	1	2	3	4	Limit
gK	1.0	0.2	0.3	0.2	0.1
reloading stiffness degradation					
	1	2	3	4	Limit
gD	0.50	0.5	2.0	2.0	0.25
strength degradation					
	1	2	3	4	Limit
gF	1.0	0.0	1.0	1.0	0.15
damage index		
gE	dmgType	
10	energy	

Table A.2. Model parameters for 32 mm drywall screws fastening 13 mm GWB to frame

envelope in positive displacement range (State 1)				
	1	2	3	4
ePf (kN)	0.250	0.440	0.580	0.050
ePd (mm)	0.25	1.25	4.00	8.00

envelope in negative displacement range (State 2)				
	1	2	3	4
eNf (kN)	-0.250	-0.440	-0.580	-0.050
eNd (mm)	-0.25	-1.25	-4.00	-8.00

unloading-reloading path (State 4)		
rDispP	rForceP	uForceP
0.65	0.35	0.05

unloading-reloading path (State 3)		
rDispN	rForceN	uForceN
0.65	0.35	0.05

unloading stiffness degradation				
	1	2	3	4	Limit
gK	1.0	0.2	0.3	0.2	0.1

reloading stiffness degradation				
	1	2	3	4	Limit
gD	0.50	0.5	2.0	2.0	0.25

strength degradation				
	1	2	3	4	Limit
gF	1.0	0.0	1.0	1.0	0.15

damage index	
gE	dmgType
10	energy

Table A.3. Model parameters for 22 ga narrow corrugated ties

envelope in positive displacement range (State 1)				
	1	2	3	4
ePf (kN)	0.085	0.150	0.250	0.150
ePd (mm)	1.0	2.5	12.5	20.0

envelope in negative displacement range (State 2)				
	1	2	3	4
eNf (kN)	-0.085	-0.150	-0.250	-0.150
eNd (mm)	-1.0	-2.5	-12.5	-20.0

unloading-reloading path (State 4)		
rDispP	rForceP	uForceP
0.65	0.35	0.05

unloading-reloading path (State 3)		
rDispN	rForceN	uForceN
0.65	0.35	0.05

unloading stiffness degradation				
	1	2	3	4	Limit
gK	1.0	0.2	0.3	0.2	0.1

reloading stiffness degradation				
	1	2	3	4	Limit
gD	0.50	0.5	2	2	0.25

strength degradation				
	1	2	3	4	Limit
gF	1.0	0.0	1.0	1.0	0.15

damage index	
gE	dmgType
10	energy

Table A.4. Model parameters for 22 ga wide corrugated ties

envelope in positive displacement range (State 1)				
	1	2	3	4
ePf (kN)	0.181	0.300	0.420	0.150
ePd (mm)	1.25	3.0	12.5	20.0
envelope in negative displacement range (State 2)				
	1	2	3	4
eNf (kN)	-0.181	-0.300	-0.420	-0.150
eNd (mm)	-1.25	-3.0	-12.5	-20.0

unloading-reloading path (State 4)		
rDispP	rForceP	uForceP
0.65	0.35	0.05

unloading-reloading path (State 3)		
rDispN	rForceN	uForceN
0.65	0.35	0.05

unloading stiffness degradation				
	1	2	3	4	Limit
gK	1.0	0.2	0.3	0.2	0.1

reloading stiffness degradation				
	1	2	3	4	Limit
gD	0.50	0.5	2	2	0.25

strength degradation				
	1	2	3	4	Limit
gF	1.0	0.0	1.0	1.0	0.15

damage index	
gE	dmgType
10	energy

VITA

Nikola Zisi was born in Skopje, Republic of Macedonia, on May 22, 1966. He went to J. H. Pestalozzi elementary school, and graduated from Orce Nikolov high school in 1984. He attended the University St. Cyril and Methodius, Skopje and received a B.S. in civil engineering in 1991, and a M.S. in technical sciences in 1995. He worked as a structural researcher in the Institute of Earthquake Engineering and Engineering Seismology in Skopje before coming to the U.S.A. in 2000. He is currently enrolled in the graduate program of the University of Tennessee, Knoxville where he is pursuing a doctorate in civil engineering.